3D CHARACTERIZATION OF ACIDIZED FRACTURE SURFACES

A Thesis

by

CAMILO MALAGON NIETO

Submitted to the Office of Graduate Studies of
Texas A&M University
in partial fulfillment of the requirements for the degree of

MASTER OF SCIENCE

May 2007

Major Subject: Petroleum Engineering

3D CHARACTERIZATION OF ACIDIZED FRACTURE SURFACES

A Thesis

by

CAMILO MALAGON NIETO

Submitted to the Office of Graduate Studies of
Texas A&M University
in partial fulfillment of the requirements for the degree of

MASTER OF SCIENCE

Approved by:

Chair of Committee,	A. Daniel Hill
Committee Members,	Stephen A. Holditch
	Yanyuan Ma
Head of Department,	Stephen A. Holditch

May 2007

Major Subject: Petroleum Engineering

ABSTRACT

3D Characterization of Acidized Fracture Surfaces. (May 2007)
Camilo Malagon Nieto, B.S., Universidad de América
Chair of Advisory Committee: Dr. A. Daniel Hill

The complex interrelations among the different physical processes involved in acid fracturing make it difficult to design, and later, to predict the outcome of stimulation jobs. Actual tendencies require the use of computational models to deal with the dynamic interaction of variables. This thesis presents a new study of acidized surface textures by means of a laser profilometer to improve our understanding of the remaining etched surface topography and its hydraulic response.

Visualization plots generated by the profilometer identified hydrodynamic channels that could not be identified by the naked eye in acidized surfaces. The plots clarified the existence of rock heterogeneities and revealed how the processes of dissolution function in chalk rock.

Experimental data showed clearly that the effect of dissolution depends on the type of rock and the fluid system; dolomite, for example, dissolves more rapidly but more roughly than limestone. Fluid leakoff rate and temperature also affect the dissolution. Further research is necessary to clarify the effects of conductivity.

DEDICATION

To Marco A. and Rosalba

ACKNOWLEDGEMENTS

The author of this work would like to thank Dr. Daniel A. Hill and Dr. Ding Zhu for their commitment to this project and their academic support and advice.

The author also highly appreciates the hard work and help received from the other members of the acidizing group Maysam Pournik, Gina Melendez and Luis Antelo whose work allowed me to collect the necessary data.

Finally, the author wants to acknowledge the Harold Vance Department of Petroleum Engineering and its sponsor companies for funding the present research project.

TABLE OF CONTENTS

Page

ABSTRACT……. iii

DEDICATION …… iv

ACKNOWLEDGEMENTS …… v

TABLE OF CONTENTS…… vi

LIST OF FIGURES……..... ix

LIST OF TABLES…….. xv

1. INTRODUCTION…….…… 1

    1.1. Acid Fracturing and Conductivity…….……..……... 1

    1.2. Development of Acid Fracturing ….……..…….…….……. 3

    1.3. Scope of Present Study……..……...……..…… 6

    1.4. Content of the Thesis. ……..……..……..……. 7

2. ACID FRACTURING EXPERIMENTS……..…… 8

3. PROFILOMETER DESCRIPTION…….…….…… 12

    3.1. Hardware Description. ……...……..……. 12

    3.2. LabView Software Description…….…….…..... 15

    3.3. Measurement Procedure…...…….…..….... 17

4. SURFACE CHARACTERIZATION. ……..…… 18

    4.1. Introduction. …….. 18

    4.2. The Surface Topography as a Random Process……...…….. 19

    4.3. Acid Etching as a Multi-event Formative Process…….…… 21

    4.4. Surface Assessment. …….…….…… 23

        4.4.1. Data Acquisition. …….…….. 25

        4.4.2. Data Pre-processing. …….……. 26

            4.4.2.1. Data File Conversion……. 27

            4.4.2.2. Filtering of the Surface Roughness and Waviness..…..… 29

        4.4.3. Data Characterization. ….…….. 33

Page

4.4.3.1. Visualization..... 36

4.4.3.2. Amplitude Property..... 38

4.4.3.3. Hybrid Property..... 40

4.4.3.4. Material Ratio Curve..... 42

5. TEXTURE OF ACIDIZED SURFACES..... 44

5.1. Experimental Work Summary..... 44

5.2. Experimental Surfaces Characterization..... 44

5.2.1. Experiment 1: Emulsified Acid and Limestone, 200°F, 0.005 ft/min 45

5.2.2. Experiment 2: Emulsified Acid and Limestone, 275°F, 0.005 ft/min..... 54

5.2.3. Experiment 3: Gelled Acid and Limestone, 200°F, 0.005 ft/min.... 63

5.2.4. Experiment 4: Gelled Acid and Limestone, 200°F, 0.010 ft/min.... 71

5.2.5. Experiment 5: Viscoelastic Surfactant Acid and Limestone, 200°F, 0.003 ft/min..... 78

5.2.6. Experiment 6: Viscoelastic Surfactant Acid and Dolomite, 200°F, 0.005 ft/min..... 86

5.2.7. Experiment 7 and 8: Straight Acid and Chalk, 100°F, 0.005 ft/min..... 93

6. CONCLUSIONS AND RECOMMENDATIONS..... 100

6.1. Characterization Technique..... 100

6.2. Profilometer..... 101

6.3. Experiments Results..... 102

6.4. Recommendations About Conductivity..... 103

6.5. General Recommendations..... 104

REFERENCES..... 106

APPENDIX A PROFILOMETER MANUAL 108

APPENDIX B MATLAB FUNCTIONS..... 115

Page

APPENDIX C SAMPLE PICTURES…….…… 122

VITA…… 129

LIST OF FIGURES

Page

Figure 1.1. Acid fracturing dissolves portions of the rock faces, thus leaving a rough surface that remains open to fluid flow……...… 1

Figure 1.2. Acid stimulation done (a) may improve flow capacity and wormhole growth (b) may extend it, but hydraulic fracturing (c) will create larger, more effective flow area..…….. 4

Figure 2.1. Rock samples are cut to the shape of the cell and coated with silicone rubber to prevent fluid bypass during experiments.……. 8

Figure 2.2. Samples are placed onto the acidizing cell (a), a gap is left to simulate a fracture gap (b).. ……..……. 9

Figure 2.3. The cell mounted on the rack to sustain internal pressure (a). Acid flows from the mixing tank through the test cell and back out through both the leakoff lines and the discharge line (b). ……. 10

Figure 2.4**.** The profilometer identifies surface changes in the acidized rock..... 10

Figure 2.5. Nitrogen gas is flow through the acidized surfaces while different loads are applied in the conductivity stack..……..….. 11

Figure 3.1. Profilometer components…….…… 13

Figure 3.2. Control box and its components…….……. 13

Figure 3.3. Data measurement path along the specified scanning area…...……. 14

Figure 3.4. Points where data is recorded for a 7 in. x 1.7 in. scanning area and 0.05 in. resolution (4935 data points)……..... 15

Figure 3.5. Profilometer software user window……...…….. 16

Figure 3.6. First rows of the text data file from the profilometer output and its trajectory……..... 16

Figure 4.1. Height probability density function (histogram) of 3D surface data set.…….……. 19

Page

Figure 4.2. Generation of a rough surface due to deposition of (a) a single drop, (b) multiple, random and cumulative process……..…….. 20

Figure 4.3. Cumulative height distribution curve. a) Polished copper etched in ferric chloride. b) Polished copper etched in nitric acid. c) Polished brass etched in ferric chloride……..……..... 21

Figure 4.4. No-symmetric height distribution shape of acidized surfaces…….… 22

Figure 4.5. Procedure for 3D surface characterization assessment...…..…… 24

Figure 4.6. Micro-roughness at smaller measurement intervals…….…... 25

Figure 4.7. a) The interaction scale of some processes (contact) does not require micro-roughness resolution. b) Large measurement interval fail capturing roughness features…….…..... 26

Figure 4.8. Simplified explanation of data matrix conversion……..... 28

Figure 4.9. Raw data visualization. …….…….. 28

Figure 4.10. Profile components a) Original profile and its waviness. b) Roughness profile after waviness subtraction….…… 29

Figure 4.11. Unfiltered surface with hydrodynamic channel (light blue)…...……. 30

Figure 4.12. a) Waviness surface after filtering. b) Roughness surface after filter, notice that the surface is leveled to zero…… 30

Figure 4.13. ISO standard 13565 filtering, a) Calculation of the first mean line over the original profile, b) Suppression of the profile data points below the first mean line. c) Second mean line calculated over the remaining profile. d) Filtered profile after subtraction of second mean line……. 31

Figure 4.14. 3D surface with major channel as main characteristic…… 32

Figure 4.15. Filter of Fig. 4.14. a) Waviness surface after filtering keeps the shape of the channel. b) Roughness surface after filter destroys the channel features (notice the color scale)……..……... 32

Figure 4.16. Classification of the characterization techniques….……..…. 35

Page

Figure 4.17. Inverted 3D gray surface visualization technique..…… 37
Figure 4.18. Cross-section plot visualization technique..…….……..…… 38
Figure 4.19. Profile digital data represented as a height distribution……. 38
Figure 4.20. The height distribution curve as profile descriptor……. 39
Figure 4.21. Skewness and kurtosis as distribution shape descriptors.……...… 40
Figure 4.22. Different profiles can exhibit same height distribution…..…… 41
Figure 4.23. Material ratio curve. a) Origin of the curve. b) MRC Hp and Hv…. 42
Figure 5.1. Exp. 1: Visualization 3D surfaces of emulsified acid and limestone—200 °F, 0.005 ft/min., 15 min.……. 46
Figure 5.2. Exp. 1: Visualization 3D surfaces of emulsified acid and limestone—200 °F, 0.005 ft/min., 30 min.……. 47
Figure 5.3. Exp. 1: Visualization 3D surfaces of emulsified acid and limestone—200 °F, 0.005 ft/min., 60 min.……. 48
Figure 5.4. Exp. 1—Volume of rock dissolved on rock surface..…….. 49
Figure 5.5. Exp. 1—Longitudinal and transversal cross-section profiles……. 50
Figure 5.6. Exp. 1—Comparative cross-section profile.…….…….. 50
Figure 5.7. Exp. 1—Comparative roughness cross-section profile. …..…… 50
Figure 5.8. Exp. 1—Roughness parameters…….……. 51
Figure 5.9. Exp. 1—Roughness comparison of material ratio curves.……. 52
Figure 5.10. Exp.1—Conductivity measurements.…….……..... 52
Figure 5.11. Exp. 1—Waviness 3D surface views…….……. 53
Figure 5.12. Exp. 1—Original surfaces comparative of material ratio curves…... 54
Figure 5.13. Pictures of experiment 2…… 55
Figure 5.14. Exp. 2: Visualization 3D Surfaces of emulsified acid and limestone—275 °F, 0.005 ft/min., 15 min..…… 56
Figure 5.15. Exp. 2: Visualization 3D surfaces of emulsified acid and limestone—275 °F, 0.005 ft/min., 30 min..…… 57

Page

Figure 5.16. Exp. 2: Visualization 3D surfaces of emulsified acid and limestone—275 °F, 0.005 ft/min., 60 min…….. 58
Figure 5.17. Exp. 2—Volume of rock dissolved on rock surface…….. 59
Figure 5.18. Exp. 2—Longitudinal and transversal cross-section profiles……. 60
Figure 5.19. Exp. 2—Comparative cross-section profile. …….. 60
Figure 5.20. Exp. 2—Comparative roughness cross-section profile. …… 60
Figure 5.21. Exp. 2—Roughness parameters……. 61
Figure 5.22. Exp. 2—Roughness material ratio curves. ……. 62
Figure 5.23. Exp. 2—Original data material ratio curves……..……. 62
Figure 5.24. Exp. 3: Visualization 3D surfaces of gelled acid and limestone—200°F, 0.005 ft/min., 15 min.……. 64
Figure 5.25. Exp. 3: Visualization 3D surfaces of gelled acid and limestone—200°F, 0.005 ft/min., 30 min.. …… 65
Figure 5.26. Exp. 3: Visualization 3D surfaces of gelled acid and limestone—200°F, 0.005 ft/min., 60 min.……. 66
Figure 5.27. Exp. 3—Volume of rock dissolved on rock surface…….. 67
Figure 5.28. Exp. 3—Longitudinal and transversal cross-section profiles……. 67
Figure 5.29. Exp. 3—Comparative cross-section profile..……. 68
Figure 5.30. Exp. 3—Comparative roughness cross-section profile.……. 68
Figure 5.31. Exp. 3—Roughness parameters…….……. 69
Figure 5.32. Exp. 3—Roughness material ratio curves.……. 69
Figure 5.33. Exp. 3—Original data material ratio curves..……. 70
Figure 5.34. Exp. 3—Conductivity measurements……..... 70
Figure 5.35. Exp. 4: Visualization 3D surfaces of gelled acid and limestone — 200 °F, 0.010 ft/min., 15 min.…… 72
Figure 5.36. Exp. 4: Visualization 3D surfaces of gelled acid and limestone—200 °F, 0.010 ft/min., 30 min.…… 73
Figure 5.37. Exp. 4—Volume of rock dissolved on rock surface……... 74

Page

Figure 5.38. Exp. 4—Longitudinal and transversal cross-section profiles……. 74
Figure 5.39. Exp. 4—Comparative cross-section profile. …….. 75
Figure 5.40. Exp. 4—Comparative roughness cross-section profile…….. 75
Figure 5.41. Exp. 4—Roughness parameters……. 76
Figure 5.42. Exp. 4—Roughness comparative of material ratio curves..... 77
Figure 5.43. Exp. 4—Conductivity measurements…… 77
Figure 5.44. Exp. 4—Waviness 3D surface view for 30-min. rock…… 78
Figure 5.45. Exp. 5: Visualization 3D surfaces of viscoelastic surfactant acid and limestone—200 °F, 0.003 ft/min., 15 min…….. 79
Figure 5.46. Exp. 5: Visualization 3D surfaces of viscoelastic surfactant acid and limestone—200 °F, 0.003 ft/min., 30 min…….. 80
Figure 5.47. Exp. 5: Visualization 3D surfaces of viscoelastic surfactant acid and limestone—200 °F, 0.003 ft/min., 60 min…….. 81
Figure 5.48. Exp. 5—Volume of rock dissolved on rock surface…….. 82
Figure 5.49. Exp. 5—Longitudinal and transversal cross-section profiles……. 82
Figure 5.50. Exp. 5—Comparative cross-section profile..…….. 83
Figure 5.51. Exp. 5—Comparative roughness cross-section profile……..... 83
Figure 5.52. Exp. 5—Roughness parameters……..... 84
Figure 5.53. Exp. 5—Original data material ratio curves…..... 85
Figure 5.54. Exp. 5—Conductivity measurements…… 85
Figure 5.55. Exp. 6: Visualization 3D surfaces of viscoelastic surfactant acid and dolomite—200 °F, 0.005 ft/min., 10 min…….. 87
Figure 5.56. Exp. 6: Visualization 3D surfaces of viscoelastic surfactant acid and dolomite—200 °F, 0.005 ft/min., 20-min……... 88
Figure 5.57. Exp. 6: Visualization 3D surfaces of viscoelastic surfactant acid and dolomite—200 °F, 0.005 ft/min., 30 min…….. 89
Figure 5.58. Exp. 6–Volume of rock dissolved on rock surface…… 90
Figure 5.59. Exp. 6—Longitudinal and transversal cross-section profiles……. 90

Page

Figure 5.60. Exp. 6—Comparative roughness cross-section profile. …… 91
Figure 5.61. Exp. 6—Roughness parameters……. 91
Figure 5.62. Exp. 6—Roughness comparative of material ratio curves..... 92
Figure 5.63. Exp. 6—Original data comparative of material ratio curves…….. 92
Figure 5.64. Exp. 6—Conductivity measurements …… 93
Figure 5.65. Exp. 7—Visualization 3D surfaces of straight acid and chalk I—
100°F, 0.005 ft/min., 3 min. …….. 94
Figure 5.66. Exp. 7: Visualization 3D surfaces of straight acid and chalk I—
100°F, 0.005 ft/min., 5 min.…… 95
Figure 5.67. Exp. 7—Volume of rock dissolved on rock surface..…….. 96
Figure 5.68. Exp. 7—Longitudinal and transversal cross-section profiles……. 96
Figure 5.69. Exp. 8: Visualization 3D surfaces of straight acid and chalk II—
100°F, 0.005 ft/min, 7.5 min..…… 98
Figure 5.70. Exp. 8—Longitudinal and transversal cross-section profiles……. 99
Figure 5.71. Exp. 7 and 8—Characterization parameters..…….. 99

LIST OF TABLES

Page

Table 1.1. Design variables…….. ……. 2

Table 4.1. Applied characterization techniques…..…..…….. 36

Table 5.1. Summary of experiments…….. 45

1. INTRODUCTION

1.1. Acid Fracturing and Conductivity

The basic principle of acid fracturing is to dissolve the surfaces of induced or natural fractures to avoid closure after the pressures declines (Fig. 1.1). The process consists of creating and opening the fracture with a fluid pumped at high pressure, then pumping an acid solution to etch the fracture walls, the pressure is reduced by flowing back the well so the fracture will close.

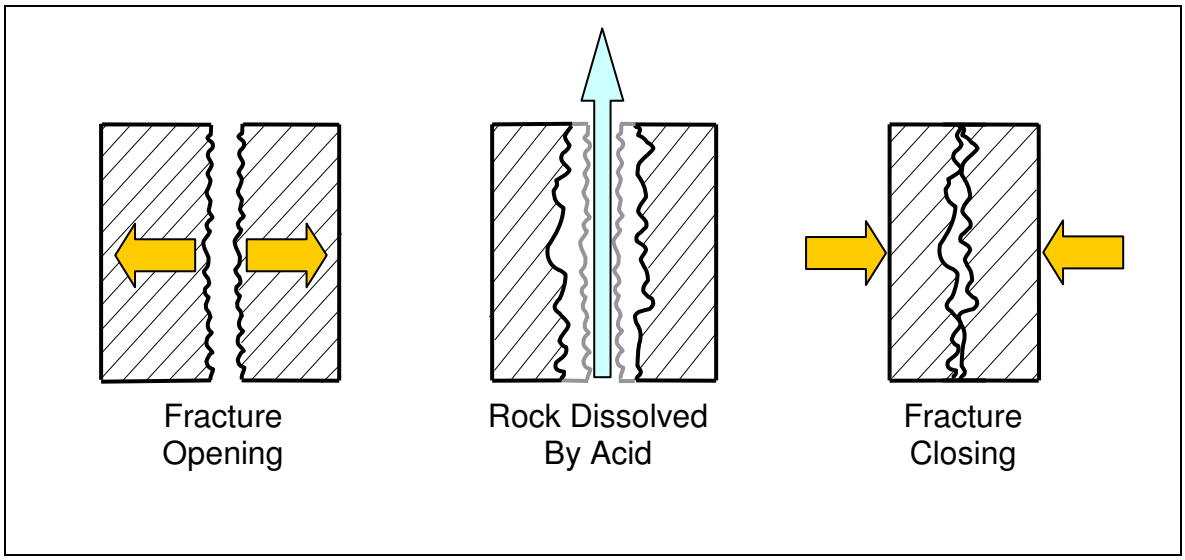

Fig. 1.1—Acid fracturing dissolves portions of the rock faces, thus leaving a rough surface that remains open to fluid flow.

The altered features on each side of the fracture create void areas along the dissolved fracture that may improve the flow capacity of the production fluid. The complexity of the process becomes evident in the large number of variables required to model it.

This thesis follows the style and format of *SPE Drilling and Completion Journal.*

Engineering design objectives and operative variables are different for each of the stages of the process (Table 1.1). Success of a design depends on how the variables are considered and manipulated.

The design of the fracture opening can be achieved by using the standard hydraulic fracturing theory including analytical or finite element calculations to determine the fracture geometry as a function of the fluid pumped.

Table 1.1— Design variables.

	Fracture Opening	**Rock Dissolution**	**Mechanical Closure**
Design Objective	• Optimum Fracture Geometry (height and long length)	• Sustain change in fracture geometry. • Deep acid penetration into the fracture. • Uniform/controlled etching along the fracture.	• Achieve conductivity • Sustain achieved conductivity on time.
Principal Operational Variables and Parameters	• Fluid Properties Flow rate Viscosity Pressure • Rock Properties In-situ stress • Leakoff	• Acid Fluid Properties Concentration Flow rate Viscosity Pressure • Rock Properties Dissolution rate • Leakoff	• Rock Properties Closure pressure • Surface Texture Rock surface strength Etched path geometry

The rock dissolution stage is much more difficult to design since the dissolution of the fracture faces changes the fracture geometry and the leakoff rate. That dynamic change occurs in both time and space; as a result, it requires the use of 3D numerical calculations.

The ultimate stage of acid fracture is the mechanical closure, where the closure pressure is a formation property that can not be influenced, and all the other variables are direct consequences of the rock-dissolution stage. Under this conceptual model, the surface texture formative process is a fundamental part of the dissolution stage design. Since the interaction between the fracture faces and the acid dissolution itself are different physical processes, two approaches can be use to model the processes; one is to create a model to up-scale the surface interaction to the size of the dissolution model grid; the other is to use the final dissolution model output as input for a specific closure-modeling application. Both of these first require more knowledge about the acidized surface interaction.

That knowledge must include an understanding of the surfaces characteristics, and its formative process, how those characteristics change depending on the acidizing conditions, and how the surfaces interact against each other depending on their texture.

1.2. Development of Acid Fracturing

Acid fracturing was developed to overcome the short penetration of acid treatments (Fig. 1.2). Barron & Hendrickson[1] identifies the interactions among variables such as fracture width, acid concentration, contact time, and fracture height that affected the reaction of acid on marble. They showed that the reaction rate is a function of the flow velocity and fracture width, so while increasing the flow rate will increase the penetration, it will also increase the reaction rate and therefore the spending. This deeper penetration could be attained by increasing the fracture width during the treatment to reduce spending and force live acid to travel farther into the fracture.

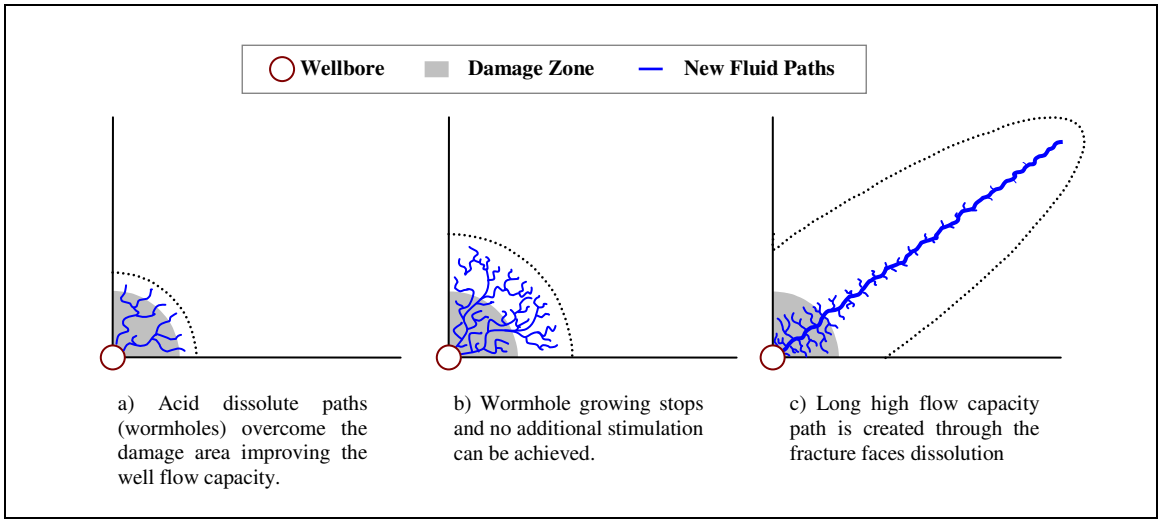

Fig. 1.2—Acid stimulation done (a) may improve flow capacity and wormhole growth (b) may extend it, but hydraulic fracturing (c) will create larger, more effective flow area.

Efforts to improve acid treatment assume that large quantities of acid and large contact times would make better treatments but ignored the fact that over etching of the rock can soften the rock faces, causing the rock to crush under closure stress and reduce flow capacity. Broaddus et al.[2] showed that different formations, acids, solutions, and temperatures all affected fluid flow. And that rock properties and surface etching pattern are of vital importance to the final fracture flow capacity.

Williams & Nierode[3] proposed a design procedure that takes into account the change in fracture geometry where the rock has been dissolved by the acid and the change in fluid volume as it leaks into the formation. Nevertheless, they recognized that the fracture conductivity after treatment cannot be predicted with certainty because it is a related to the degree of formation heterogeneity.

In theory, avoiding leakoff into the formation will sustain deeper acid penetration; furthermore, retarded acid will allow less over-etching in the near-wellbore region, more homogenous concentration along the fracture, and long penetration distance. This

concept led to the use of improved fluid systems such as gelled, emulsified, or viscosified acids, in which the dynamic fluid properties supposedly act as both fluid-loss control and retardant.

Addressing the use of specialized fluid systems, Nierode and Kruk[4] developed a correlation for conductivity estimation that takes into account the rock strength and the applied closure stress. Assuming that the fracture walls dissolve uniformly, they developed the dissolved rock equivalent conductivity (DREC) concept, which is calculated from the rock weight loss. The authors conclude that since the heterogeneities and fingering can lead to channels along the fracture, any measurement of conductivity, in the laboratory or by correlation, will show the lower boundary of the attainable conductivity.

Using an acidizing cell that allows leakoff, Beg et al.[5] observed that sometimes the increase in contact time results in lower conductivity, and that the fluid loss can increase the fracture conductivity. They also discovered that increased acid exposures will weak the rock structure so that it is prone to crush under closure pressure. Beg et al.[5] also observed that different experiments with leakoff exhibited different etching patterns, such as channels and valleys, which illustrated the importance of characterizing the acidized surface.

Ruffet et al.[6] characterized the etched surfaces quantitatively and evaluated their relation with acid injection conditions. In their approach Ruffet et al.[6] measured the 2D surface profile with a mechanical profilometer after each etching experiment and used these digital data to calculate the statistical measurements of the data distribution and the linear and absolute roughness values. Their global roughness parameter encapsulates all these measurements to compare between different treatment conditions. In addition, Ruffet et al.[6] estimated the mechanical behavior of the surface under closure stress, using

digitalized profile data to calculate specific topographic descriptors, which are used to estimate the fracture conductivity behavior.

In their model for acid fracture conductivity, Gong et al.[7] assumed plastic deformation closure of the asperities after closure stress is applied and achieved close agreement between the laboratory conductivity measurements and the model output.

Dong et al.[8] used synthetic surfaces from geostatistical methods to validate a computational model for acidizing carbonates. This model uses mass conservation for acid solution, acid transport, and change in fracture caused by dissolution. The experimental work identified three different kind of etching patterns: wormhole features, channeling, and pure surface roughness. The differentiation of those three patterns indicates that normal profilography (2D unidirectional measurement) will not be able to effectively characterize the features of the surfaces because of the nature of the profile.

1.3. Scope of Present Study

The complex interrelations among the different physical processes involved in acid fracturing make it difficult to design and, later, to predict the outcome of stimulation jobs. Actual tendencies require the use of computational models to deal with the dynamic interaction of variables. This project presents a new study of acidized surface textures by means of the use of a laser profilometer to improve the understanding of the remaining etched surface topography and its hydraulic response.

The project developed a preliminary surface assessment technique to characterize the acidized surfaces. It developed computer programs to handle, visualize, and analyze the data sets and to characterize the 3D digital recorded data, and identified relevant

variables for future mathematical modeling and a more robust theory of etched surface interaction.

1.4 Content of the Thesis

Section 2 presents a brief description of the equipment used to perform the experiments. Section 3 is dedicated specifically to describing the profilometer apparatus software and hardware; it includes a brief description of the procedure to measure the surfaces. Section 4 presents the theory of profilometry and surface characterization; it contains the explanation of the characterization stages and presents the characterization technique. Section 5 contains the characterization of the surfaces using the techniques proposed in section 4, this section starts with a summary of the experiments followed by the sequential analysis for each one. Finally, section 6 presents the conclusions regarding the experiments results and the characterization technique; additionally, it presents a set of recommendations for future work.

2. ACID FRACTURING EXPERIMENTS

A complete acid fracture experiment in this project consists of four main stages: rock preparation, acid fracture treatment, profile scanning, and conductivity measurement. Initially, the rock is cut to the shape of the cell; those dimensions are 7.11 in. length, 1.61 in. width, and 3 in. height; the rock sides are covered with a silicone rubber compound to assure a complete seal and to prevent fluid bypass around the rock during the experiments (Fig. 2.1). Then, an initial surface scan is made to record the surface before the acidizing. Finally, the sample is taken to a vacuum vessel to saturate it with brine.

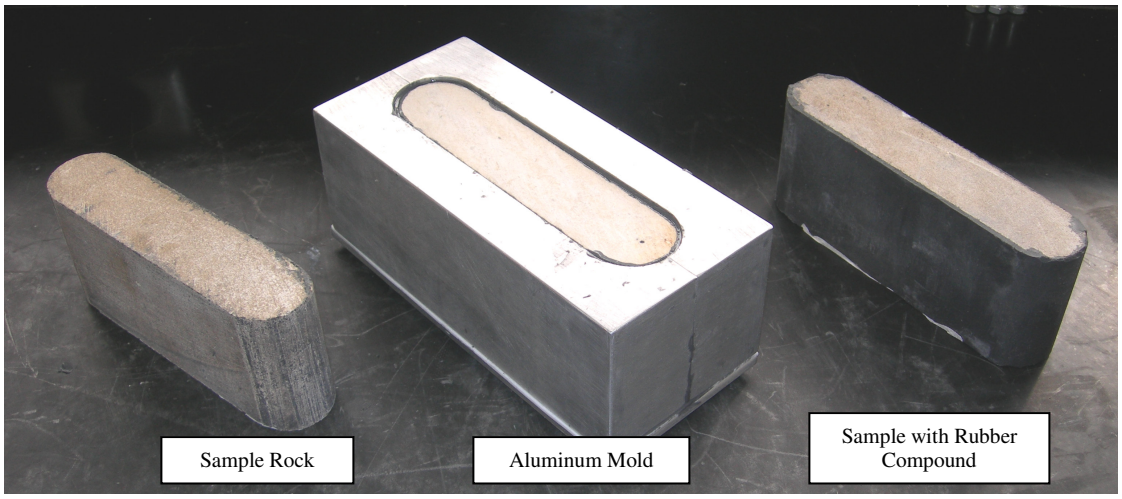

Fig. 2.1—Rock samples are cut to the shape of the cell and coated with silicone rubber to prevent fluid bypass during experiments.

For the acid treatment, the two rocks are fitted into an API cell (Fig. 2.2.a), leaving a gap to simulate the fracture width, typically 0.12 in. (Fig. 2.2.b). The cell is mounted on a frame and connected to the acid flow lines and the pressure sensors (Fig. 2.3.a).

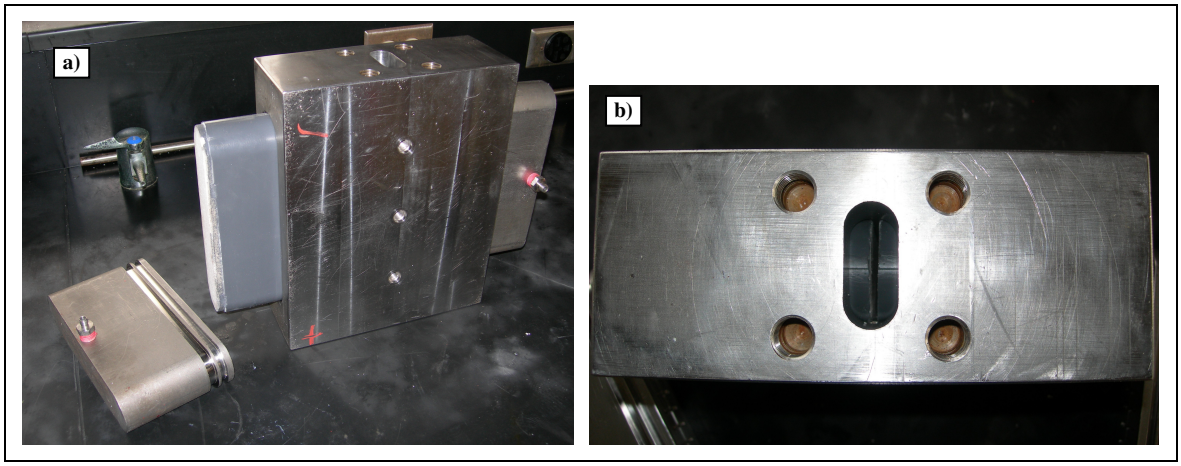

Fig. 2.2—Samples are placed onto the acidizing cell (a), a gap is left to simulate a fracture gap (b).

During the acidizing, the acid solution is pumped from the mixing tank through a tubing line which passes through heater jackets to heat the fluid to the desired temperature. From the heater the fluid goes to the cell inlet. Consequently, part of the fluid leaves the cell through the outlet and part leaves the cell through the pistons leakoff tubing; the fluid leaving from the outlet goes through a backpressure regulator which assures an internal cell pressure of ~1,000 psi and later to a disposal tank. The fluid leaving from the leakoff tubing goes to another backpressure regulator and finally to a leakoff recipient (Fig. 2.3.b).

When the acidizing stage finishes, the rock samples are pulled out of the cell and scanned in the profilometer (Fig. 2.4.). For the final stage, the rocks are again put together in the cell at the same initial position; then, the cell is mounted in the conductivity stack (Fig. 2.5.). There, the piston applies pressure to the rocks through the pistons, while nitrogen is flowed through the etched fracture.

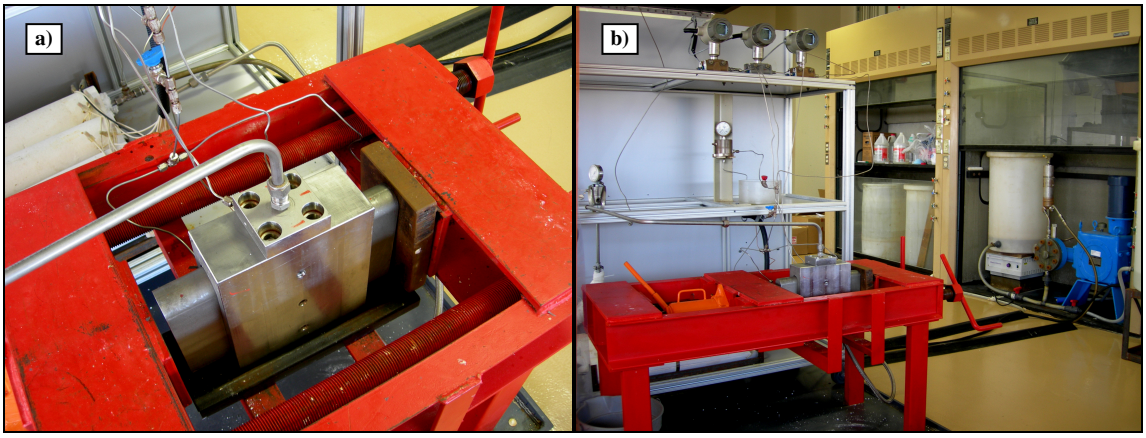

Fig. 2.3—The cell mounted on the rack to sustain internal pressure (a). Acid flows from the mixing tank through the test cell and back out through both the leakoff lines and the discharge line (b).

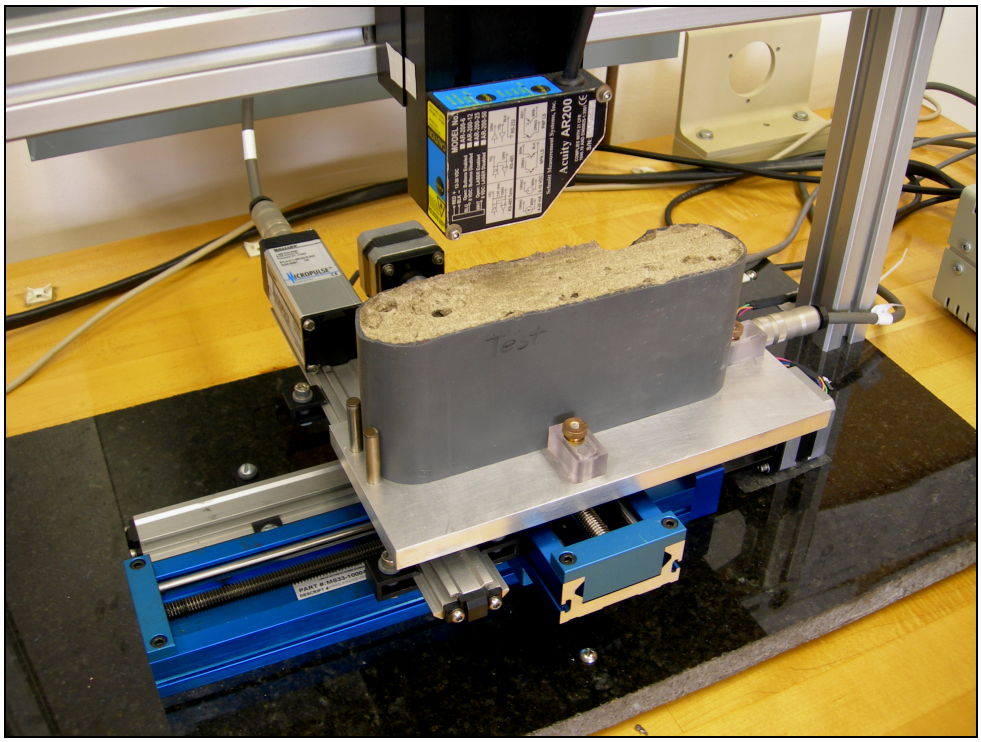

Fig. 2.4—The profilometer identifies surface changes in the acidized rock.

Fig. 2.5—Nitrogen gas is flow through the acidized surfaces while different loads are applied in the conductivity stack.

3. PROFILOMETER DESCRIPTION

A profilometer is a precision vertical distance measurement device; it can measure small surface variations in vertical surface topography as a function of the sample position. The vertical measurement is made with a laser displacement sensor while the sample is moved along its length on a moving table. That measurement is repeated several times over the width of the sample to cover the entire surface area. The resolution on the vertical measurement is 0.002 in.; the horizontal X and Y resolution is 0.05 in. At that resolution the scanning time is 2 hours.

3.1. Hardware Description

The principal profilometer components are a laser displacement sensor, two micro-pulse linear transducers, two stepping motor units, and a horizontal milling table. All the components are mounted on a heavy marble plate except for the laser sensor that is attached to the vertical milling table on an aluminum frame. All the components of the profilometer can be seen in Fig. 3.1.

All the component hardware controllers are connected inside the control box through a multichannel board. This board receives signals from the laser and the micro-pulse transducer drivers; it also sends signals to the motor driver board. In this way, the control box contains the multichannel board, the laser signal receiver, two motor drivers, and a power supply (Fig. 3.2).

The entire control box is controlled automatically with a Data Acquisition Board (DAQ) on a personal computer. The DAQ is cabled to the multichannel board socket in the back of the control box. The movement of the horizontal table can also be controlled manually from the control box front panel.

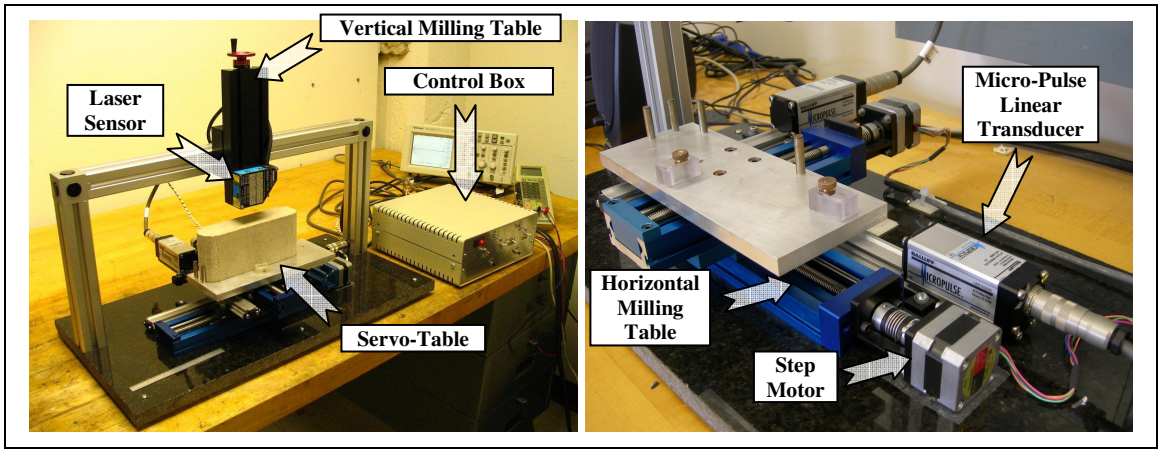

Fig. 3.1—Profilometer components.

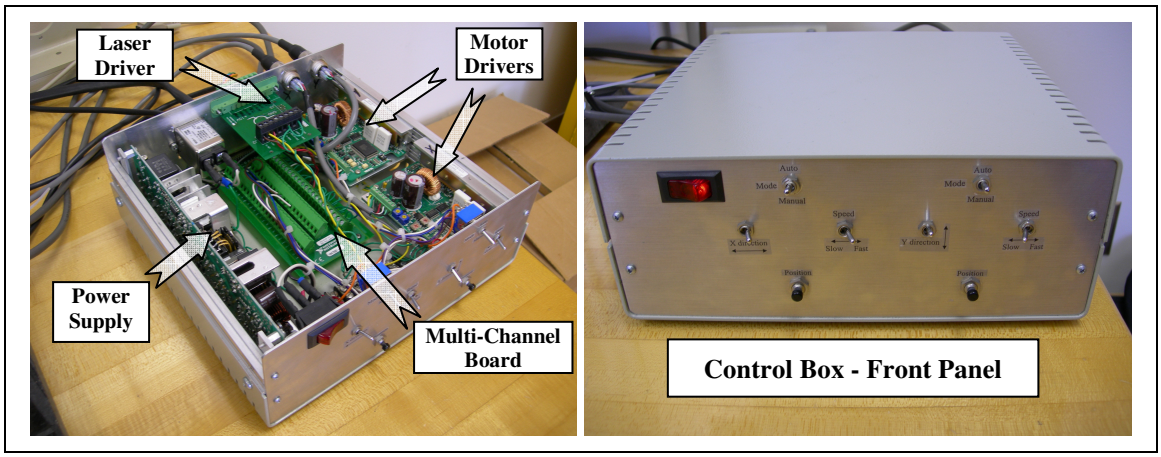

Fig. 3.2—Control box and its components.

The Laser Displacement Sensor is an AR200-25 from Acuity Laser Measurement Inc. This device is a laser diode measurement sensor that uses triangulation to measure distance. It projects a laser beam and captures the reflection from the target surface into collection lenses. The lenses focus the laser spot image on an array camera; the position of the image on the camera pixel sensors is processed to determine the distance to the target.[9] The device accuracy is 50.8 μm (0.002 in.), and its measurement range is 25.4 mm (1.0 in.).

The two micro-pulse linear transducers use magnetic wave sensors to measure the horizontal displacement; since the movable magnet element is attached to the sample table, it measure the milling table position. Each of them measures in the X and Y directions.

The stepping motor units are high-torque, low-vibration devices attached to each of the milling table screws. Their function is to move the table during the measurement. The table moves dynamically in the X direction during the data reading, while the motor moves only in small steps in the Y direction for each X profile measurement. A diagram of the path followed for a measurement set is presented in Fig. 3.3. The small Y steps are equal to the resolution distance (i.e. 0.05 in.); the measurements on X are recorded each time the laser passes over the specified measurement point i.e. each 0.05 in. (Fig. 3.4).

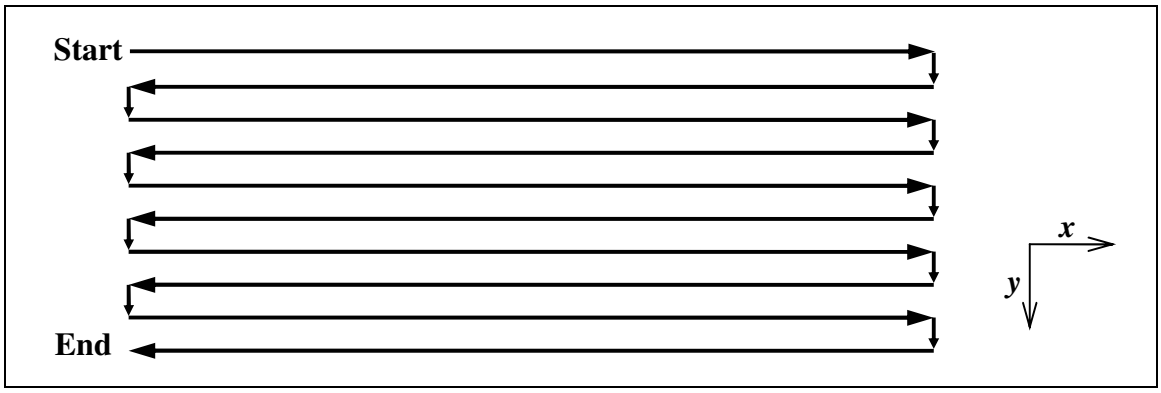

Fig. 3.3—Data measurement path along the specified scanning area.

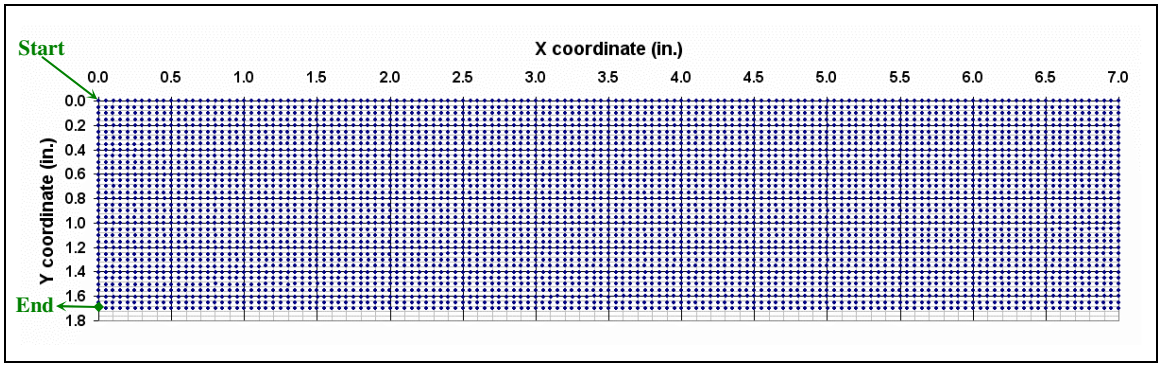

Fig. 3.4—Points where data is recorded for a 7 in. x 1.7 in. scanning area and 0.05 in. resolution (4935 data points).

3.2. LabView Software Description

The data acquisition board allows control of the profilometer devices by means of LabView software. LabView primarily controls the servo-table movement, as seen on Fig. 3.3 through the operation of the step motors and depending on the sample dimension and measurement interval setup. The software receives the signals from the laser and from the micro-pulse sensors and records the data in a text file as coordinates and heights.

Fig. 3.5 shows the software window while scanning is being performed. First the user establishes the filename and the directory path for the data file; next, the sample information and the sample dimensions are entered; and then the scanning is started by clicking the Start Scan button. The window will automatically show the updated information of the laser position and height measurement during the entire scanning time.

The software was provided by the profilometer manufacturer, and some adjustments have been performed on the display and data input dialog boxes. The output is an ASCII text file consisting of a header and scan data values (Fig. 3.6). The header records the

sample information entered on the software screen; that includes the name of the file, experiment number, sample dimensions and measurement interval. The scanning data is recorded in three columns, two for position and the third for the height, so that each row corresponds to a 3D coordinate. The extension of the file is equal to the number of data points recorded. (i.e. 4,935 rows for a 7 in. x 1.7 in. sample and 0.05 in. resolution). The order of the data follows the laser trajectory over the sample.

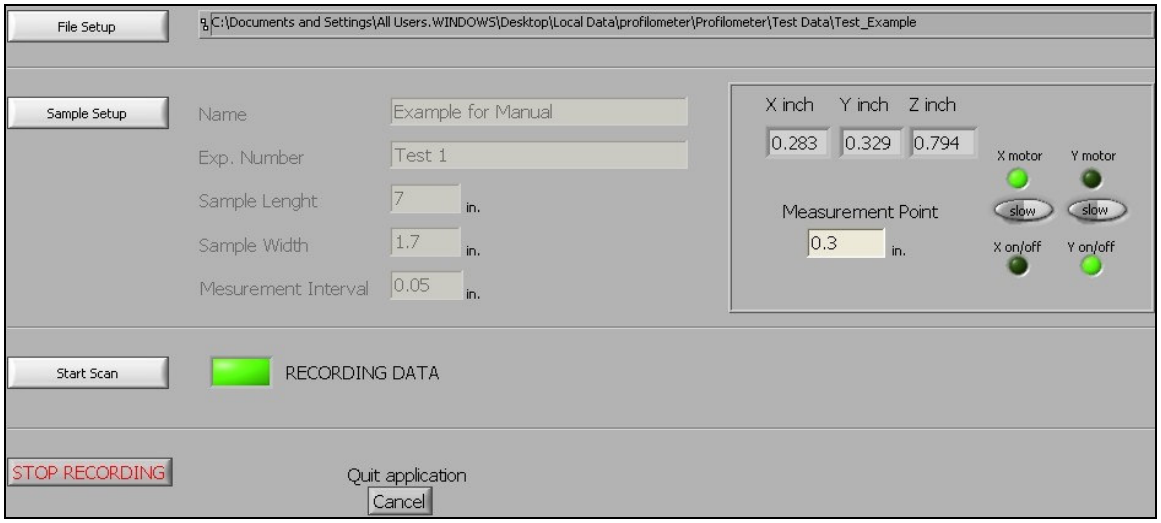

Fig. 3.5—Profilometer software user window.

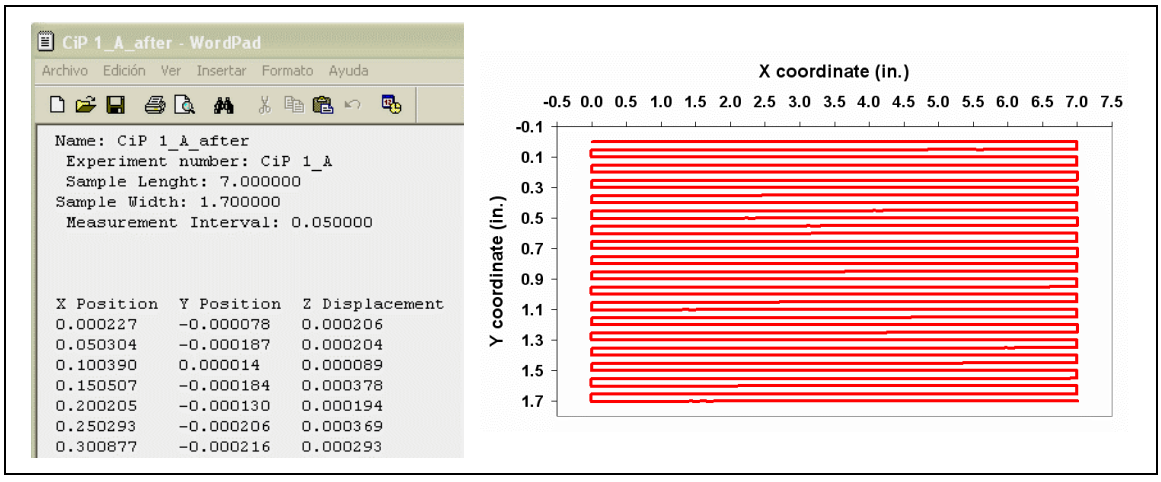

Fig. 3.6—First rows of the text data file from the profilometer output and its trajectory.

3.3. Measurement Procedure

The measurement procedure consists of six steps described below; however, a detailed explanation and special warnings are presented in the profilometer manual in Appendix A.

1. Place the rock sample on the table and secure it using the table screws.
2. Adjust the laser sensor using the vertical milling table screw to assure full range measurements over the surface topography.
3. Set the X and Y distance indicators to zero manually using the control box front panel.
4. Switch the control panel to automatic.
5. Input the data file location, experiment information, and sample dimensions on the software user window.
6. Start scanning by clicking on the Start Scan button on the software screen.

4. SURFACE CHARACTERIZATION

4.1. Introduction

Traditionally, the meaning of surface characterization is misunderstood. The common thought is that the surface does not need to be described; instead, the real importance is its response to the physical process under study rather than its multiple surface features and attributes. This is clearly a common statement in tribology science, where the question is not how to characterize the surface, but how to effectively model the response of the surface from the characterization parameters.[10]

Nevertheless, specialized fields and physics research recognize the strong influence of surface texture on understanding surface behavior. Unfortunately, there is no common consensus on which characteristics are decisive or irrelevant for each of the different applications.

Therefore, the characterization of the surface topography is intended to accomplish two objectives. The first is to provide a general understanding of the surface and to serve as a guide to interpret and envision its properties. This is accomplished by applying different techniques such as statistical, spatial, or functional approaches. The second objective is to relate those parameters to some other physical process. This objective is intrinsically related to the specific phenomenon physical response, and then, the analyst must pick those parameters that represent the expected response of the surface.[11]

Historically, a considerable amount of characterization techniques has been proposed. As a result of the broad spectrum of techniques and data analysis theories, an international effort arose to review and propose a standard for 3D characterization.[12] This work uses the techniques proposed in the first edition of that compendium.

4.2. The Surface Topography as a Random Process

To understand the significance of the surface shape, we must understand how the surface acquires that shape. We define surface texture to means the affectation of the original material topography from its original nominal shape.[1] For the case of etching as it is proposed in this work, this affectation is based on the mixture of different processes as will be discussed in Section 4.3.

The height distribution of many surface profiles has a Gaussian shape product of a random process (Fig. 4.1). In theory, if the engineering surface acquires its shape from to the occurrence of a very large number of separate events that occur randomly along the whole surface and whose effects are cumulative, then the histogram shape will be Gaussian. This is observed in surfaces from processes like deposition (Fig. 4.2) or extrusion.

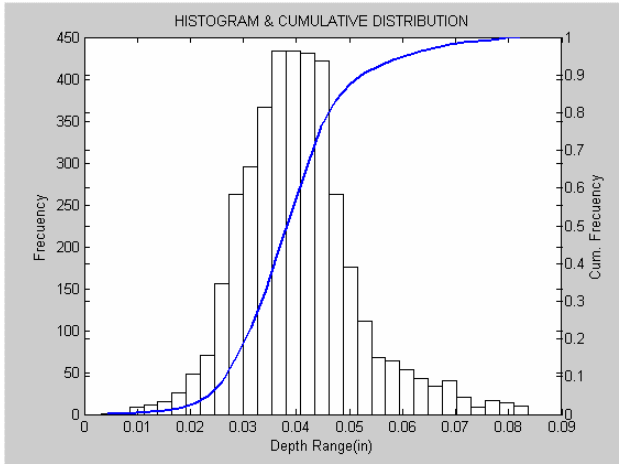

Fig. 4.1—Height probability density function (histogram) of 3D surface data set.

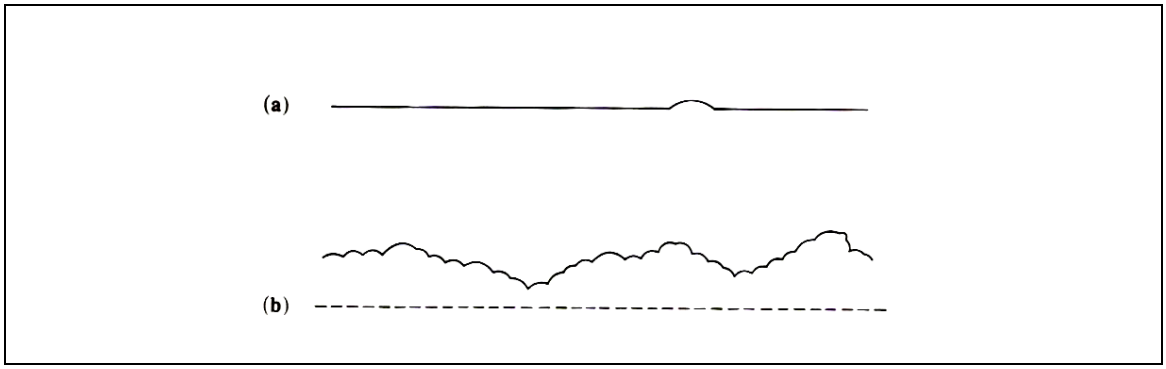

Fig. 4.2—Generation of a rough surface due to deposition of (a) a single drop, (b) multiple, random and cumulative process. (After Thomas[12]).

If the surface height histogram follows the Gaussian shape, a plot of the cumulative distribution will be a straight line (Fig. 4.3). But deviation from the Gaussian behavior starts appearing for other creation processes like sanding, milling, or grinding. Therefore, as Fig. 4.3 shows, the curve behavior for other processes is different.

The change in the shape of the cumulative distribution curve can be attributed to two situations; first, that the creation process is not strictly random (independent multiple single events, random and cumulative), and second, that the surface is affected by more than one random process. Those secondary processes such as wear will affect the surface or a stratum of it, adding or destroying the primary surface defined by processes such as etching.

For the more complex case, formative processes can also be a mixture of random and nonrandom processes, some affecting only part of the surface spectrum. Those are called multi-event formative processes.

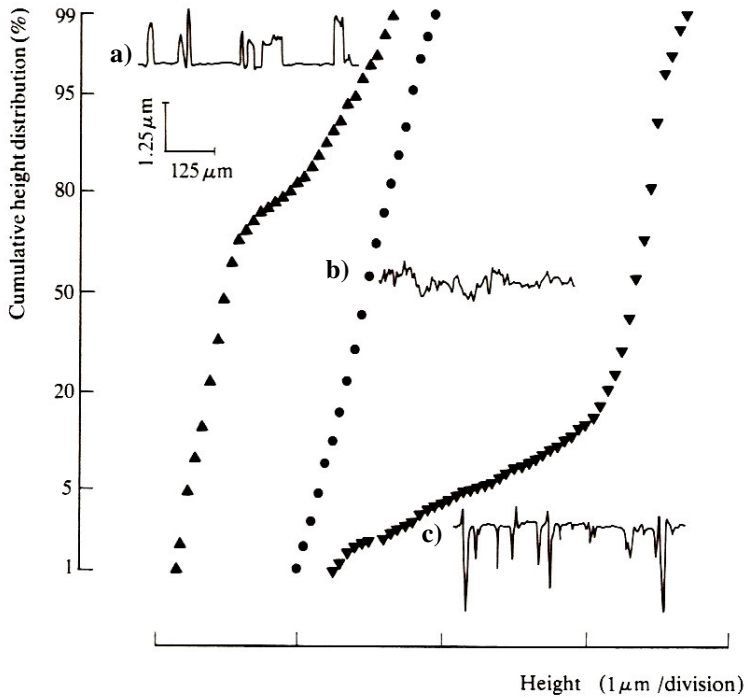

Fig. 4.3.—Cumulative height distribution curve. a) Polished copper etched in ferric chloride. b) Polished copper etched in nitric acid. c) Polished brass etched in ferric chloride. (After Thomas[12]).

4.3. Acid Etching as a Multi-event Formative Process

Surface topography of etched surfaces appears to have an additional complexity to other engineering surfaces, mainly because the formative processes responsible for surface shape have two totally different components, the acid and the surface material. Although in theory the acid attacks the entire surface uniformly, in reality, the dissolution is affected spatially by the original fracture surface topography. Furthermore, the rock features can cause nonrandom dissolution; such features include the type of minerals present and their distribution, micro-structural features, heterogeneities, granules, and pores.

Under this theoretical frame, the combined action of the two intrinsic components (acid and rock) make the acidized surface texture a mixture of formative events that may also change its mechanism dynamically during the extent of the surface dissolution.

This is clearly visible when surface wormholes are analyzed. A wormhole will start growing from a micro-structural feature or heterogeneity that allows its development. But after that first set of random occurrences, older, larger wormholes will take control over the appearance of new ones; so their effect on the surface texture changes with time and destroys part of the simple surface dissolved by acid. This additional process causes the height distribution to be asymmetric and to acquire a gamma distribution shape (Fig. 4.4); that shape is representative of consecutive, rare, random events occurring in a process with no memory.[13]

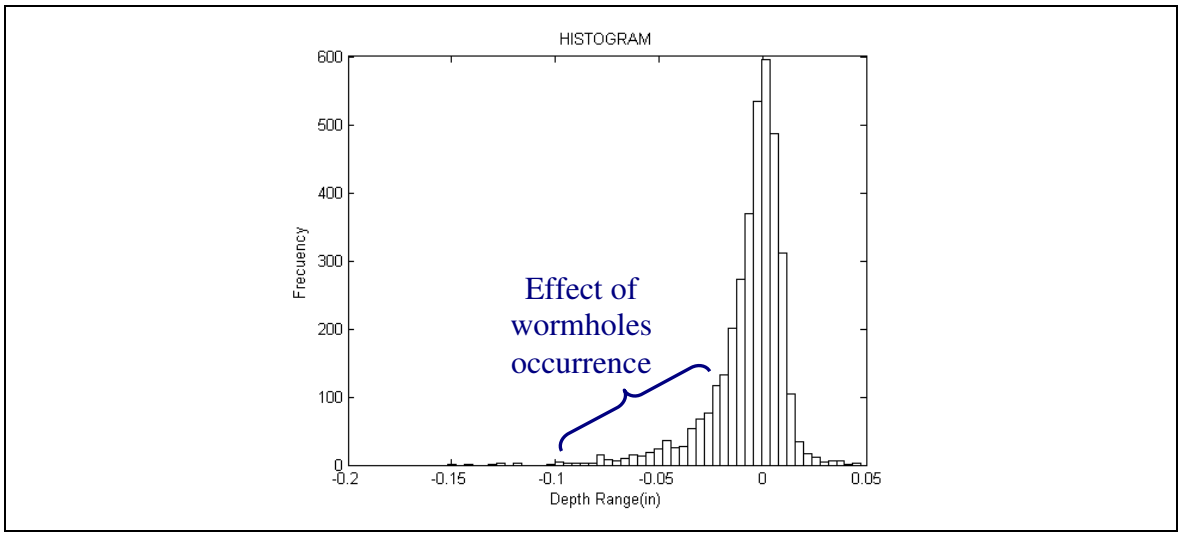

Fig. 4.4—No-symmetric height distribution shape of acidized surfaces.

4.4. Surface Assessment

The main goal of the 3D surface texture assessment is to establish a correspondence between the surface shape and its physical characteristics. Therefore, a measurement of a spatial property has to be expressed in a way that more complicated physical variables (hardness, deformation, thermal or electrical conductance or conductivity) can be deducted. Traditionally, a 2D profile will accomplish this task for the case of standardization or quality control (especially of machined surfaces), but for more complex processes (such as radiation, adherence, fluid flow capacity, deformation, friction) 3D surface measurements are necessary.

The surface assessment is an integrated process that includes three main stages: data acquisition, data pre-processing, and data characterization. Fig. 4.5 presents the surface characterization assessment work flow as proposed by the standard compendium.[11] Notice the three main components: surface data acquisition, pre-processing, and characterization.

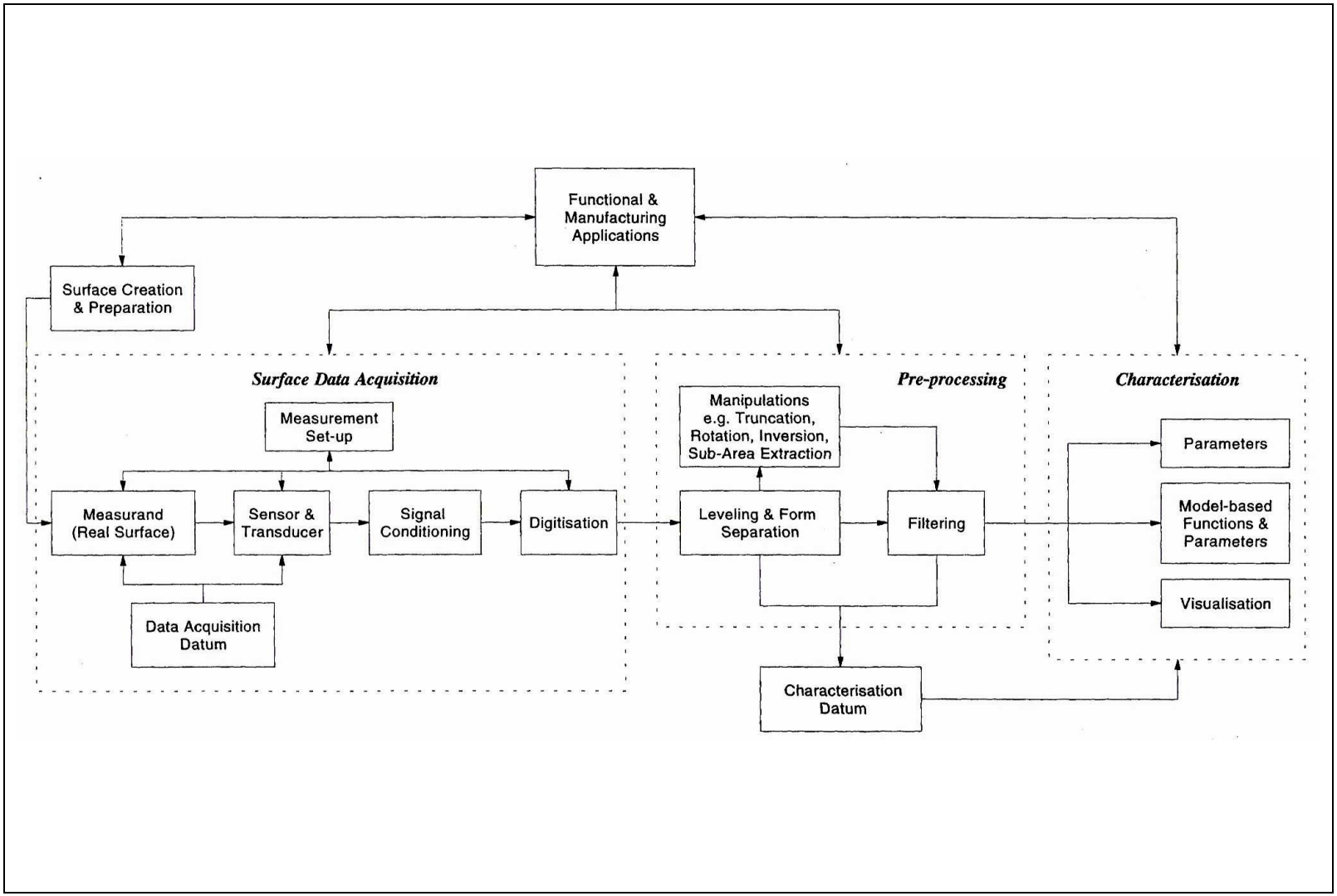

Fig. 4.5—Procedure for 3D surface characterization assessment. (After Stout[11]).

4.4.1. Data Acquisition

Data acquisition starts by establishing the physical set-up; it consist of mounting the rock sample on the servo-table and establishing the sampling dimensions, measurement interval, and the measurement datum on the profilometer software window. Secondarily, the measurement system (profilometer device) is used to measure and record the heights from the laser as a matrix of data.

A detailed explanation of the physical setup is available in the profilometer manual in Appendix A. Special care should be take in maintaining the same laser measurement datum if the same rock sample is scanned before and after acidizing for rock volume loss calculations.

The importance of the measurement intervals lies in the fact that the profile roughness is dependent of the measurement scale. As shown in Fig. 4.6, each small profile section has micro-roughness that continues until molecular dimensions are reached.

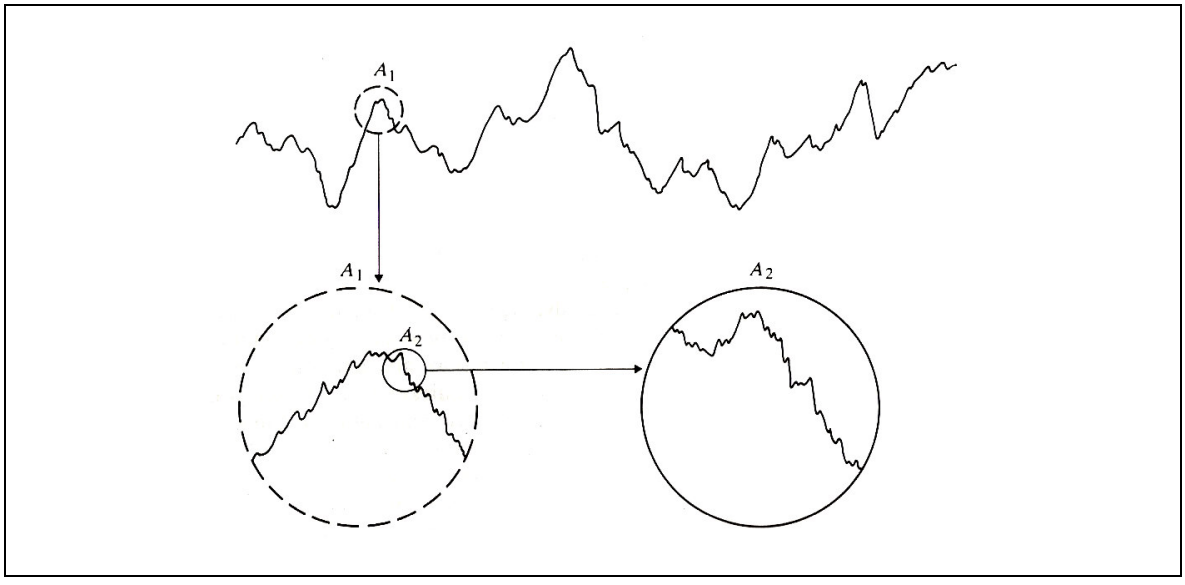

Fig. 4.6—Micro-roughness at smaller measurement intervals. (After Thomas[12]).

Although a fine measurement interval is a better representation of the surface, Fig4.7a shows that exceeding a resolution that allows us to study the process is unnecessary; on the other hand, Fig. 4.7b shows that a large measurement interval will produce a false roughness profile. In this way an optimum resolution should be found to capture the accurate resolution roughness without compromising the scanning time.

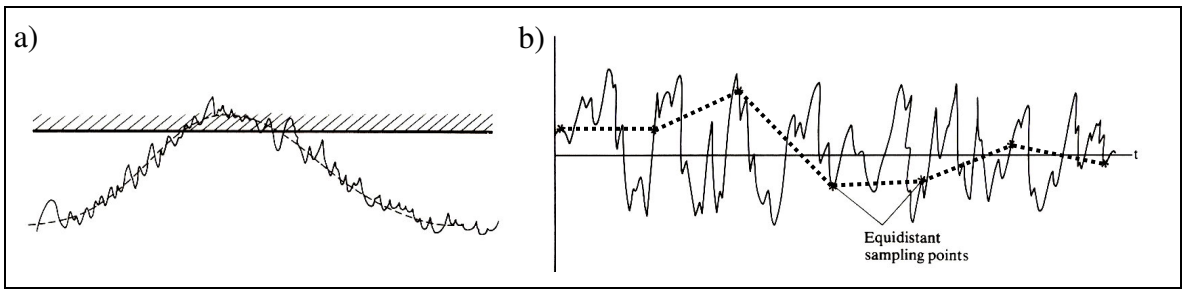

Fig. 4.7—a) The interaction scale of some processes (contact) does not require micro-roughness resolution. b) Large measurement interval fail capturing roughness features. (After Thomas[12]).

All the surfaces presented in this study have a measurement interval of 0.05 in.; that is the profilometer specification resolution. Although increasing the resolution may be desirable to collect more data points for evaluation, the increase in scanning time is unacceptable.

4.4.2. Data Pre-processing

Data pre-processing consists of preparing the data for future analysis. That preparation includes, leveling the raw data to measurement datum, inverting the axes, selecting the evaluation area, and filtering roughness-waviness. This data processing is done using MatLab; the two main steps involved are explained below:

- Convert the text data file from profilometer output to a matrix data file.
  - Level to a determined measurement datum (phase).
  - Invert data from rocks that acidized in inverse direction (by mistake).
- Filter the surface roughness and waviness.

This basic concept of these two steps is explained next; however, a detailed explanation of the MatLab functions used to perform the tasks is presented in Appendix B.

4.4.2.1. Data File Conversion

The profilometer output text file comes in three columns of coordinates (Fig. 4.8); the length of the file corresponds to the number of data points and follows the scanning path. For simple data manipulation, the data is converted to three matrixes of two dimensions ($X_{(i,j)}$, $Y_{(i,j)}$, $Z_{(i,j)}$). In each one, the matrix positions correspond to the number of data points in each direction; and the data itself contains the distance for the case of the X and Y matrixes, and height for the case of the Z matrix. This structure of the Z height matrix allows the calculations between different data sets (i.e. after/before, roughness/waviness), the other two matrixes are used to easily plot the axes of surfaces and profiles.

Fig. 4.9 presents a 3D plot of data in the raw form; notice that the Z direction range is referred to as the laser measurement range (1 in.) and not to any specific datum. Additionally, the corners of the sample are recorded as zero values since the laser falls outside the range. For this reason, the program requests the user to input a datum value, specifically for the case when the rock volume loss is going to be calculated but the "before" and "after" scans do not have the same datum (the laser device was at different static height positions).

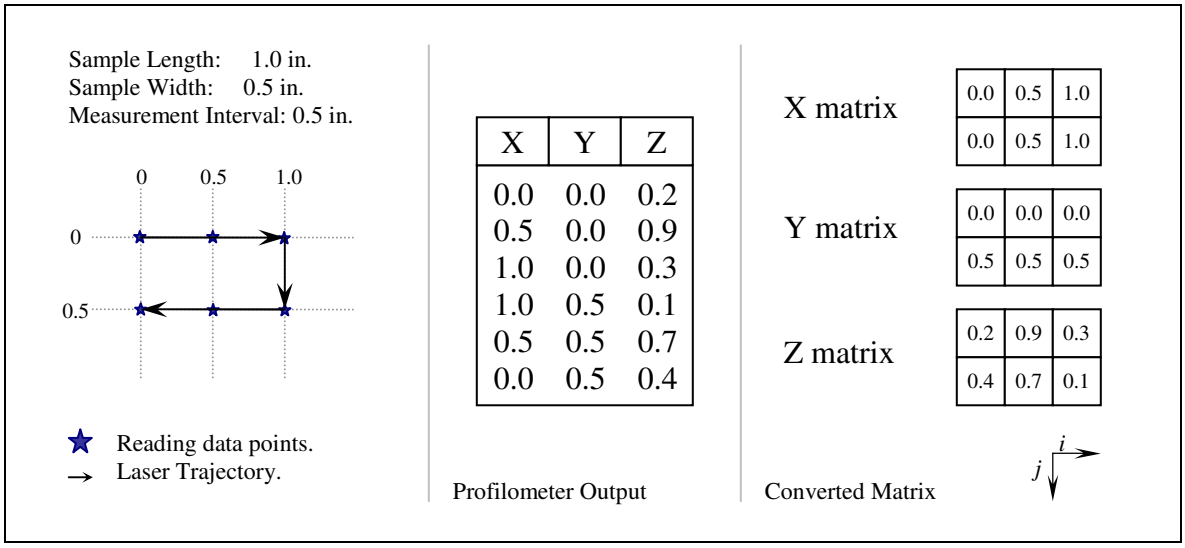

Fig. 4.8—Simplified explanation of data matrix conversion.

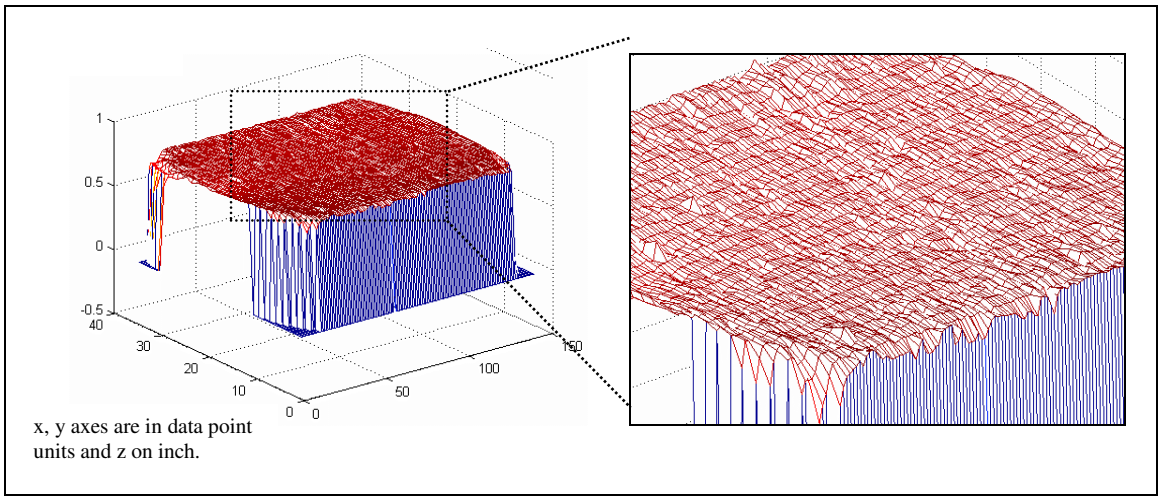

Fig. 4.9—Raw data visualization.

For the case where the sample is acidized or set on the table on the wrong direction, the data processor MatLab program asks the user if the data should be inverted in the Y direction (see Appendix B). Finally, the converted MatLab file saves the three matrixes as well as the sample name, length, width, and measurement interval.

4.4.2.2. Filtering of the Surface Roughness and Waviness

The original texture profile is a summation of two components, waviness and roughness (Fig. 4.10). The roughness is associated with the formative process by itself, while the waviness is associated with other processes[12] like hydrodynamic effects for the case of acidized surfaces. If we assume that a profile is similar to an electrical signal, the roughness corresponds to the small-spectrum wavelengths, and the waviness to the long wavelengths.[14]

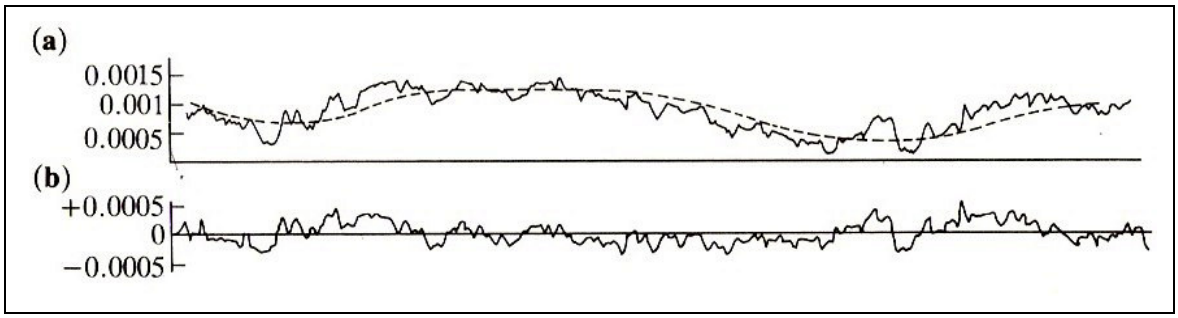

Fig. 4.10—Profile components a) Original profile and its waviness. b) Roughness profile after waviness subtraction. (After Thomas[12]).

Filtering of the data allows separating both components; thus, roughness can be analyzed independently. This is especially important for samples that present a channel like shape at the inlet (Fig. 4.11). On the other hand, the filtering aligns the profile to a mean line that is requirement for most of the characterization parameters. Fig. 4.12 presents the filtered roughness and waviness from the surface presented in Fig. 4.11.

The filtering process is performed according to the ISO Standard[15] (replacement of DIN 4776 proposed by Stout[11]) but using a moving average algorithm instead of the proposed weighted-function Fourier transformation. The filtering process is performed in two dimensions; hence, it is applied to each of the X direction profiles that make the 3D

surface. A detailed explanation is presented next; however, a detailed explanation of the calculations algorithms is available in Appendix B.

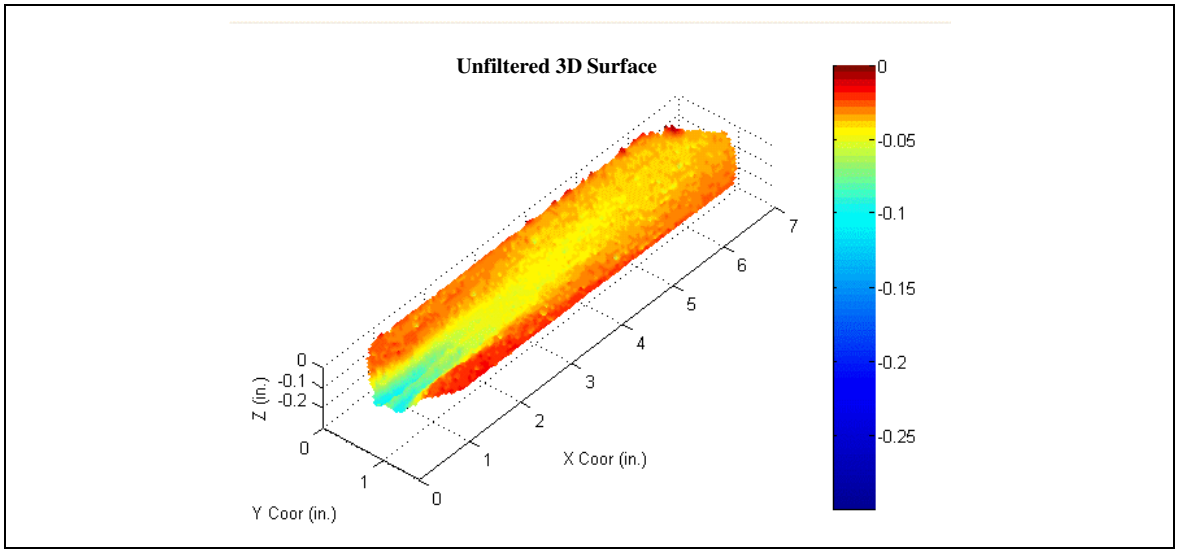

Fig. 4.11—Unfiltered surface with hydrodynamic channel (light blue).

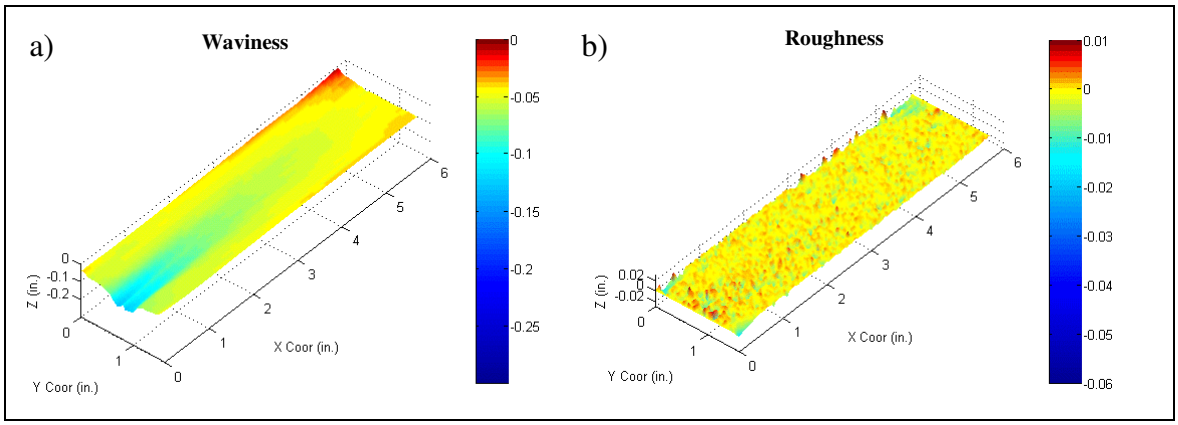

Fig. 4.12—a) Waviness surface after filtering. b) Roughness surface after filter, notice that the surface is leveled to zero.

The basic filter principle is to find the profile mean line and subtract it from the profile to eliminate the waviness. That mean line is calculated at each data point as the average

among the point, the next, and the previous data point. This process can be repeated until the mean-line profile follows the waviness of the original profile.

Because most of the acidized profiles have valleys caused by the wormholes, the ISO Standard proposes to calculate the mean line, suppress the data points that fall below that line, and calculate a second mean line over the remaining profile; that second mean line is finally subtracted from the original profile to obtain the filtered roughness profile (Fig. 4.13). Although the difference between the first and second mean line seems to be small, if the filter is made using only the first mean line, the filtered profile will exhibit exaggerately high values for the data points next to the valleys.

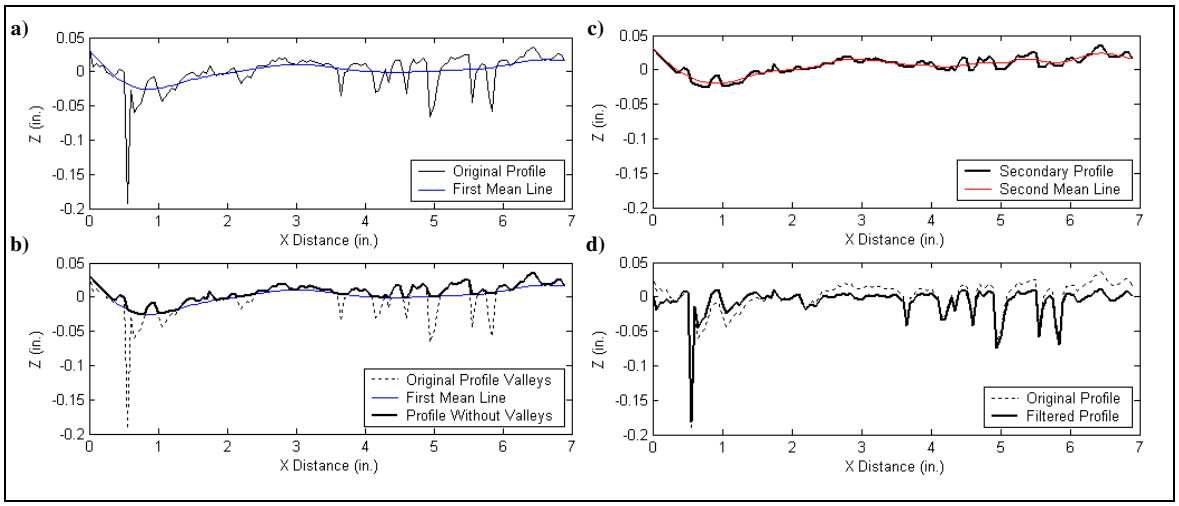

Fig. 4.13—ISO Standard 13565 Filtering. a) Calculation of the first mean line over the original profile. b) Suppression of the profile data points below the first mean line. c) Second mean line calculated over the remaining profile. d) Filtered profile after subtraction of second mean line.

Since the filter process separates the long wavelengths of the profile, it can not be used when a big channel is the main characteristic of the acidized surface (Fig. 4.14). For that

case, the waviness surface keeps the channel features, and the roughness surface exhibits the roughness inside and outside of the channel (Fig. 4.15).

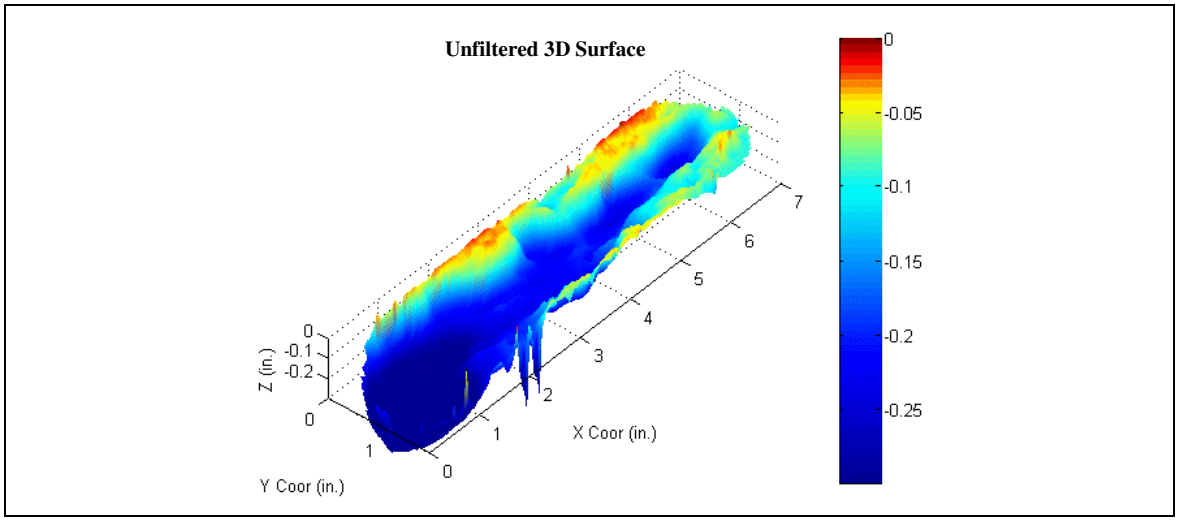

Fig. 4.14—3D surface with major channel as main characteristic.

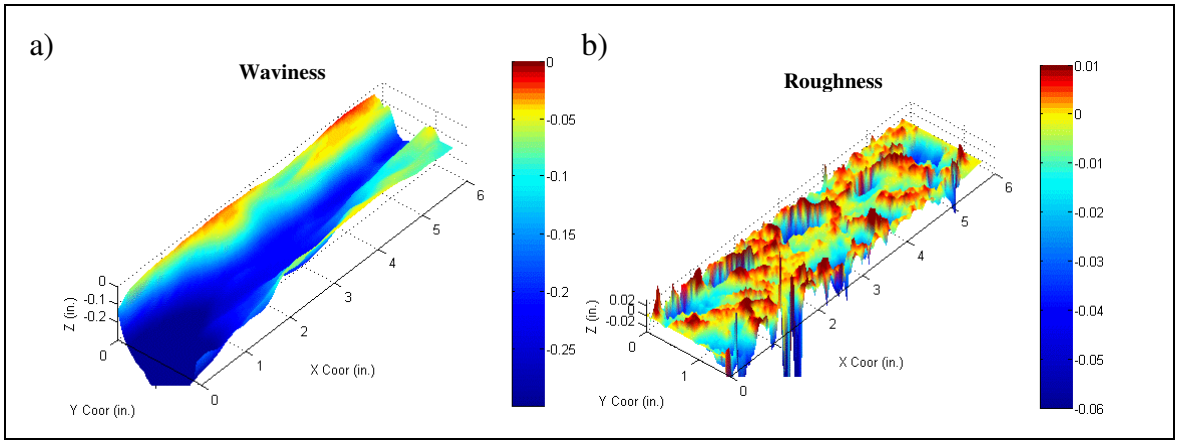

Fig. 4.15—Filter of Fig. 4.14. a) Waviness surface after filtering keeps the shape of the channel. b) Roughness surface after filter destroys the channel features (notice the color scale).

Because profile filtering must have sound characterization parameters but will eliminate channel features, the filter should be used when the roughness (small wavelengths) is the main object of study and precise characterization values are desired, as in modeling.

In contrast, the original surface (no filter) should be used when the channel features need to be preserved and to correlate the surface with the laboratory experiment conductivity measurements. For that instance, the characterization parameters should be used carefully and only for qualitative proposes.

4.4.3. Data Characterization

As explained before, surface characterization has two goals: to provide ways to understand the surface, and to supply parameters for modeling (i.e. conductivity prediction). Fig. 4.16 presents a classification of the actual characterization techniques.

Three techniques have been selected from the proposed characterization techniques from the 3D characterization compendium.[11] The first is the use of 3D visualization and 2D profiles; second, the statistical characterization by calculation of amplitude parameters; and third, the use of hybrid and functional parameters. A summary of the parameters is presented in Table 4.1.

The other techniques were considered but not selected for various reasons. All of them are mathematically complex, some are still under development and the available literature is limited. Secondly, the output of the techniques is also complex and difficult to relate to the physical and functional meaning. Third, some techniques are dedicated to the study of machined surfaces with periodic features; that is not the case for acid dissolution. Explanation of those techniques, usage, and weaknesses are available in the Stout compendium.[11]

Fractal characterization was also considered, but two main constraints prohibited its use. First, although the wormholes can be described under fractal geometry theory, the laser is not able to capture their internal shape; as a result, the acquired data only represents the surface that can be measured by the vertical laser beam. Additionally, the lower resolution dataset does not allow satisfy the fractal basic requirement of recognizing self-similarity; that is, every segment of the curve should be indistinguishable from the entire surface.[16] Secondarily, assuming that the first can be neglected, since the acidizing is a multi-event process, it requires the use of at least two fractal signatures, but that development is theoretically complex.

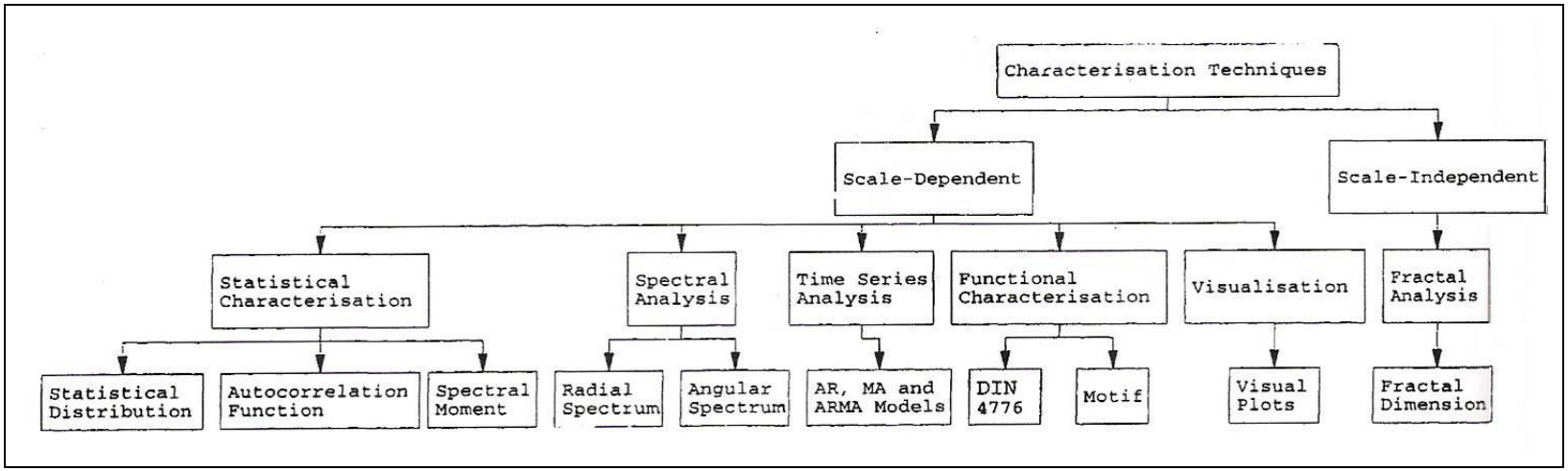

Fig. 4.16—Classification of the characterization techniques. (After Stout[11]).

Table 4.1—Applied characterization techniques.

	TECHNIQUE	PARAMETER
1	**Visualization**	Unfiltered color 3D surface Z inverted gray 3D surface Filtered color 3D surface Longitudinal and transversal cross-section plot
2	**Statistical (Amplitude)**	(S_a) Arithmetic Mean Deviation (Sq) Root-Mean-Square Deviation (S_z) Ten Point Height (S_{sk}) Skewness Height Distribution (S_{ku}) Kurtosis Height Distribution
3	**Hybrid**	($S_{\Delta q}$) RMS Slope (S_{dr}) Developed Area Ratio
	Functional	(S_c) Core Roughness depth from the material Ratio Curve

4.4.3.1. Visualization

The objective of the visualization technique is to allow the human eye to visualize features that are not visible at normal conditions. This can be achieved by the use of colors, different views, and scale increments. This project uses four techniques:

Unfiltered Color 3D Surface. This is an isometric plot of the original image from the profilometer with the shape of the original sample. The image is rotated 50° and inclined to an angle of 40°; the Z scale is amplified 3 times. The color bar represents height and it has been modified to be logarithmic in color so more contrast can be seen at small sizes close to the zero point. The color bar starts from zero and goes to -0.3 in. (Fig. 4.11).

Z Inverted Gray 3D Surface. The purpose of this image is allow a better visualization of the topographic valleys since those are an important characteristic of the acidized surfaces. For this purpose, the data is inverted in the Z direction and the color bar is a black-to-gray linear scale (Fig. 4.17).

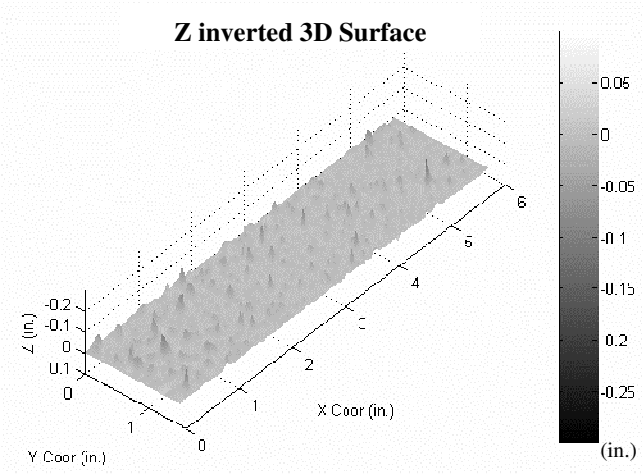

Fig. 4.17—Inverted 3D gray surface visualization technique

Filtered Color 3D Surface. This plot shows the roughness of the surface after filtering. It has the same setting as the unfiltered plot but the Z scale is increased 10 times, and the color bar is logarithmic from 0.1 to -0.6 in. (Fig. 4.12b).

Longitudinal and Transversal Cross-Section Plot. Two cross-section plots are generated, one each longitudinal and transversal directions. The longitudinal plot has three profiles at 1/4, 1/2, and 3/4 of the surface width; the transversal section has four profiles at 1/5, 2/5, 3/5, and 4/5 of the surface length. The plots purpose is to visualize clearly the change in topography at determined distances (Fig. 4.18).

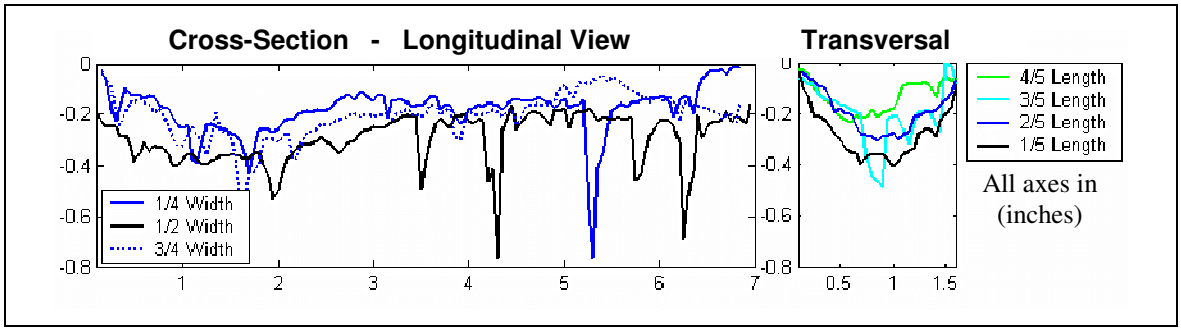

Fig. 4.18—Cross-section plot visualization technique.

4.4.3.2. Amplitude Property

A digital profile can be defined as a set of data points located in space. The data distribution, grouped by height, corresponds to an inverted axis histogram (Fig. 4.19). The shape of that height distribution is representative of the profile characteristics (Fig. 4.20) and can be described using statistical parameters such as dispersion, extremes, asymmetry, and peakedness.

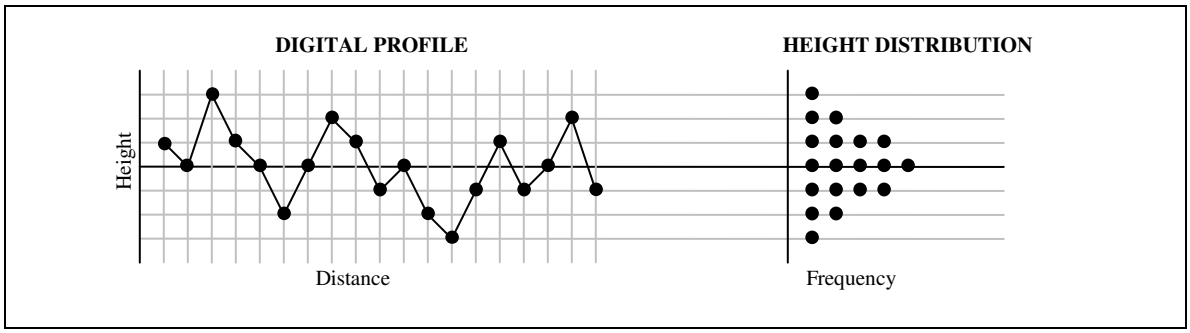

Fig. 4.19—Profile digital data represented as a height distribution.

The digital 3D data is evaluated as a Z(x,y) 2D height matrix where *M* is the number of rows and *N* the number of columns, and Δx and Δy the measurement interval.

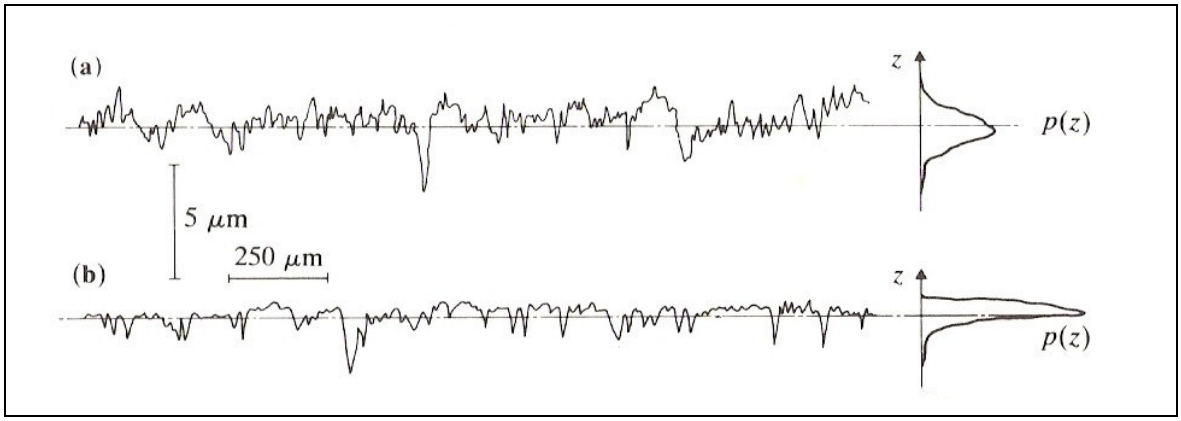

Fig. 4.20—The height distribution curve as profile descriptor. (After Thomas[12]).

Arithmetic Mean Deviation (S_a). Since the surface has been normalized to a mean plane during the prepossessing, this measurement gives the absolute value above and below the mean plane; it is calculated using Eq. 4.1;

$$S_a = \frac{1}{MN}\sum_{j=1}^{N}\sum_{i=1}^{M} Z_{(x_i,y_j)} \cdot \quad \text{.....(4.1)}$$

Root-Mean-Square Deviation (S_q). This is the measurement of the data dispersion from the mean line, it is equivalent to the statistics standard deviation and is calculated using Eq. 4.2;

$$S_q = \sqrt{\frac{1}{MN}\sum_{j=1}^{N}\sum_{i=1}^{M} Z^2_{(x_i,y_j)}} \cdot \quad \text{.....(4.2)}$$

Ten-Point Height (S_z). This is a measurement of the extreme values; it uses the five highest surface summits and the five lowest surface valleys.

$$S_z = \frac{\sum_{i=1}^{5}\left|Z_{pi}\right| + \sum_{i=1}^{5}\left|Z_{vi}\right|}{5} \quad \text{.} \quad \text{.....(4.3)}$$

Skewness Height Distribution (S_{sk}). This is the measurement of asymmetry of the data to each side of the mean line (Fig. 4.21a); it is calculated by Eq. 4.4;

$$S_{sk} = \frac{1}{MNS_q^3}\sum_{j=1}^{N}\sum_{i=1}^{M} Z^3_{(x_i, y_j)} \quad \text{.} \quad \text{.....(4.4)}$$

Kurtosis Height Distribution (S_{ku}). This is the surface height distribution measurement for peakedness or sharpness (Fig. 4.21b); calculated by Eq. 4.5;

$$S_{ku} = \frac{1}{MNS_q^4}\sum_{j=1}^{N}\sum_{i=1}^{M} Z^4_{(x_i, y_j)} \quad \text{.} \quad \text{.....(4.5)}$$

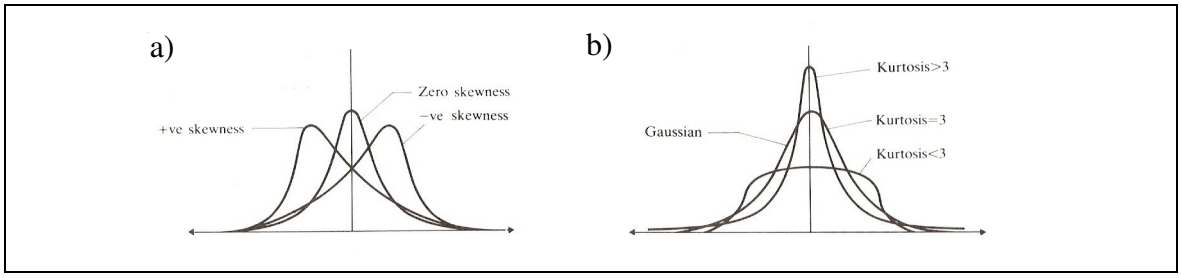

Fig. 4.21—Skewness and kurtosis as distribution shape descriptors. (After Thomas[12]).

4.4.3.3. Hybrid Property

The amplitude parameters can describe the shape of the height distribution, but that distribution can be assigned to totally different profiles, since if does not consider the

spatial (distance) interrelation of the data points (Fig. 4.22). For this reason the hybrid parameters are a combination of amplitude and space. Therefore, they vary with the amplitude changes but they are affected by the sampling interval.

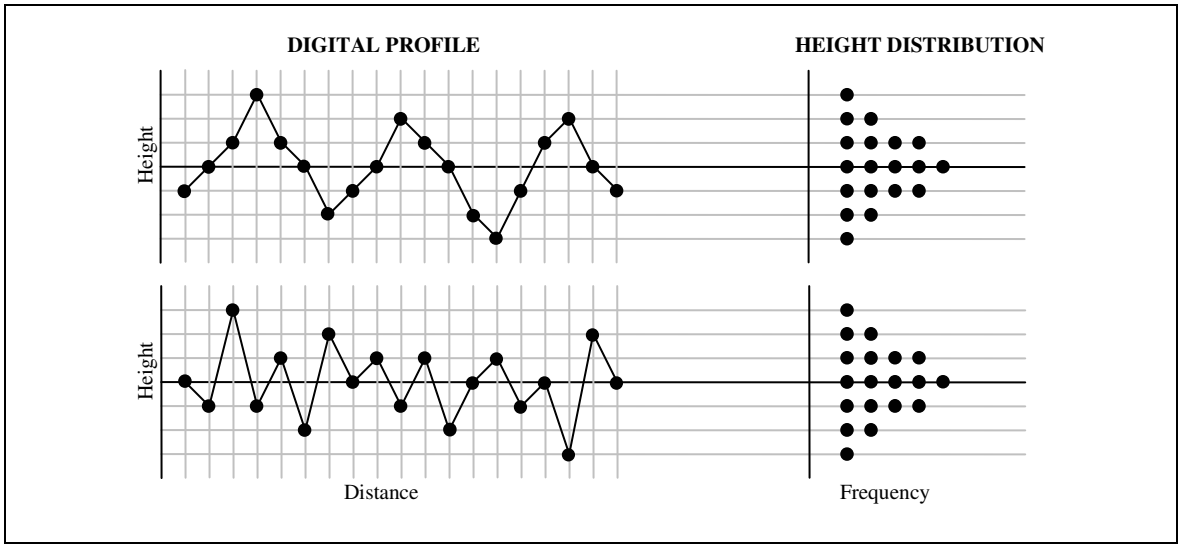

Fig. 4.22—Different profiles can exhibit same height distribution.

RMS Slope ($S_{\Delta q}$). This is the root-mean-square value of the surface slopes in between data points and along the entire sampling area. It is calculated using Eq. 4.6;

$$S_{\Delta q} = \sqrt{\frac{1}{(M-1)(N-1)} \sum_{j=2}^{N} \sum_{i=2}^{M} \left[\left(\frac{Z_{(x_i, y_j)} - Z_{(x_i-1, y_j)}}{\Delta x} \right)^2 + \left(\frac{Z_{(x_i, y_j)} - Z_{(x_i, y_j-1)}}{\Delta y} \right)^2 \right]} \quad \text{.....(4.6)}$$

Developed Area Ratio (S_d). The developed area parameter measures the increment of the area over the assumed flat surface. It is calculated using Eqs. 4.7 through 4.9;

$$A_{ij} = \frac{1}{4}\left(\left[\Delta y^2 + \left(Z_{(x_i, y_j)} - Z_{(x_i, y_j+1)} \right)^2 \right]^{1/2} + \left[\Delta y^2 + \left(Z_{(x_i+1, y_j+1)} - Z_{(x_i+1, y_j)} \right)^2 \right]^{1/2} \right) \bullet$$

$$\frac{1}{4}\left(\left[\Delta x^2 + \left(Z_{(x_i, y_j)} - Z_{(x_i+1, y_j)} \right)^2 \right]^{1/2} + \left[\Delta x^2 + \left(Z_{(x_i, y_j+1)} - Z_{(x_i+1, y_j+1)} \right)^2 \right]^{1/2} \right). \quad \text{.....(4.7)}$$

$$A = \sum_{j=1}^{N-1}\sum_{i=1}^{M-1} A_{ij} \,. \quad \text{.....(4.8)}$$

$$S_{dr} = \frac{A - (M-1)(N-1)\Delta x \Delta y}{(M-1)(N-1)\Delta x \Delta y} \cdot 100\% \,. \quad \text{.....(4.9)}$$

4.4.3.4. Material Ratio Curve

The material ratio curve describes topographic features that are related to some specific physical behavior. The material ratio curve is the cumulative distribution curve of the height distribution curve and its calculation is explained in Appendix B (Fig. 4.23a).

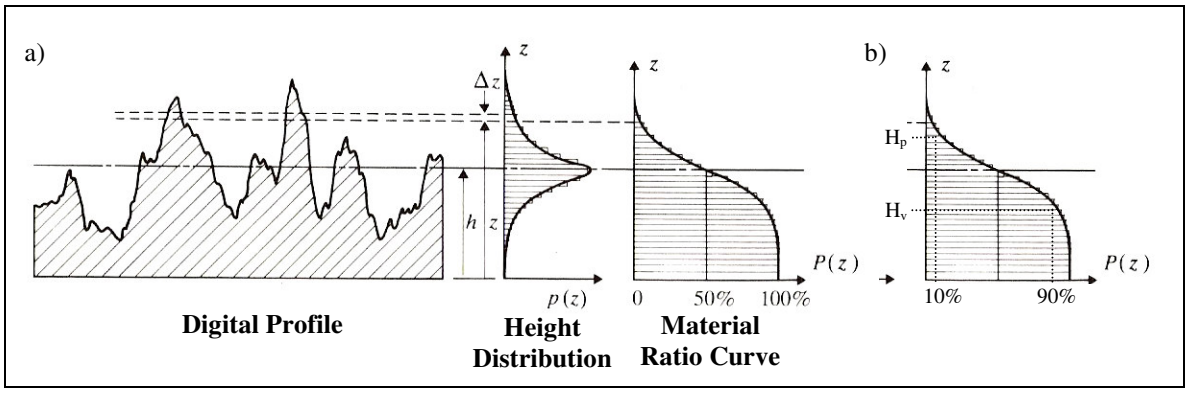

Fig. 4.23—Material ratio curve. a) Origin of the curve. b) MRC Hp and Hv. (Modified from Thomas[12]).

The ISO 13565-2 Standard[17] indicates how to geometrically obtain several parameters to describe the curve. Those parameters depend upon the amount of material below the curve at determined percentages. Nevertheless, we propose the use of a single modified parameter, S_c explained below.

Core Roughness Depth (S_c). Considering H_p and H_v as the heights where the material ratio curve corresponds to the 10% and 90% of the material, the core roughness depth is calculated as the difference between H_p and H_v (Fig. 4.23b). This parameter accounts for the core roughness profile that excludes the protruding peak and deep valleys of the material ratio curve.

Volumetric. This technique simply consists of calculating the volume of rock dissolved. It is calculated over the matrix resulting from the subtraction of the "after" and "before" measurements (Z') not over the filtered Z matrix.

$$V_R = \sum_{j=1}^{N-1} \sum_{i=1}^{M-1} Z'_{(x_i, y_j)} \Delta x \Delta y \,. \quad \text{.....(4.10)}$$

5. TEXTURE OF ACIDIZED SURFACES

5.1. Experimental Work Summary

We performed eight sets of experiments, all of them having three different contact times except for the Experiments 4 and 8, for a total of 21 pairs of rocks acidized. The rocks were limestone, dolomite, and two types of chalk. Four different fluids were used. Table 5.1 presents a summary of the nine experiments and their treatment conditions.

The acid fluids used include straight acid, emulsified acid, gelled acid, and viscoelastic surfactant acid. The emulsified acid is an oil external emulsion stabilized with an emulsifier. The gelled acid is simply a straight acid with a gelling agent. The viscoelastic surfactant acid is a self-diverting acid system in which the acid viscosifies in-situ, blocking dominant wormholes.

5.2. Experimental Surfaces Characterization

This section presents the 3D images and the characterization parameters obtained for the complete set of experiments presented in Table 5.1. Since both sides of the rock exhibit the same etching pattern, the results are presented for only one of the rock faces. Nevertheless, the pictures of the rock samples for each experiment can be seen in Appendix C.

Table 5.1—Summary of experiments.

Exp. #	Fluid & Rock	Temperature (°F)	Leak-off Rate (ft/min)	Contact Time (min))
1	Emulsified Acid Limestone	200	0.005	15
				30
				60
2	Emulsified Acid Limestone	275	0.005	15
				30
				60
3	Gelled Acid Limestone	200	0.005	15
				30
				60
4	Gelled Acid Limestone	200	0.010	15
				30
5	Self-Diverting Viscoelastic Limestone	200	0.003	15
				30
				60
6	Self-Diverting Viscoelastic Dolomite	200	0.005	10
				20
				30
7	Straight Acid 7% North Sea Chalk	100	0.005	3
				5
				7
8	Straight Acid 7% North Sea Chalk II	100	0.005	7

5.2.1. Experiment 1: Emulsified Acid and Limestone, 200°F, 0.005 ft/min.

Figures 5.1, 5.2 and 5.3 show the visualization results for the experiment 1 (Table 5.1); the figures present, for each contact time, the 3D unfiltered surface, the 3D view of valleys and the 3D view of the filtered roughness.

Fig. 5.3 shows that the acid dissolves more rock at longer contact time since the surface color falls on the blue spectrum of the color scale. Fig. 5.4 also shows the plot of the volume loss for each contact time. The gray surfaces in Fig. 5.3 indicate that the wormhole development starts appearing at 60 min. Even though, the surfaces do not show any important roughness increase until 60 min., small wormholes begin to appear before then. This behavior is the result of the emulsified system that acts as an acid retardant.

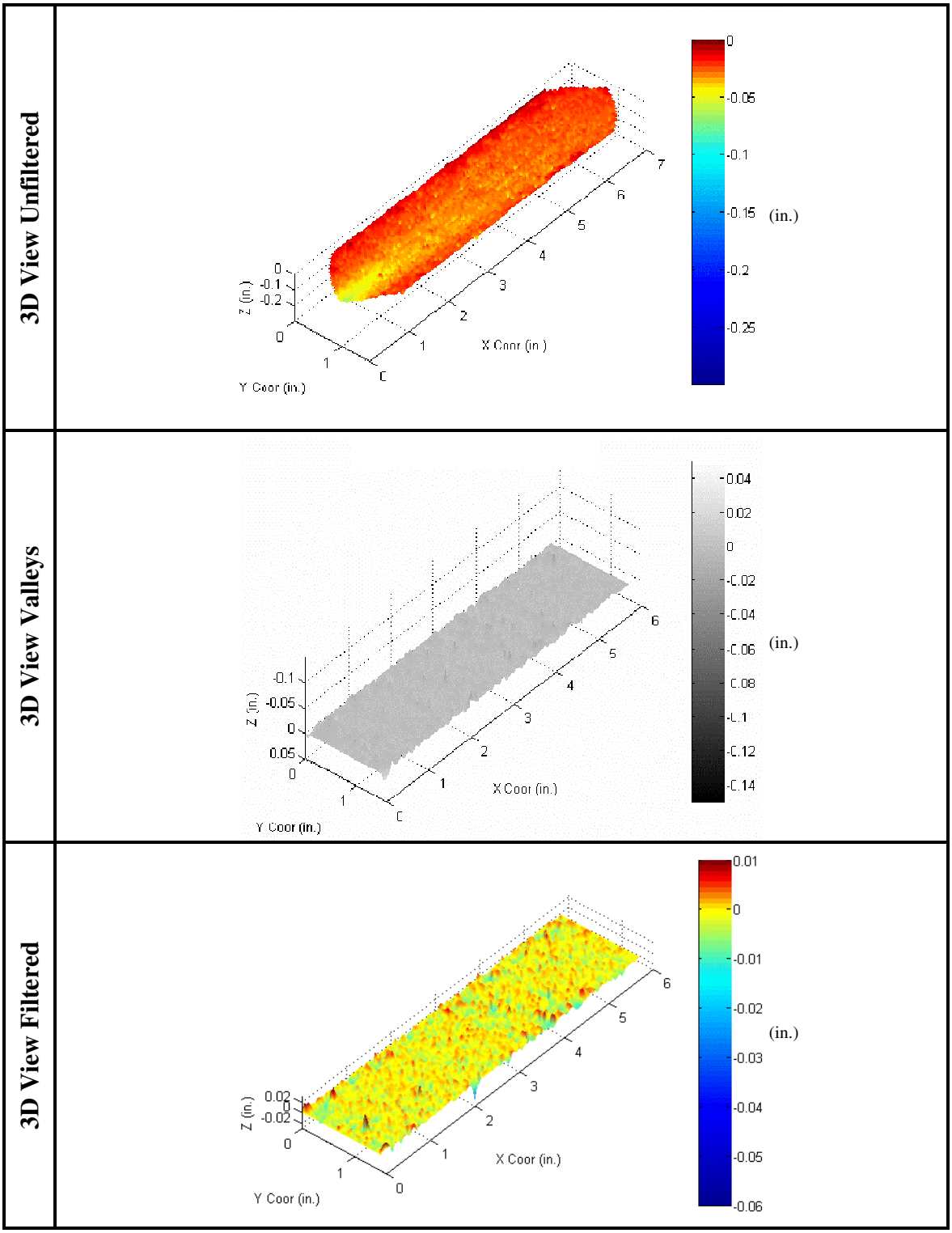

Fig. 5.1—Exp. 1: Visualization 3D surfaces of emulsified acid and limestone—200 °F, 0.005 ft/min., 15 min.

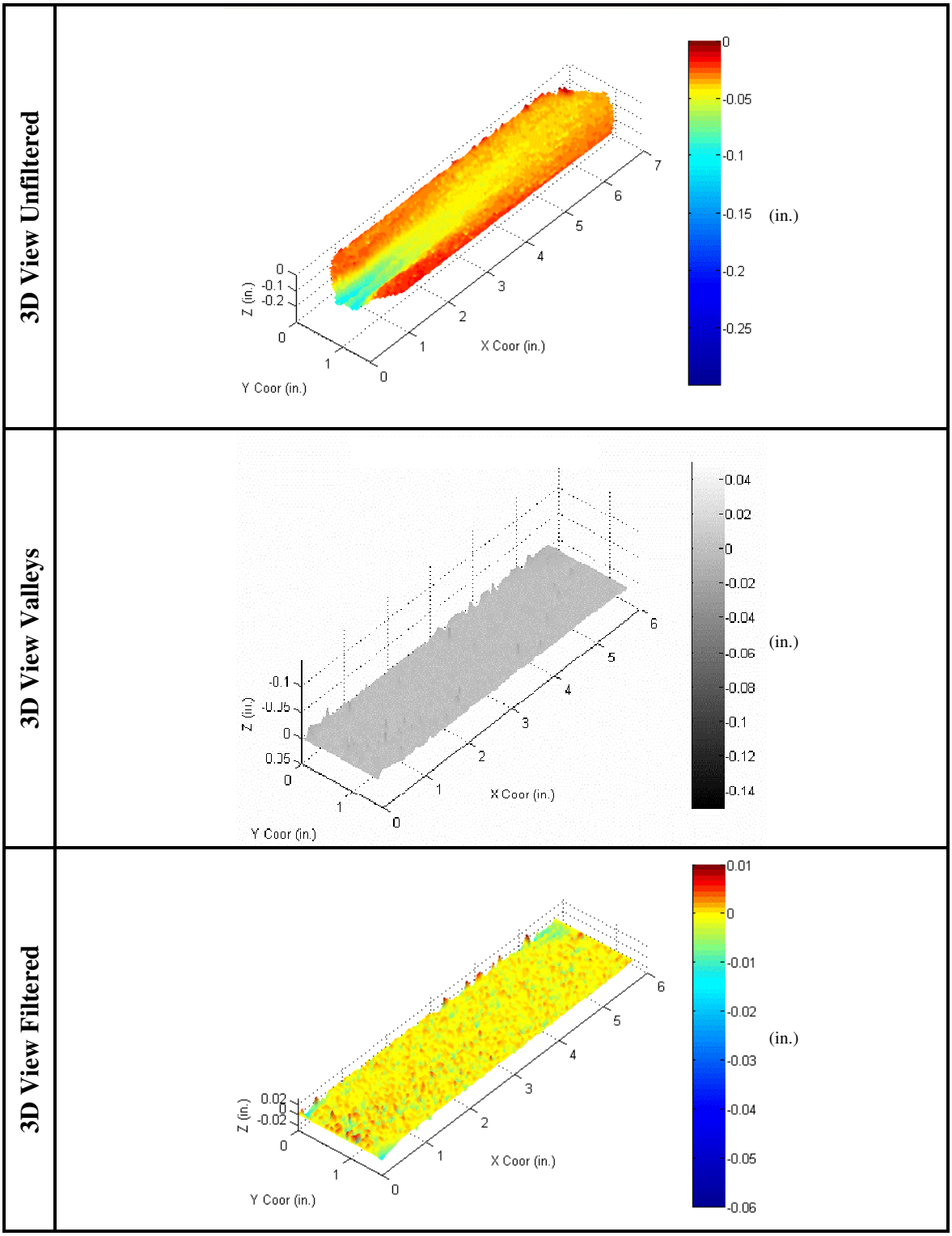

Fig. 5.2—Exp. 1: Visualization 3D surfaces of emulsified acid and limestone—200 °F, 0.005 ft/min., 30 min.

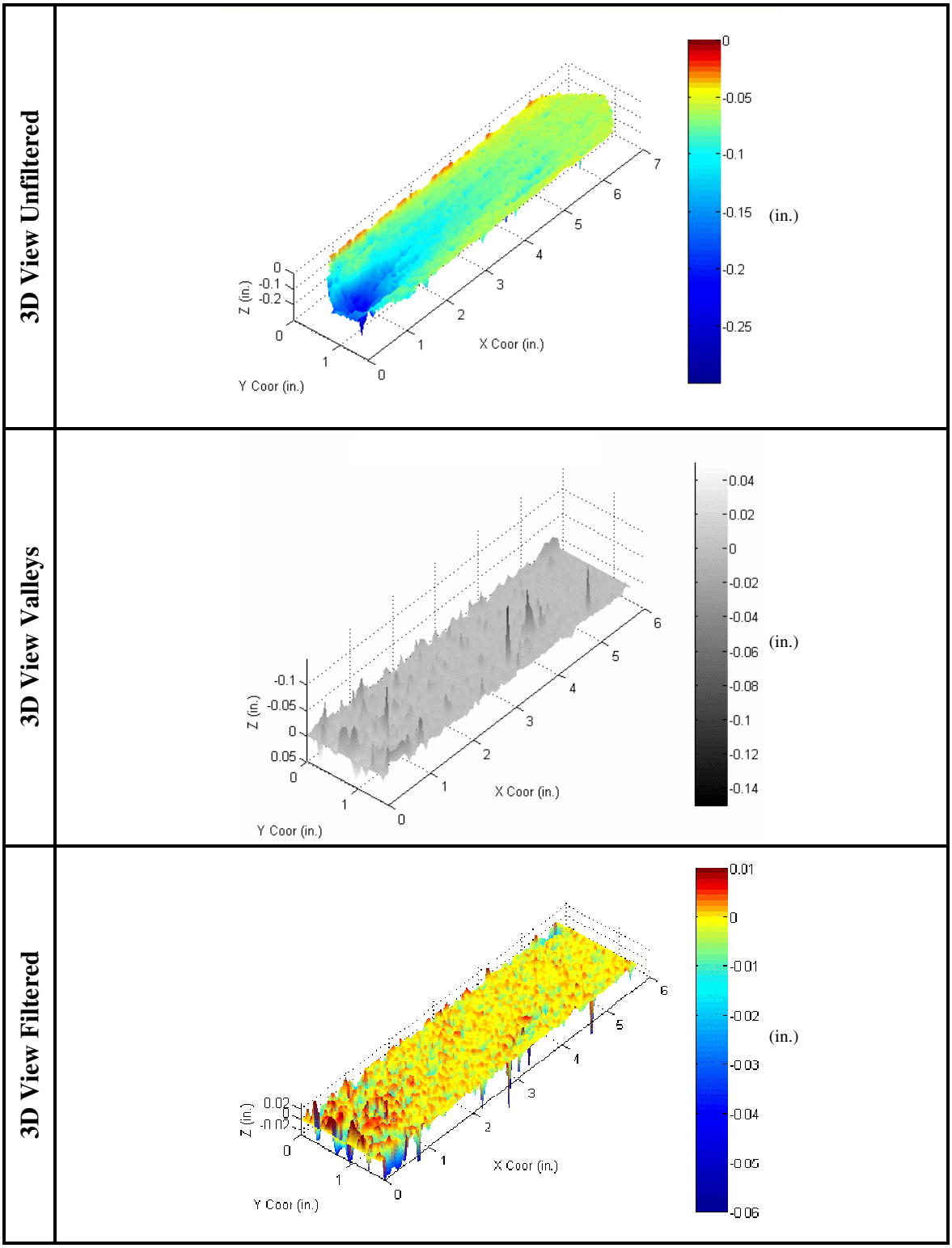

Fig. 5.3—Exp. 1: Visualization 3D surfaces of emulsified acid and limestone—200 °F, 0.005 ft/min., 60 min.

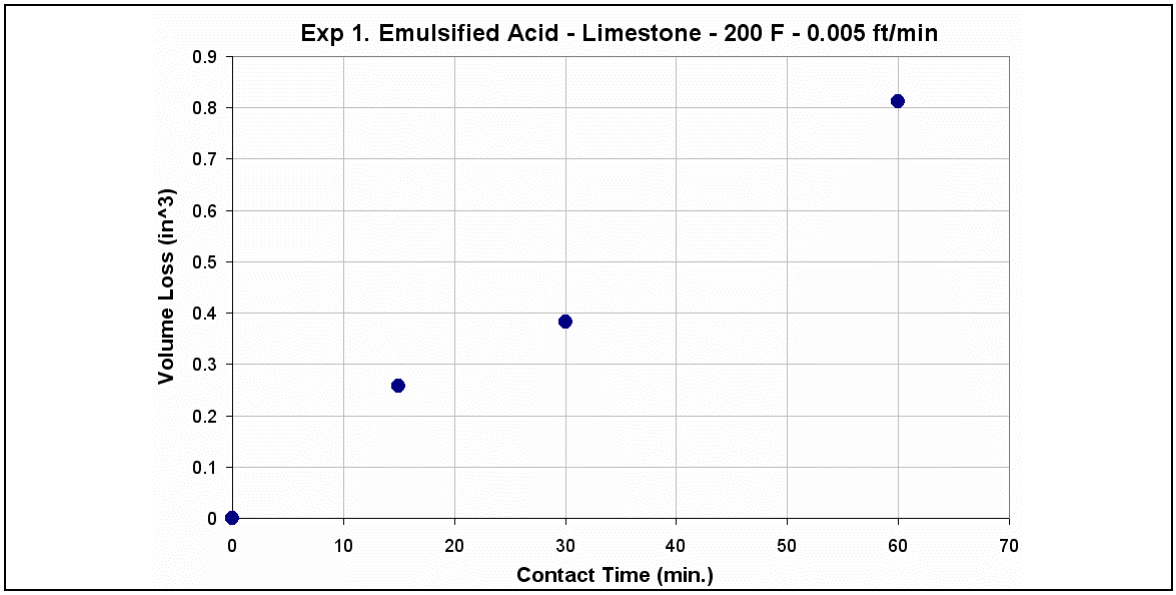

Fig. 5.4—Exp. 1—Volume of rock dissolved on rock surface.

Fig. 5.5 presents the profiles for each contact time experiment. It clearly shows how a hydrodynamic effect occurs at the inlet of the cell; the black line on the longitudinal cross-section plots shows the gradual dissolution from the inlet (left side). Fig. 5.6 presents the comparative profile development for the three experiments showing how the rock gradually dissolves along the entire surface. This central plot illustrates the inlet channel that may affect the conductivity measurement. Fig. 5.7 compares roughness profiles for the experiment. The amount of roughness created at each contact time shows how little the roughness increases, as even at 60 min. the rock roughness is still slightly higher than for lower contact times.

The roughness change can be better understood by looking of Fig. 5.8, which presents the roughness parameters for the experiment. The different parameters have been grouped on three plots because the magnitude of its values does not allow them to be combined in one single plot. The values of all those parameters are low for the entire set of values obtained for the 21 experiments.

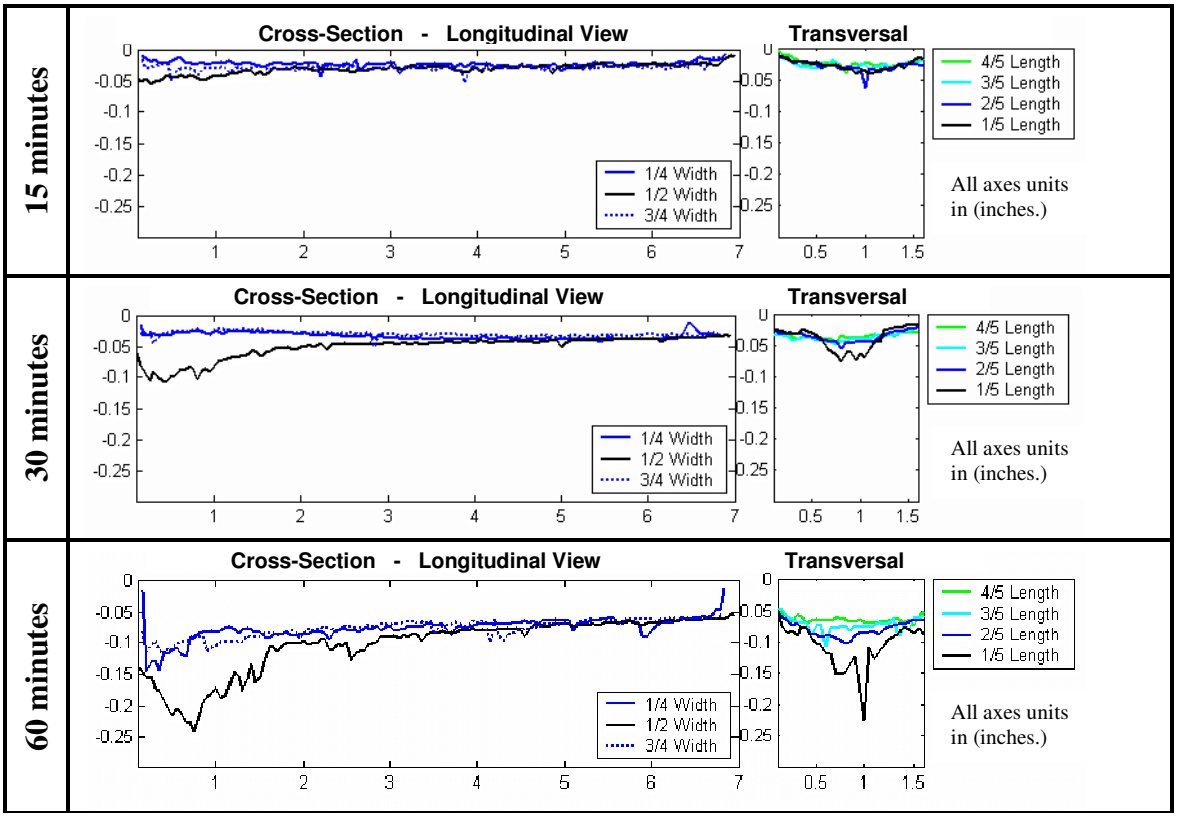

Fig. 5.5—Exp. 1—Longitudinal and transversal cross-section profiles.

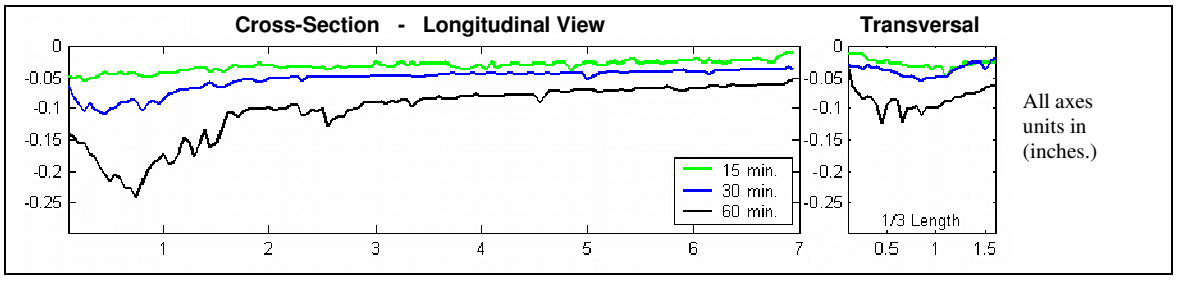

Fig. 5.6—Exp. 1—Comparative cross-section profile.

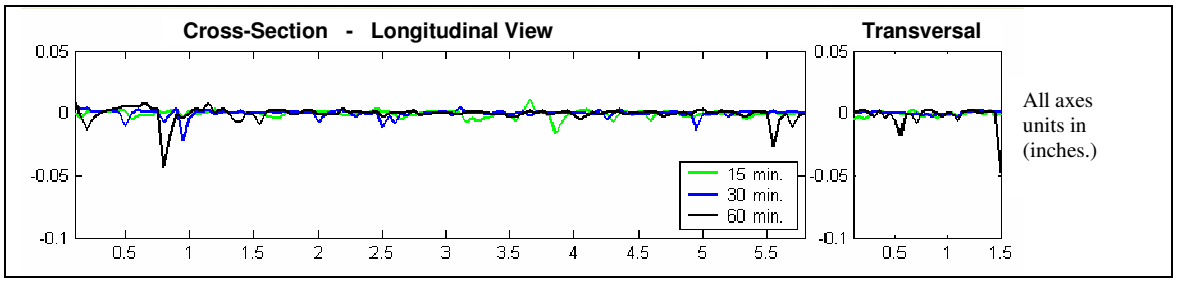

Fig. 5.7—Exp. 1—Comparative roughness cross-section profile.

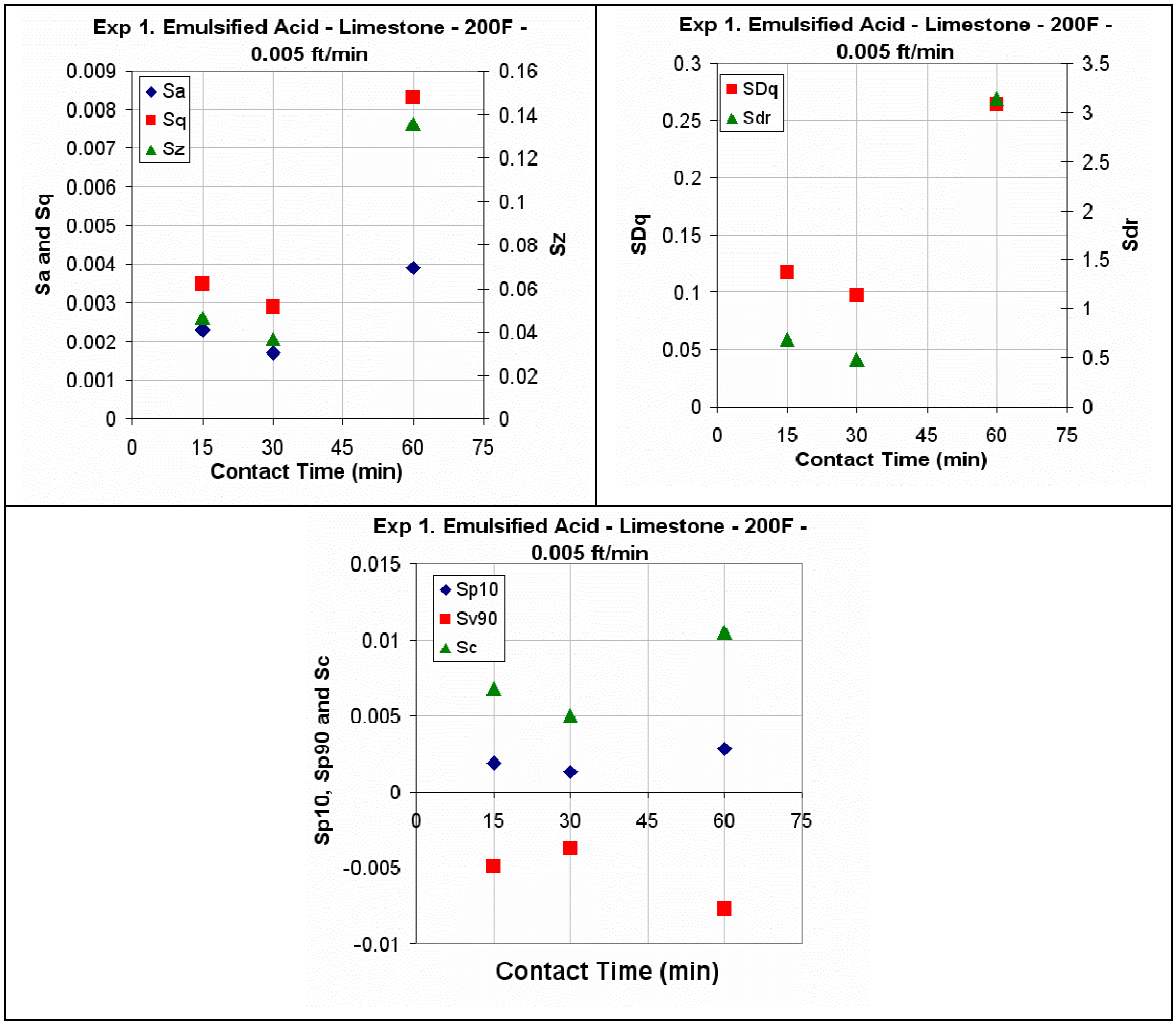

Fig. 5.8—Exp. 1—Roughness parameters.

Fig. 5.9 compares the roughness material ratio curve for the three experiments; the small change in the roughness can be seen since all the curves overlap along the entire curve; notice that the 60-min. test deviates after 90% because of the small wormholes.

The conductivity measurements (Fig. 5.10) show that the 60-min. rock has very low conductivity from the beginning of the measurement; it is also barely affected by the increasing load. The 30-min. rock starts with higher conductivity than the 15-min.

sample; this is not surprising since it has a hydrodynamic channel that may increase the conductivity readings, but the 30-min. rock loses conductivity faster with load.

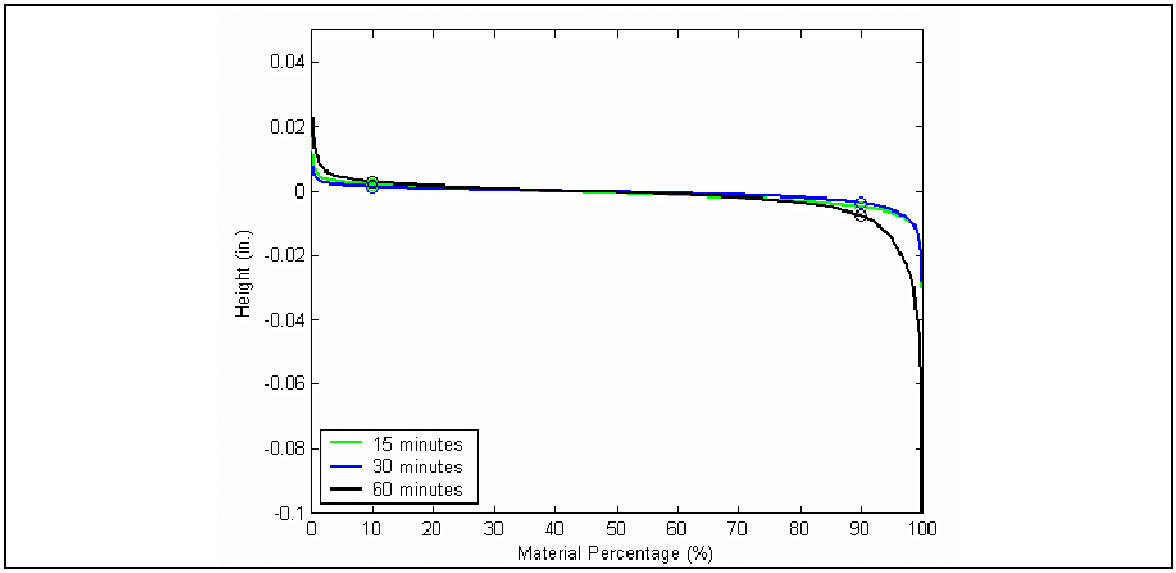

Fig. 5.9—Exp. 1—Roughness comparison of material ratio curves.

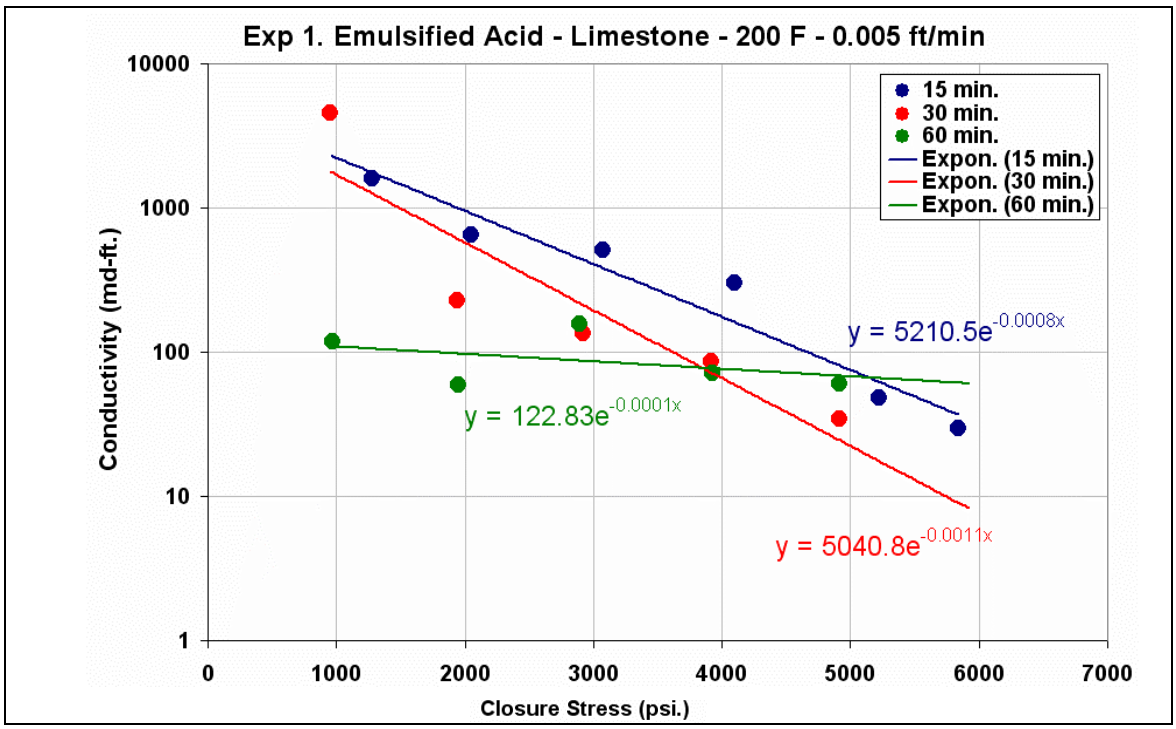

Fig. 5.10—Exp.1—Conductivity measurements.

The filtered waviness of the samples shows that the degree of empty space increases with contact time (Fig. 5.11). The same characteristic can be seen on the material ratio curve for the original data set (Fig. 5.12) where the surface core parameter S_c is higher for the 60-min. rock.

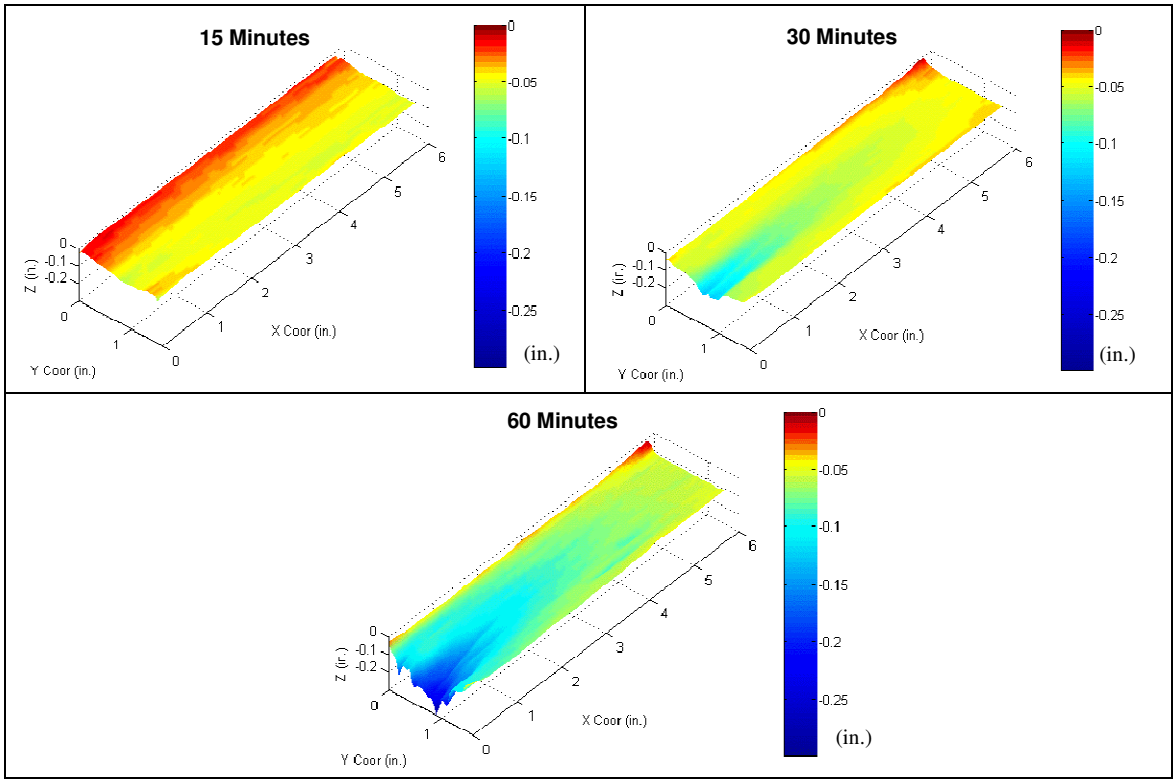

Fig. 5.11—Exp. 1—Waviness 3D surface views.

The roughness parameters reveal that the roughness of the surfaces is small and similar for all three contact times; but Fig. 5.12 shows that the core height (S_c) of the 60-min. rock is bigger than the other two samples. This implies that the 60-min. rock has more empty space available for flow; thus, the 60-min. rock has very low conductivity, a different behavior than we expected.

If we speculate that the initial conductivity depends on the waviness, the 60-min. rock should not start which such low conductivity unless the weakening is so high that the rock crushes at a load less than 1,000 psi. In contrast, little can be concluded from the roughness since the fluid system successfully maintains low roughness at every contact time because wormholes do not form.

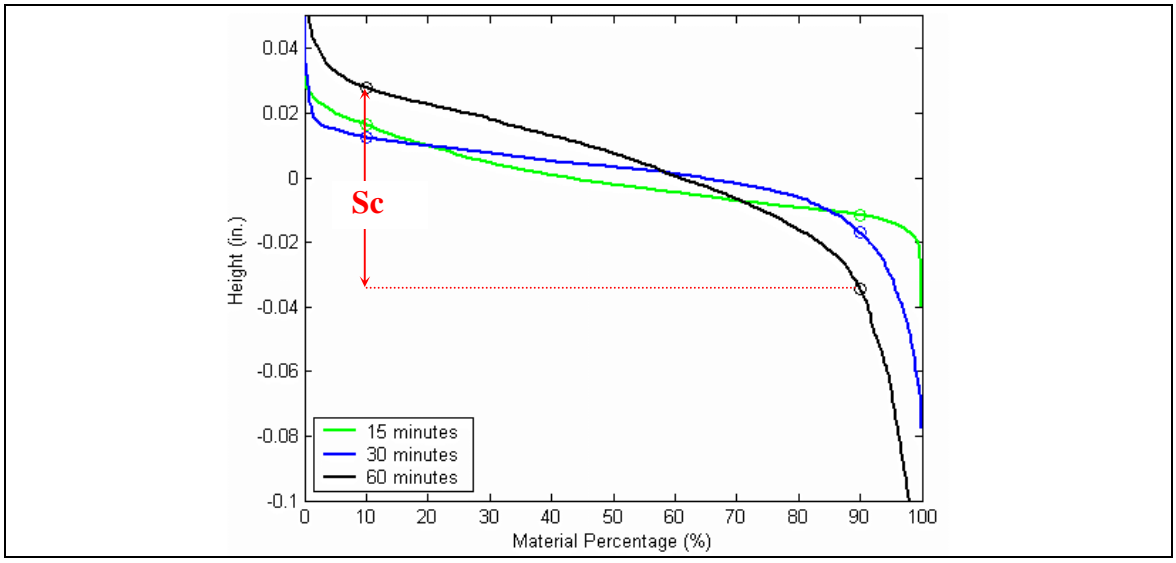

Fig. 5.12—Exp. 1—Original surfaces comparative of material ratio curves.

5.2.2. Experiment 2: Emulsified Acid and Limestone, 275°F, 0.005 ft/min.

Fig. 5.13 shows the pictures corresponding to each of the contact times for the Exp. 2 (Table 5.1). Fig. 5.14 shows how the acid has dissolved a large amount of rock at 15-min. and some wormholes start appearing. Fig. 5.15 shows larger wormholes at 30-min. The 60-min. rock in Fig. 5.13 and Fig. 5.16 shows how the wormhole has penetrated the rock entirely; those holes are very clear on the 3D view valleys surface in Fig. 5.16. This set of experiments shows more dissolution than Exp. 1, which has the same conditions except the temperature.

Fig. 5.13—Pictures of experiment 2.

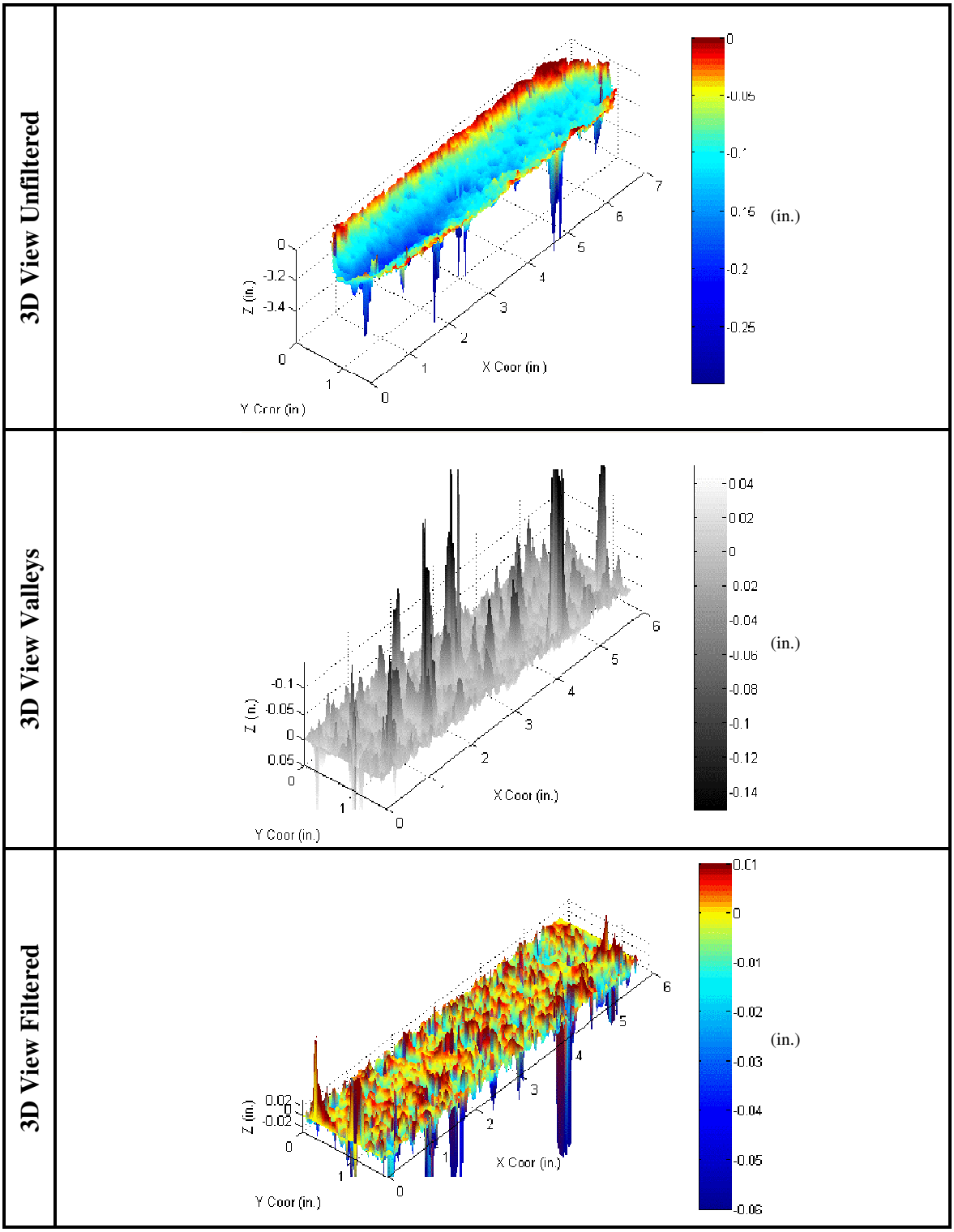

Fig. 5.14—Exp. 2: Visualization 3D Surfaces of emulsified acid and limestone—275 °F, 0.005 ft/min., 15 min.

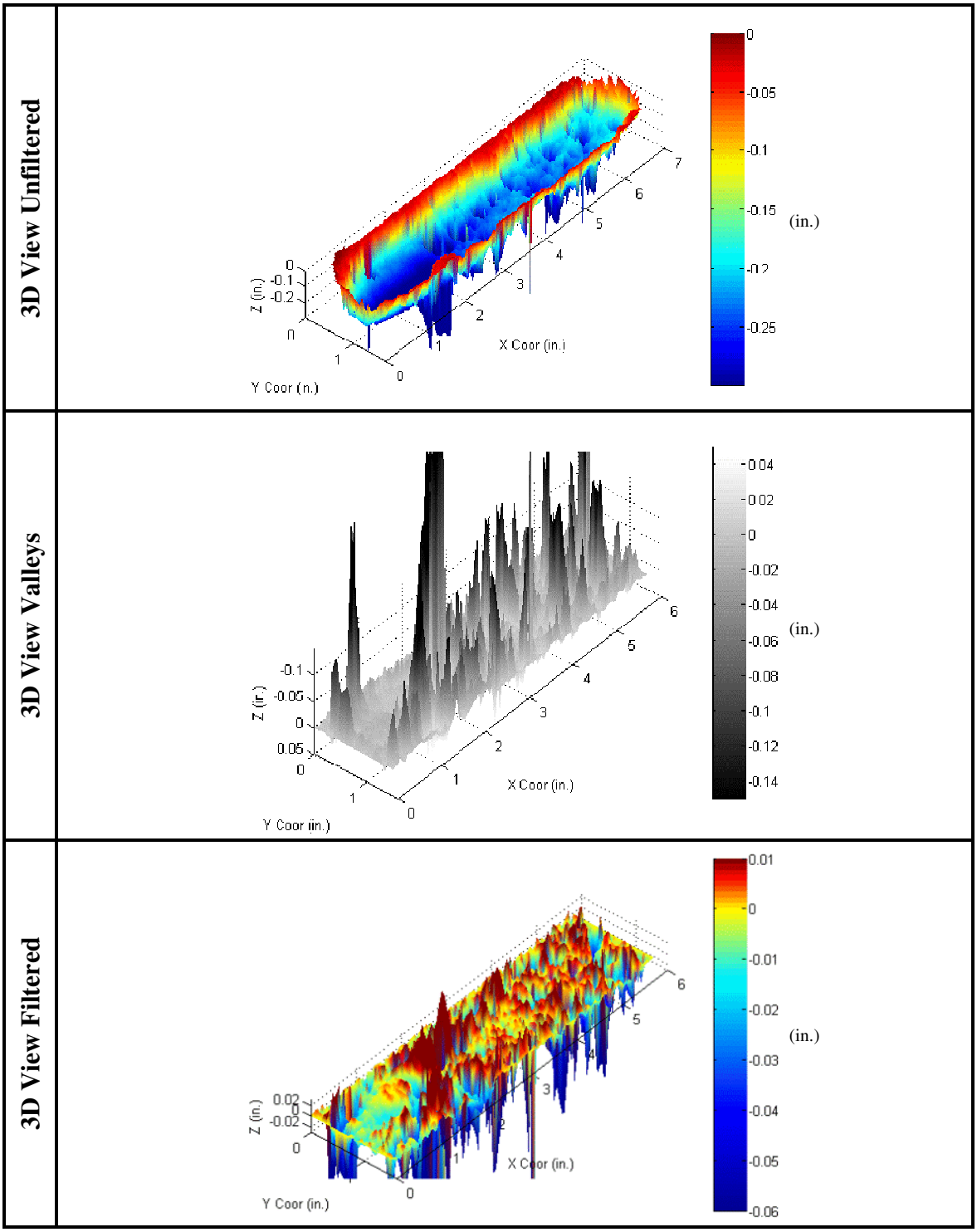

Fig. 5.15—Exp. 2: Visualization 3D surfaces of emulsified acid and limestone—275 °F, 0.005 ft/min., 30 min.

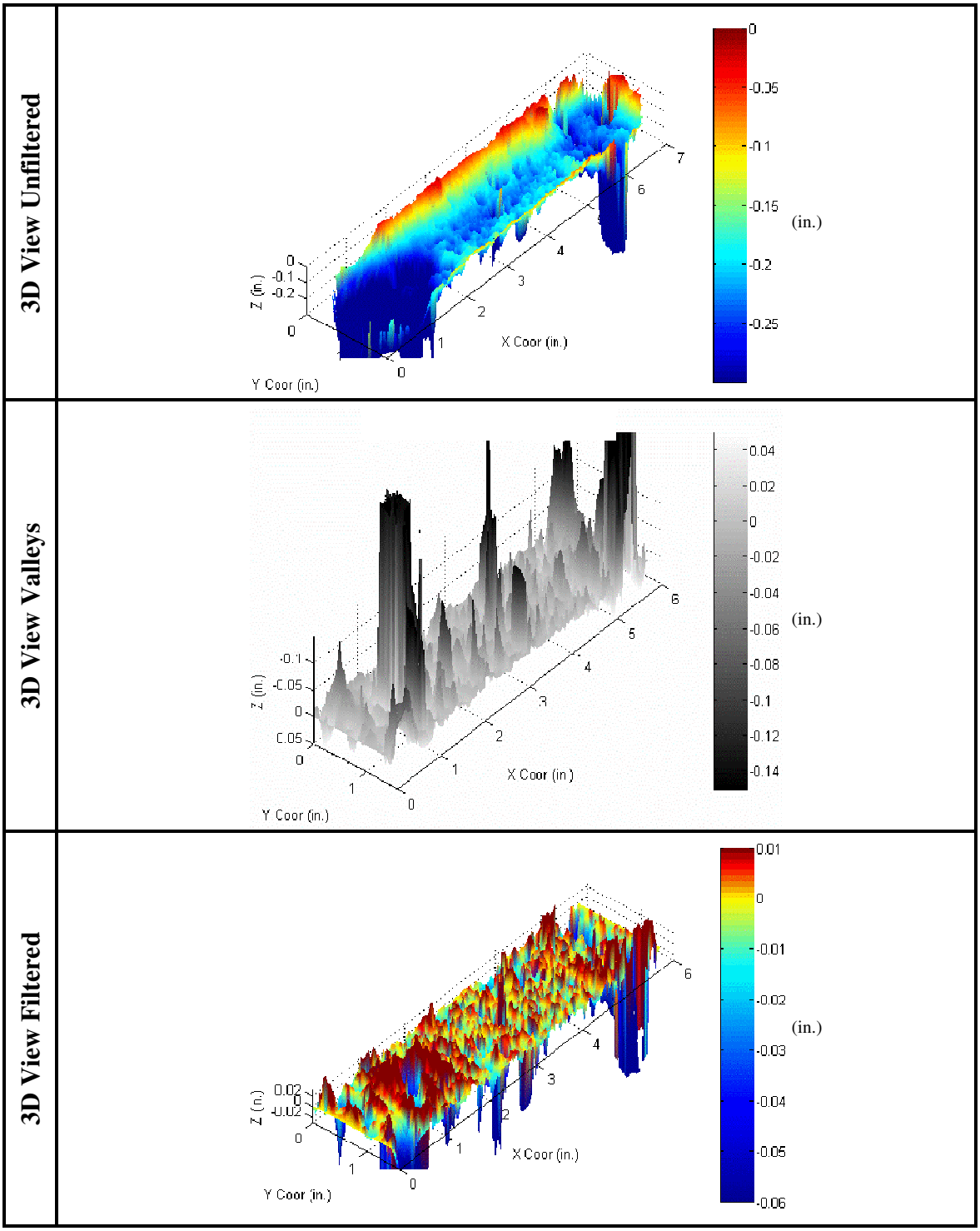

Fig. 5.16—Exp. 2: Visualization 3D surfaces of emulsified acid and limestone—275 °F, 0.005 ft/min., 60 min.

Fig. 5.17 presents the volume of rock dissolved for each contact time. The data points on this plot show an increase in the amount of rock dissolved for each increase in contact time. The 60-min. point does not follow the increase tendency because the big wormholes take control of the dissolution on the surface and also because the range of the laser can not measure to the total depth of the holes.

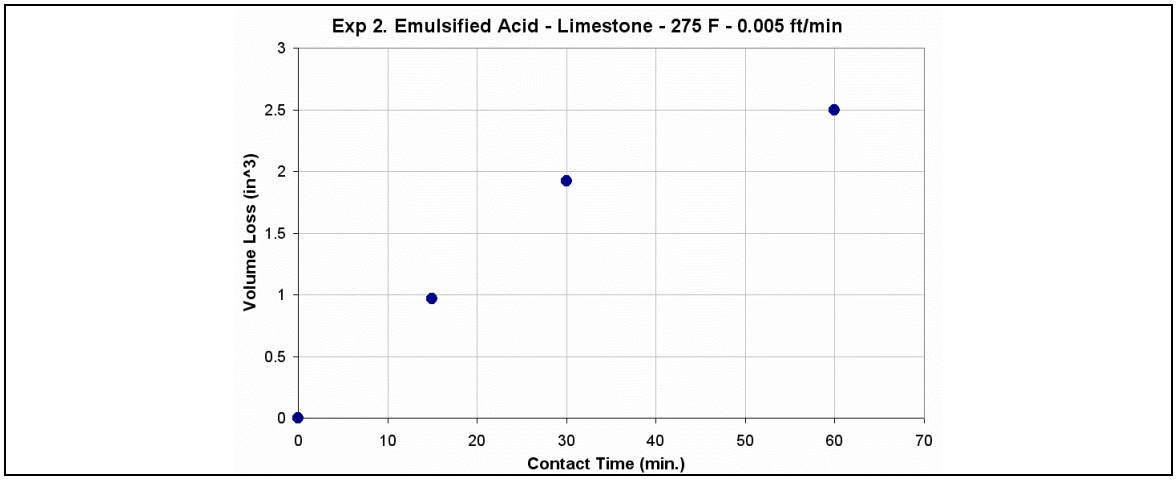

Fig. 5.17—Exp. 2—Volume of rock dissolved on rock surface.

Fig. 5.18 presents the profiles for each contact-time experiment. The vertical scale has been increased with respect to the other profile plots to clarify the entire wormhole penetration along the rock, especially for the 60-min. rock. Although the hydrodynamic effect can be seen, the degree of dissolution creates a central channel, as shown by the transversal view at 30- and 60-min. contact times.

Fig. 5.19 compares the profile development for the three experiments, and Fig. 5.20 compares the roughness profiles. These profiles are in the extreme of the filter capabilities and some overshooting appears on the corners of the wormholes. The roughness profiles are dominated by the big wormhole features.

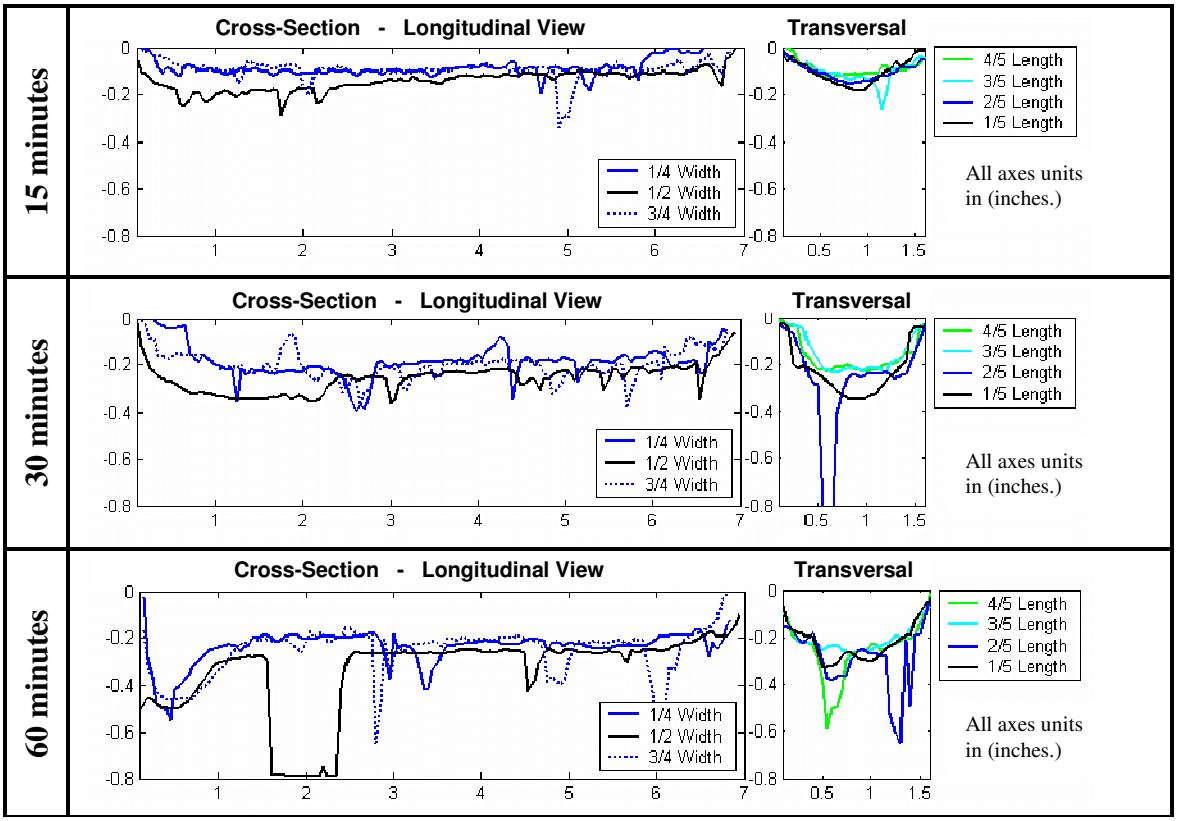

Fig. 5.18—Exp. 2—Longitudinal and transversal cross-section profiles.

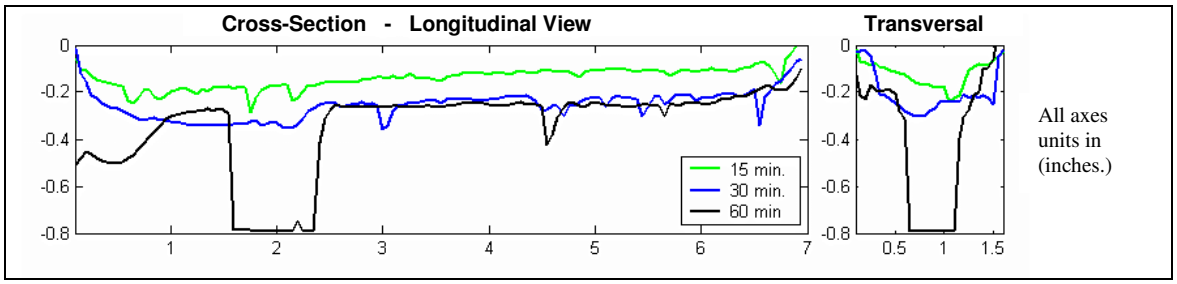

Fig. 5.19—Exp. 2—Comparative cross-section profile.

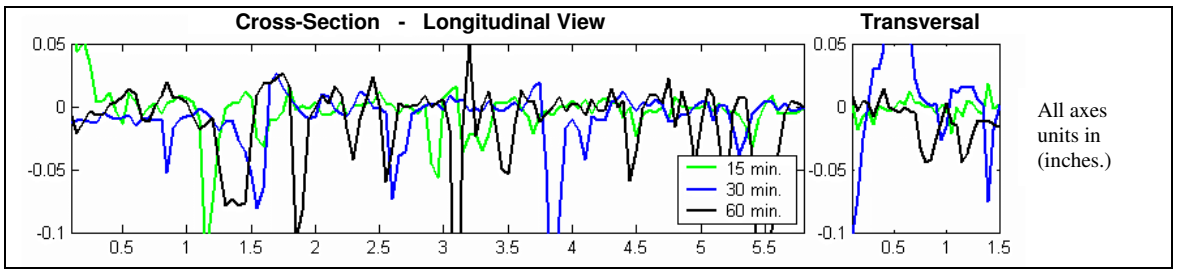

Fig. 5.20—Exp. 2—Comparative roughness cross-section profile.

Fig. 5.21 shows that the roughness parameters have high values and that the roughness increases with contact time for all the parameters but S_z which is altered because the filter overshoot of the samples.

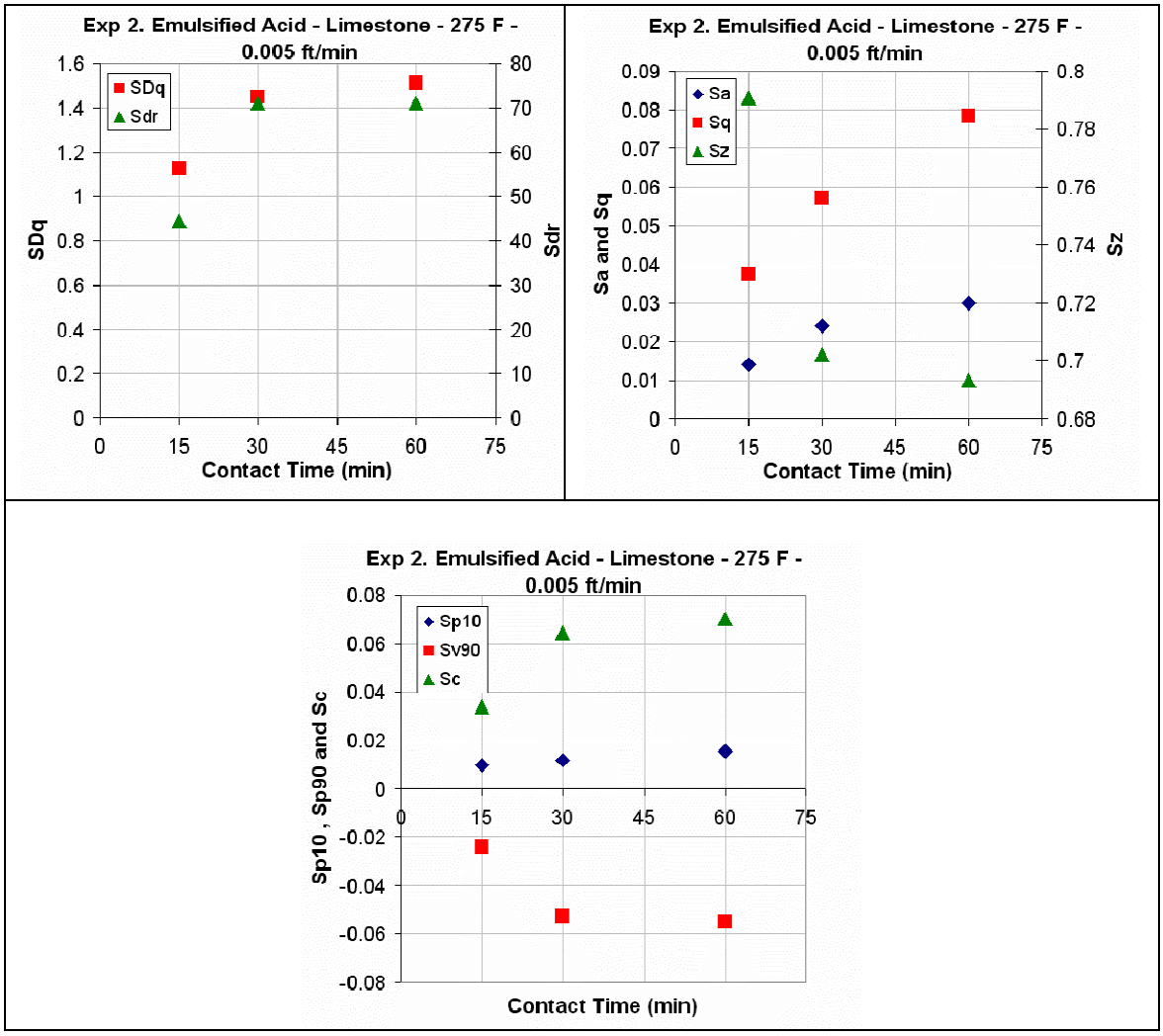

Fig. 5.21—Exp. 2—Roughness parameters.

Fig. 5.22 and 5.23 show the roughness and original data material ratio curves (MRC) for the experiments. The roughness MRCs of the 30- and 60-min. samples exhibit a significant decrease on the portion of the curve after the 90% value; this indicates the growth of the wormholes. On the other hand, the original data MRC in Fig. 5.23

exhibits curves with different plateaus for each contact time. The upper plateau on the 30-min. rock corresponds to the data points that remain on the sides of the rock; the plateau on the 60-min. rock corresponds to the lower inlet height of the sample.

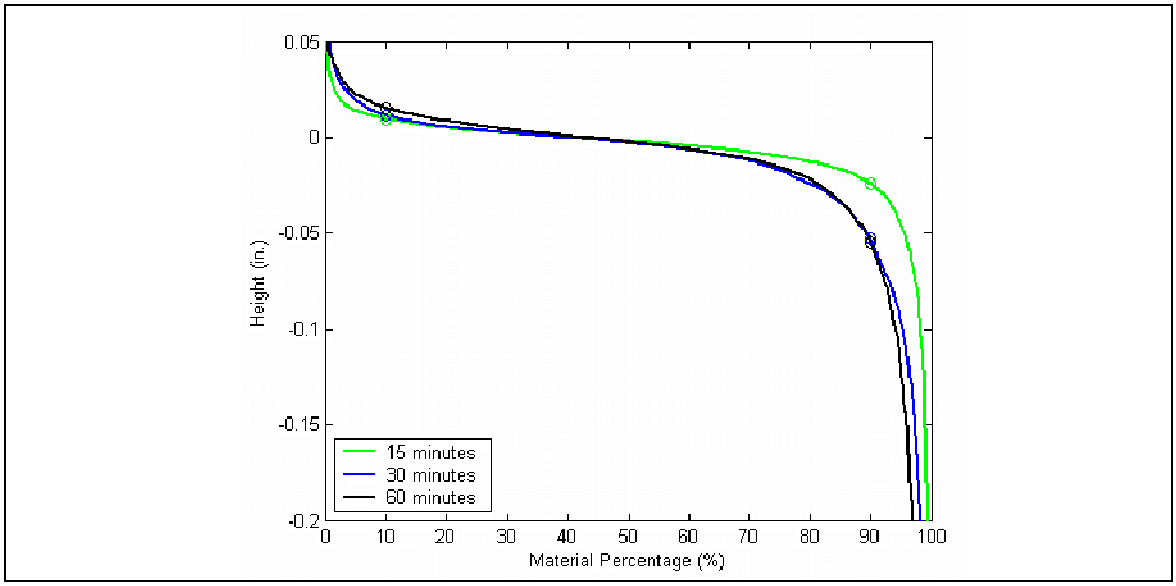

Fig. 5.22—Exp. 2—Roughness material ratio curves.

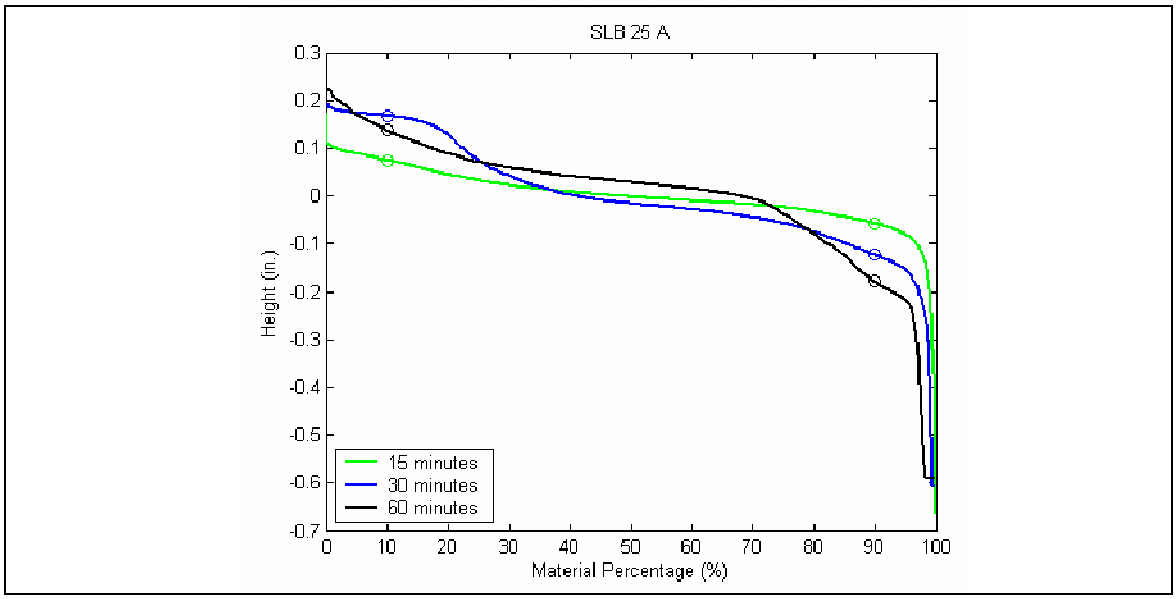

Fig. 5.23—Exp. 2—Original data material ratio curves.

Since all the samples present a concave dissolution (transversal view on Fig. 5.14) and the rocks after 30-min. were highly affected by the acid, no conductivity measurements were performed on this set of rocks.

5.2.3. Experiment 3: Gelled Acid and Limestone, 200°F, 0.005 ft/min.

Exp. 3 (Table 5.1) is like Exp. 1 but with a different fluid system. Fig. 5.24, 5.25 and 5.26 present the visualization results for the experiment. Notice that the 15-min. rock presents heterogeneity at the rock outlet; that heterogeneity was a feature of the rock before acidizing; pictures of the rocks are presented in Appendix C. The gray 3D views show how more wormholes develop at higher contact times. The increase in the amount of rock dissolved can also be seen on Fig. 5.27.

The gelled fluid does not cause a large hydrodynamic effect, but minor channeling appears at the middle of the rock sample. Fig. 5.28 illustrates the behavior of the fluid for each contact time. Fig. 5.29 verifies that the dissolution occurs along the entire rock surfaces at all contact times. Fig. 5.30 presents the successive increase of roughness with increase in contact time.

The roughness of the samples has a significant increase at 60 minutes, when a great number of wormholes start appearing. That increase can be seen in all the roughness parameters (Fig. 5.31). Assuming that the 30-min. rock is representative of the dissolution, the fluid system appears to control the wormholes up to a certain time.

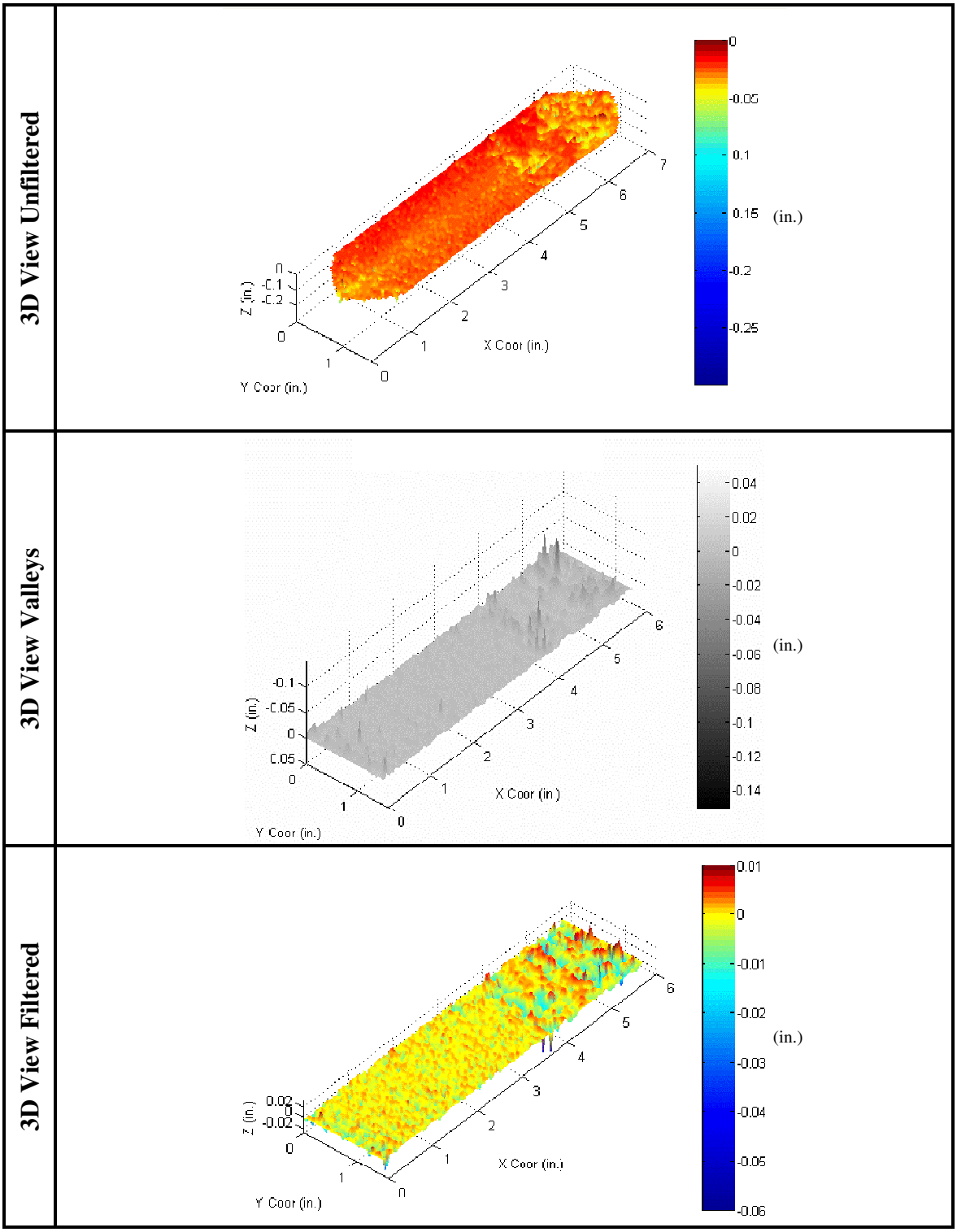

Fig. 5.24—Exp. 3: Visualization 3D surfaces of gelled acid and limestone—200°F, 0.005 ft/min., 15 min.

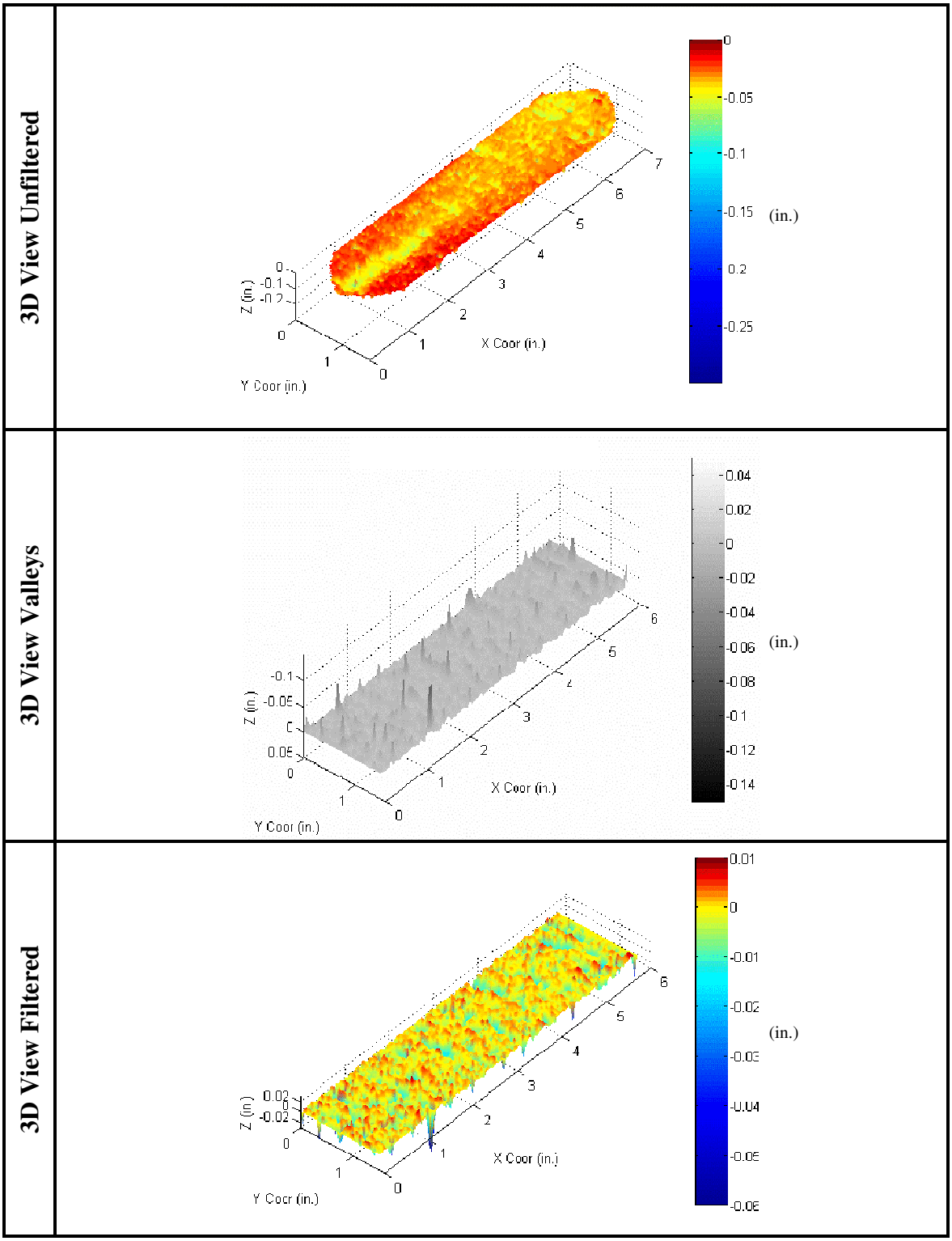

Fig. 5.25—Exp. 3: Visualization 3D surfaces of gelled acid and limestone—200°F, 0.005 ft/min., 30 min.

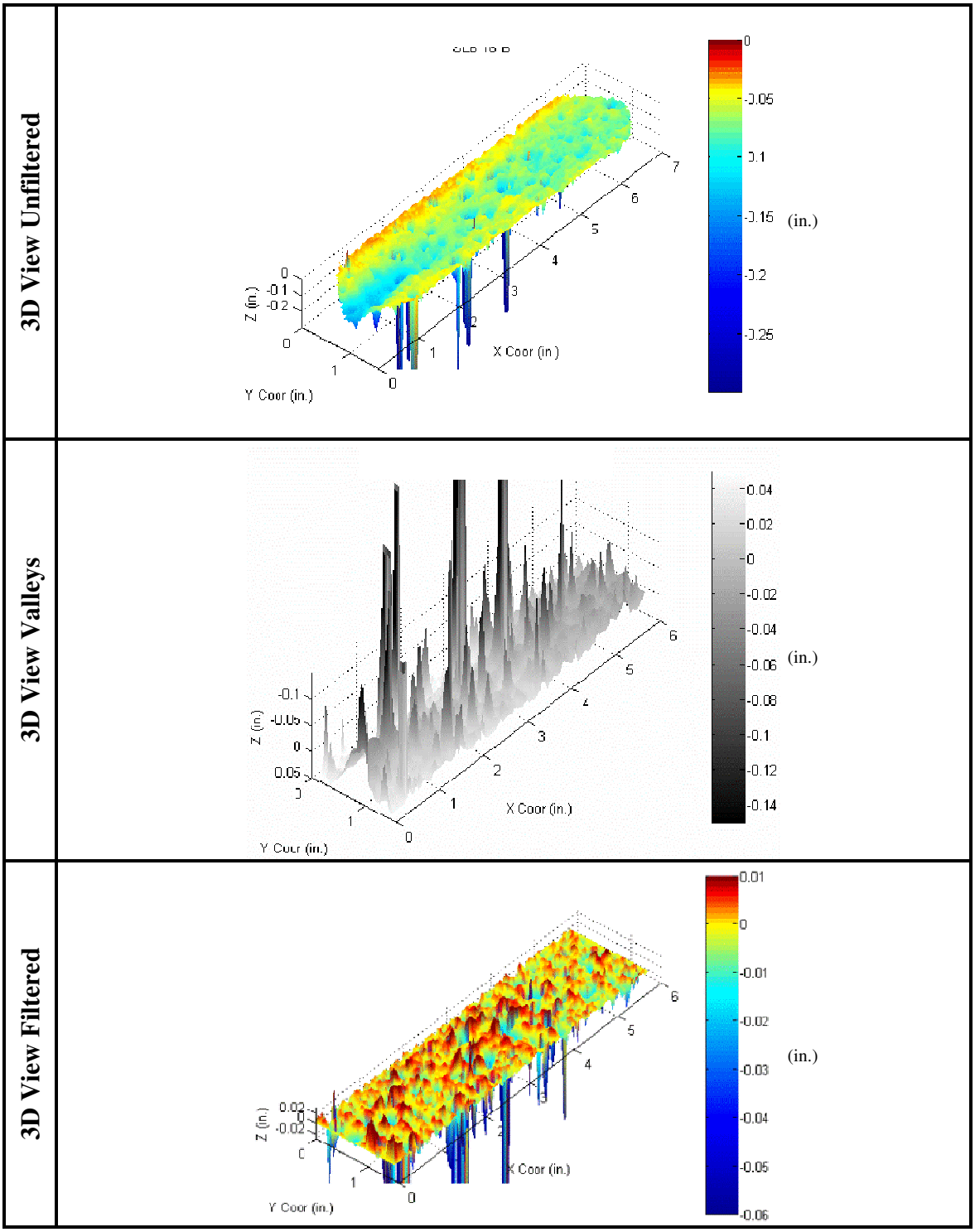

Fig. 5.26—Exp. 3: Visualization 3D surfaces of gelled acid and limestone—200°F, 0.005 ft/min., 60 min.

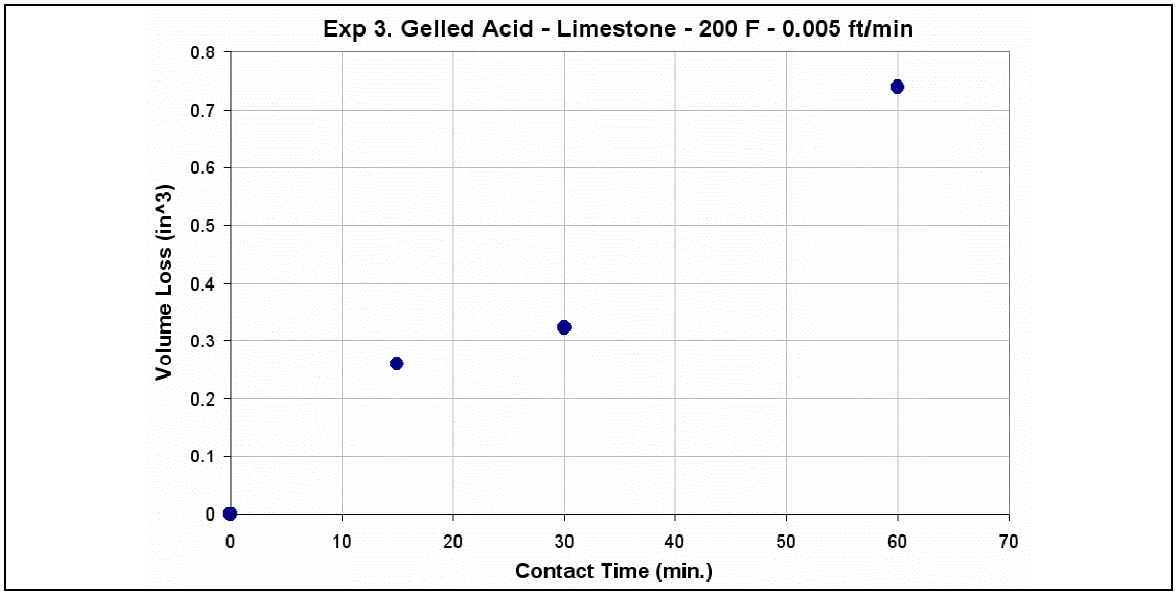

Fig. 5.27—Exp. 3—Volume of rock dissolved on rock surface.

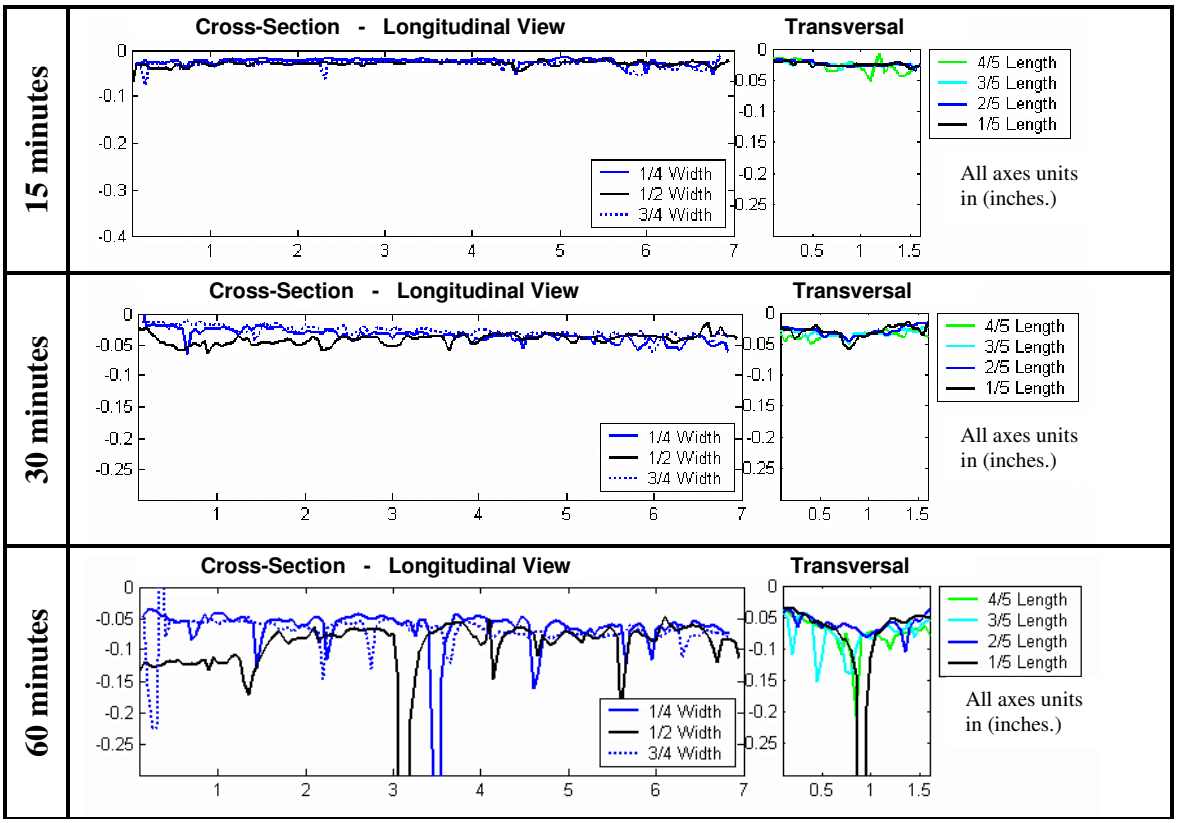

Fig. 5.28—Exp. 3—Longitudinal and transversal cross-section profiles.

Figs, 5.32 and 5.33 serve for comparison between the present the roughness and original data MRC. The curves of 15- and 30-min. almost overlap showing that the surface has barely been affected; the 60-min. roughness curve deviates at 90%, representing the increase of wormholes in the rock. Better understanding can be seen on the original data MRC plot where the distance between the 10% and 90% (S_c parameter) increases for higher contact times.

The conductivity measurements show that the initial conductivity is proportional to the acidizing contact times; this can be attributed to the combined effect of roughness and the size of the hydrodynamic channels. The slope of the curves increases with contact time also, causing the conductivity of all three samples to reach almost the same final conductivity. In particular the 60-min. conductivity exhibits the greatest decrease of conductivity with closure stress (Fig. 5.34).

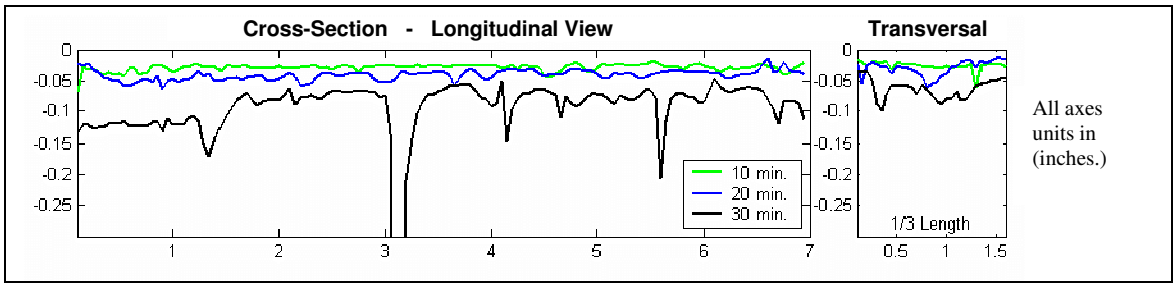

Fig. 5.29—Exp. 3—Comparative cross-section profile.

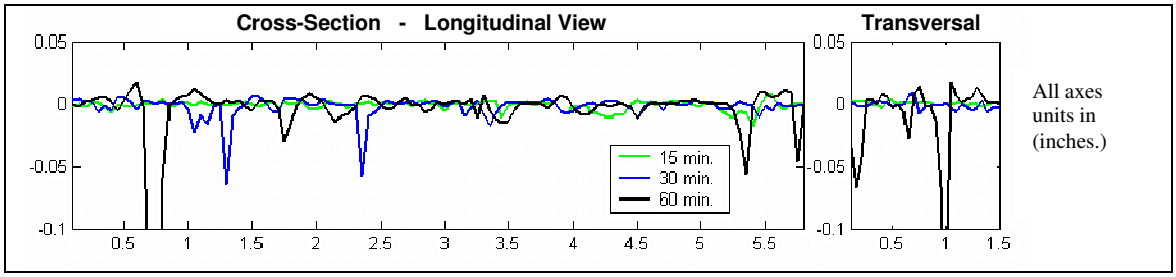

Fig. 5.30—Exp. 3—Comparative roughness cross-section profile.

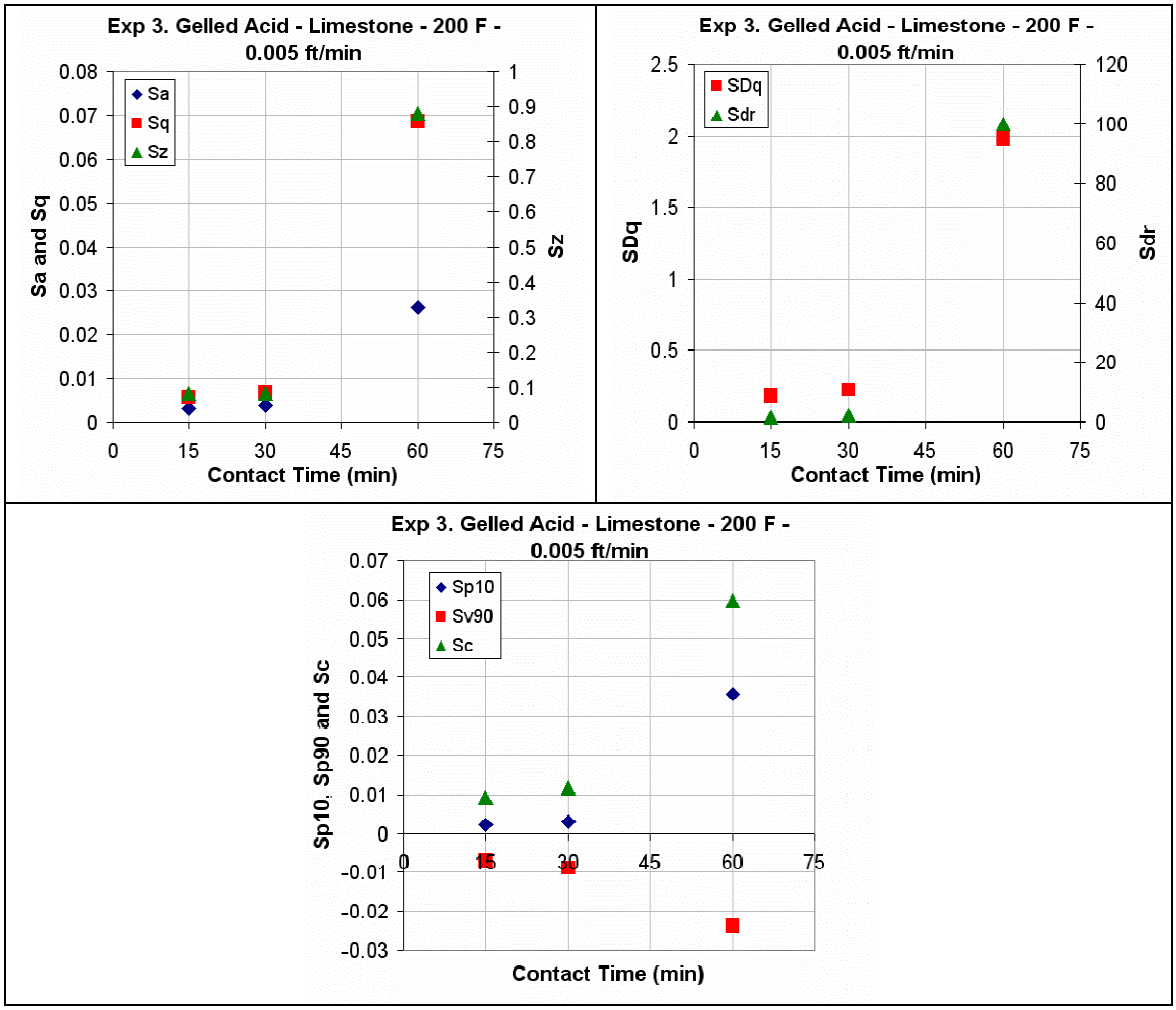

Fig. 5.31—Exp. 3—Roughness parameters.

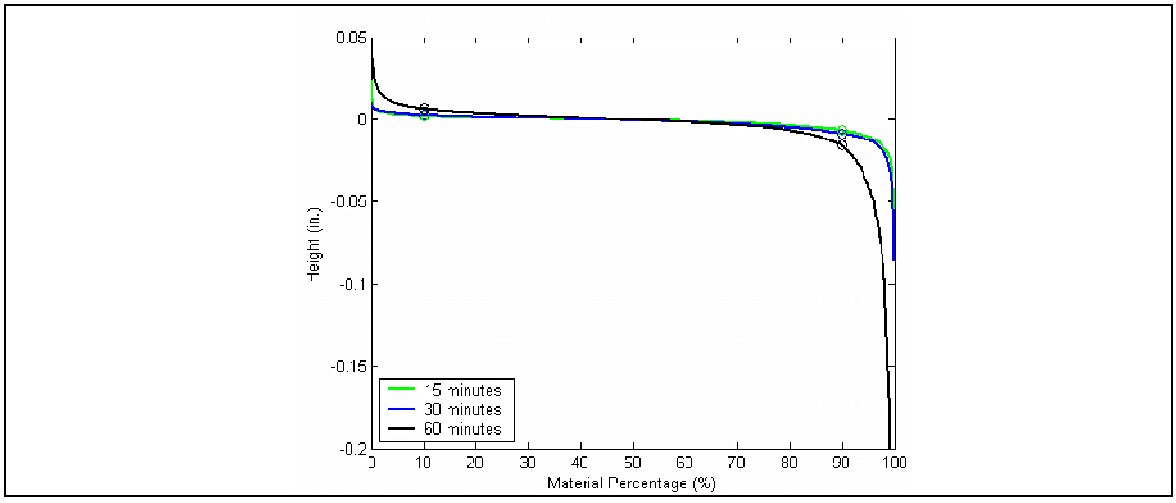

Fig. 5.32—Exp. 3—Roughness material ratio curves.

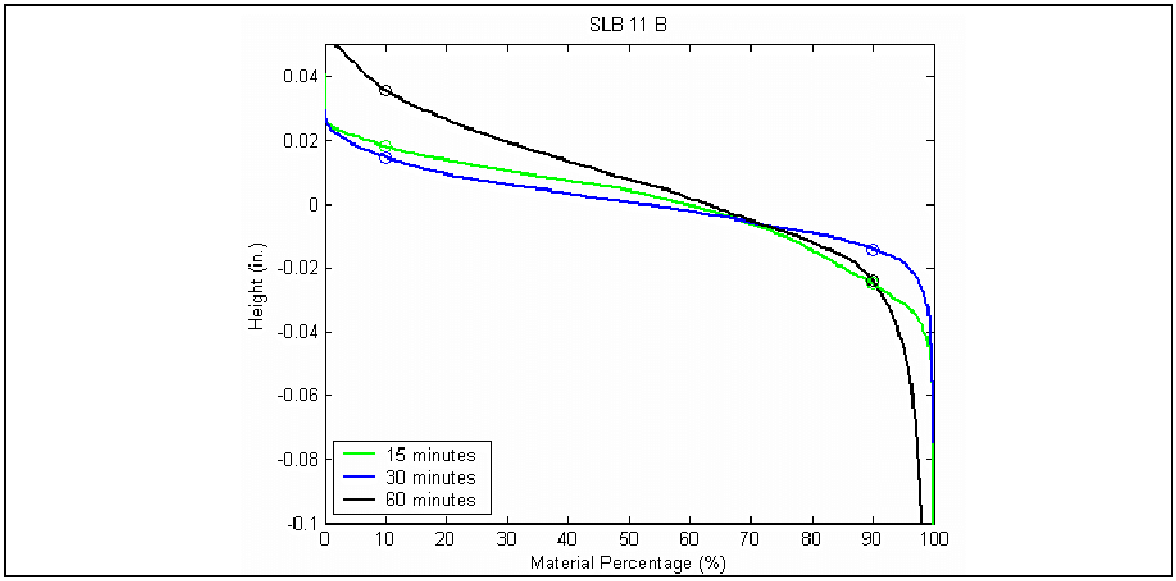

Fig. 5.33—Exp. 3—Original data material ratio curves.

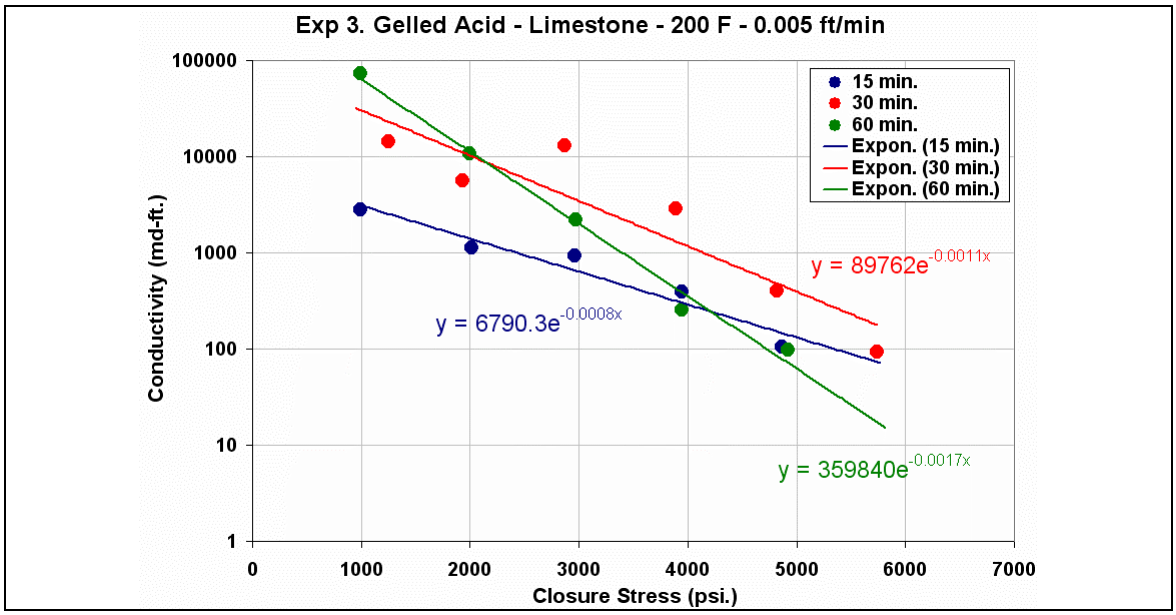

Fig. 5.34—Exp. 3—Conductivity measurements.

5.2.4. Experiment 4: Gelled Acid and Limestone, 200°F, 0.010 ft/min.

Exp. 4 is similar to Exp. 3 but with double the leakoff rate. Fig. 5.35 and 5.36 show the visualization plots. The 30-min. rock exhibits more wormholes than the 30-min. sample of Exp. 3 (See Fig. 5.25). This indicates that the leakoff facilitates the wormhole development. Longer contact time creates more volume loss, as can be seen in Fig. 5.37.

The increase in wormholes can be observed on the profile plots (Fig. 5.38). The 30-min. rock presents more surface roughness and a small channel in the middle of the rock; this channel has bigger dimensions that its counterpart on Exp. 3.

Fig. 5.39 shows that the dissolution is uniform along the sample surface. Fig. 5.40 compares the roughness, showing that the 30-min. rock is rougher.

All the roughness parameters have an increase from the 15-min. contact time to the 30.min. contact time (Fig. 5.41). This increment is greater than the one seen on other experiments, proving the quick development of wormholes because of the high leakoff rate.

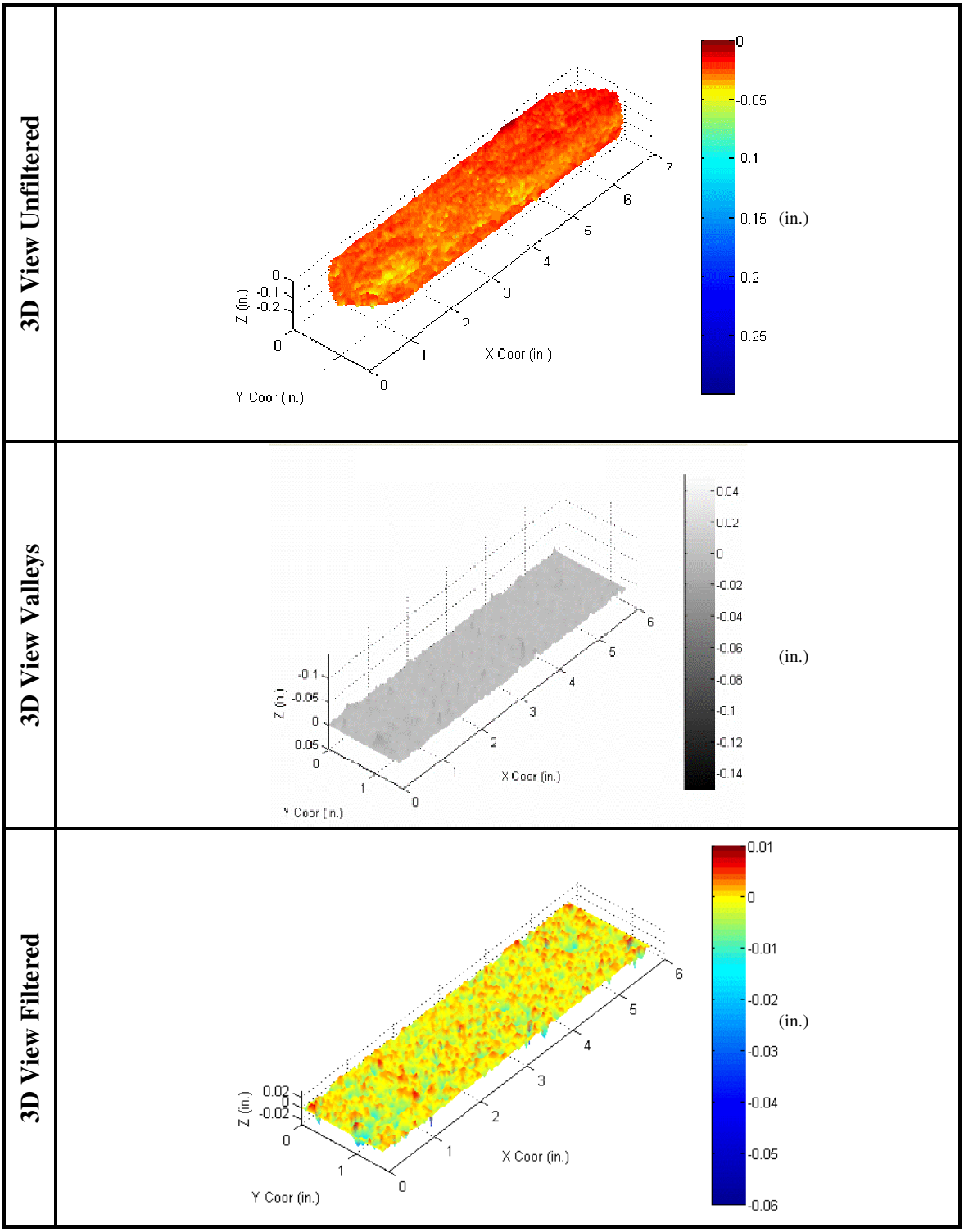

Fig. 5.35—Exp. 4: Visualization 3D surfaces of gelled acid and limestone —200 °F, 0.010 ft/min., 15 min.

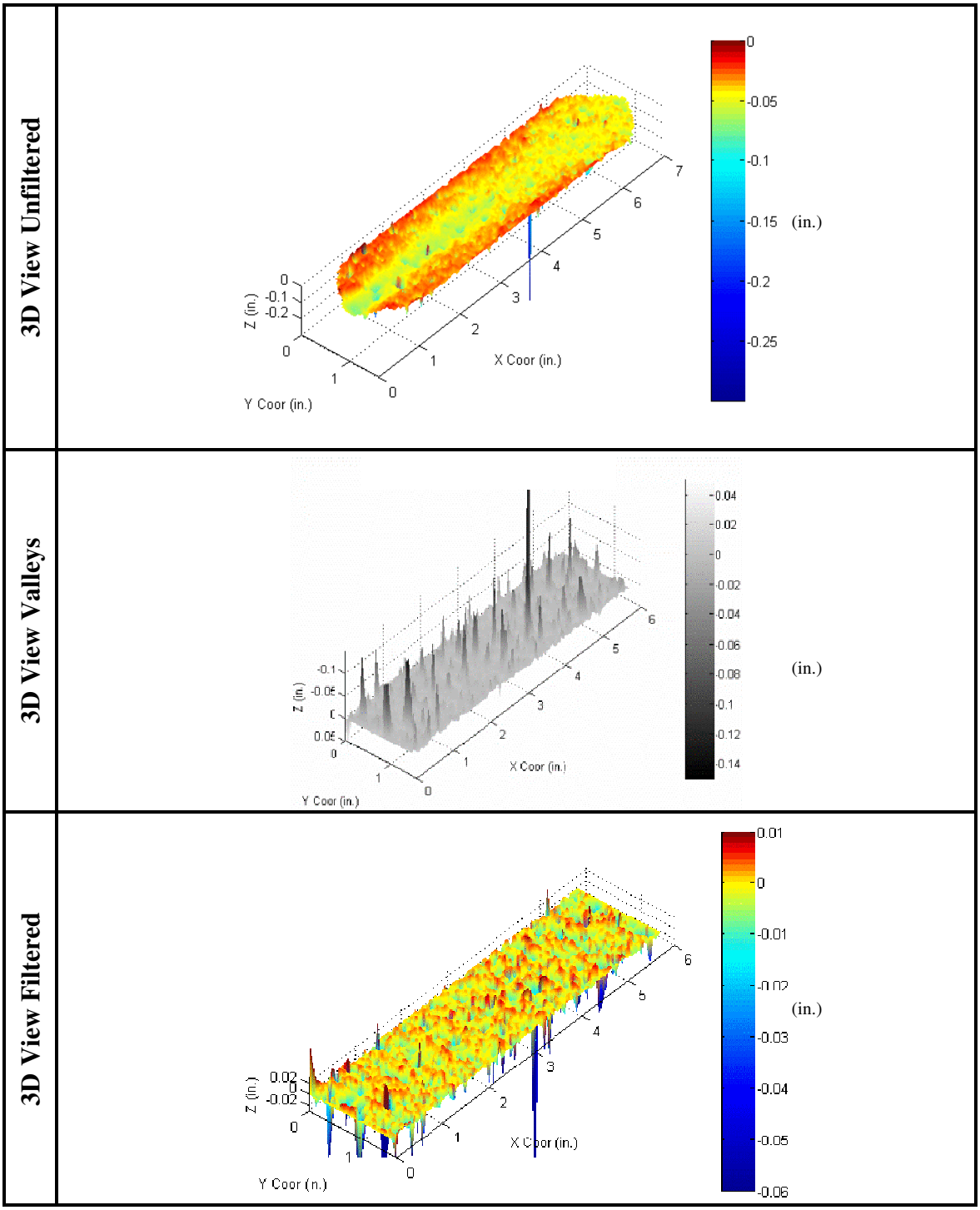

Fig. 5.36—Exp. 4: Visualization 3D surfaces of gelled acid and limestone—200 °F, 0.010 ft/min., 30 min.

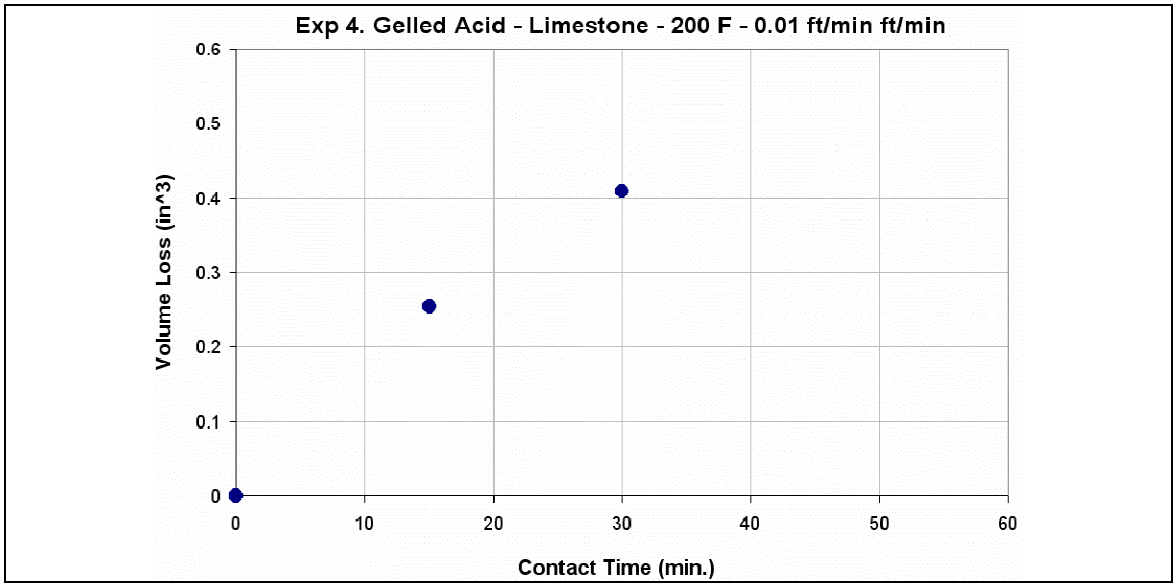

Fig. 5.37—Exp. 4—Volume of rock dissolved on rock surface.

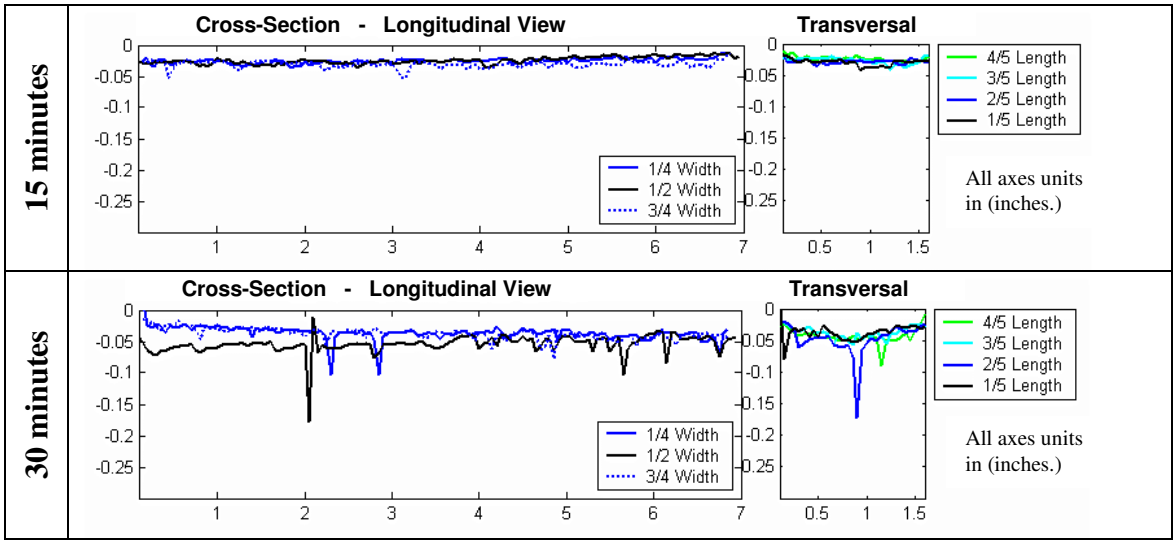

Fig. 5.38—Exp. 4—Longitudinal and transversal cross-section profiles.

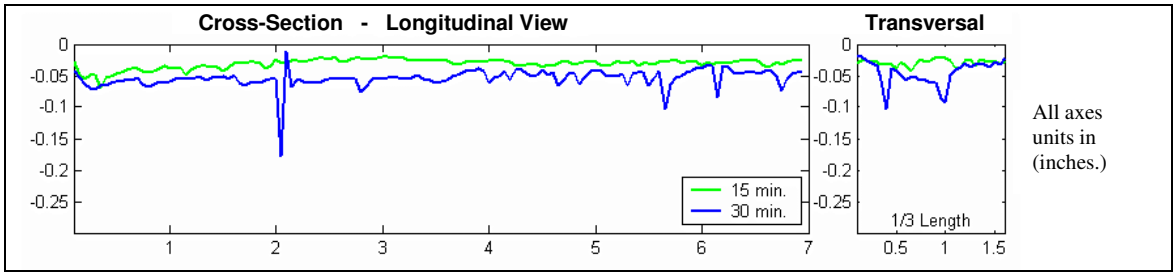

Fig. 5.39—Exp. 4—Comparative cross-section profile.

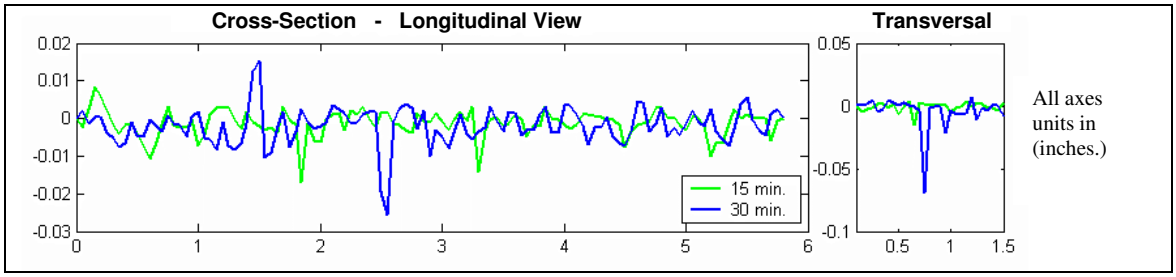

Fig. 5.40—Exp. 4—Comparative roughness cross-section profile.

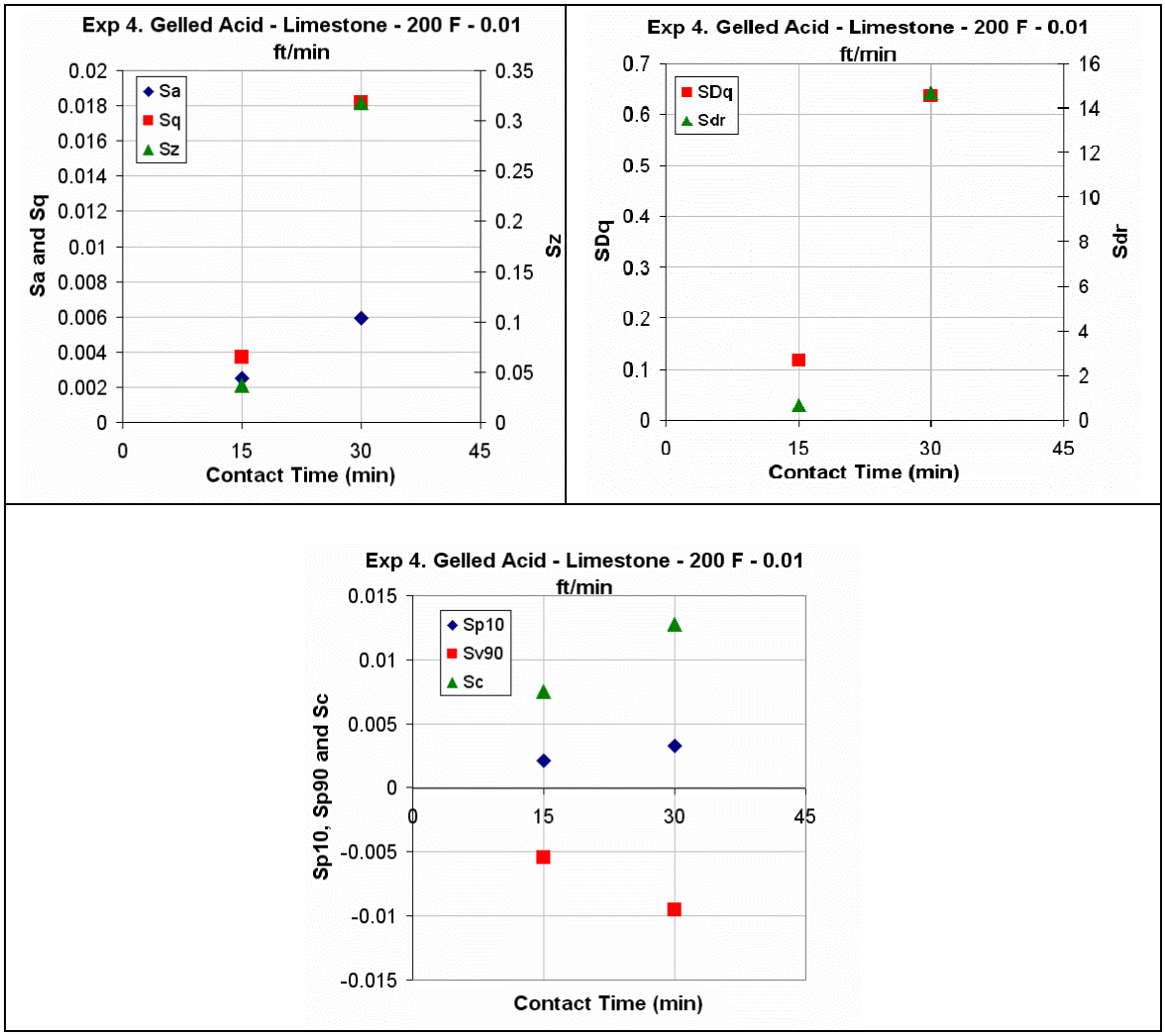

Fig. 5.41—Exp. 4—Roughness parameters.

Fig. 5.42 compares the experiment roughness MRCs; the main characteristic on that plot is the displacement of the 30-min. curve after 80% as the wormholes develop.

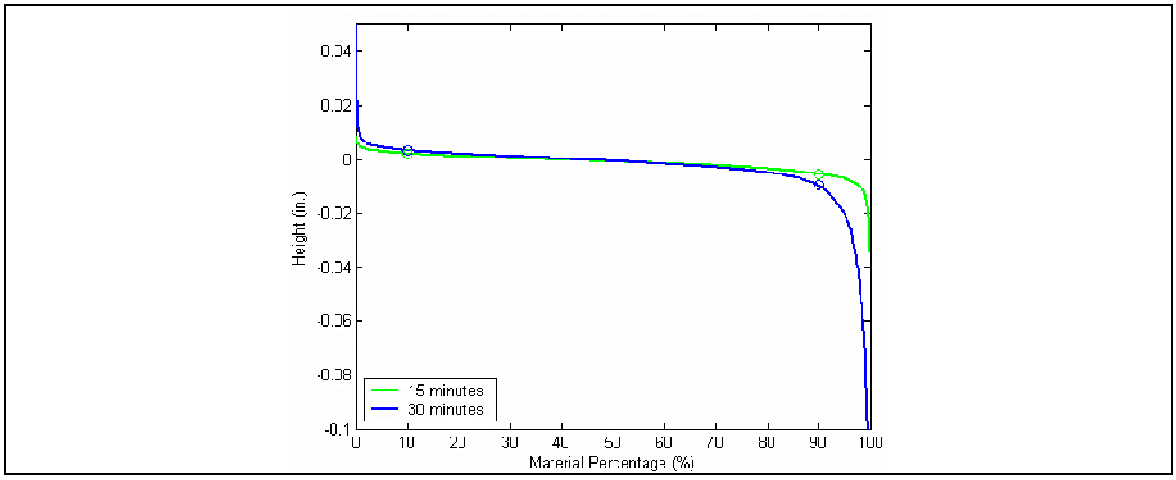

Fig. 5.42—Exp. 4—Roughness comparative of material ratio curves.

The conductivity measurements exhibit an inverse behavior with respect to the acidized time and the roughness. The 15-min. rock shows excessively high values even at pressures of 5,000 psi. In contrast, the 30-min. rock shows less initial conductivity and its expected decrease with compression (Fig. 5.43). This high value of the 15-min. rock is abnormal since the 30-min. rock has a channel that is expected to contribute at least to the initial conductivity (see Fig. 5.44).

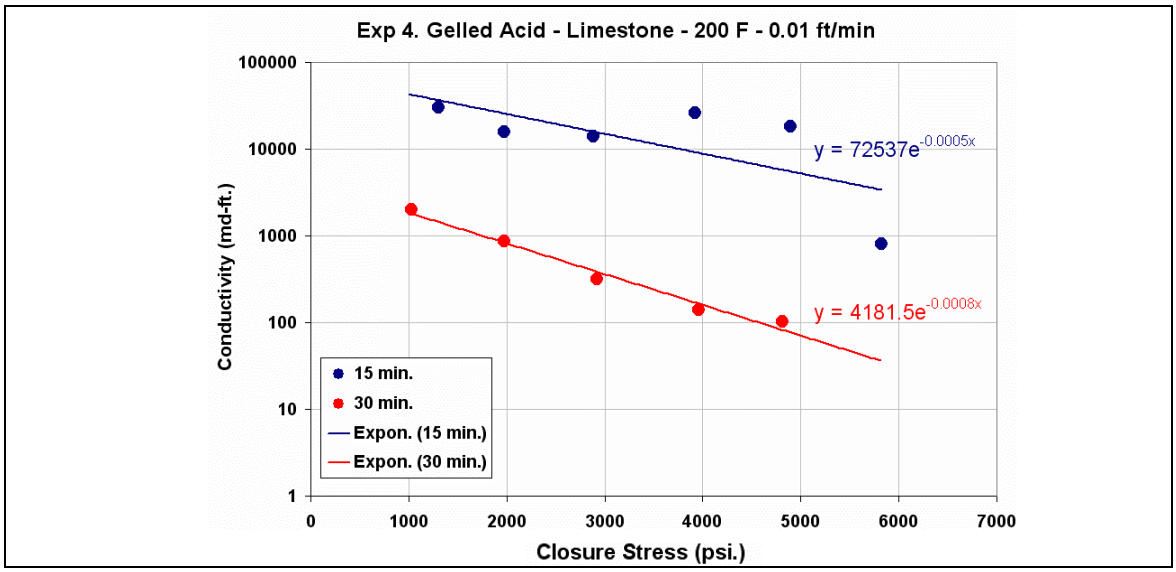

Fig. 5.43—Exp. 4—Conductivity measurements.

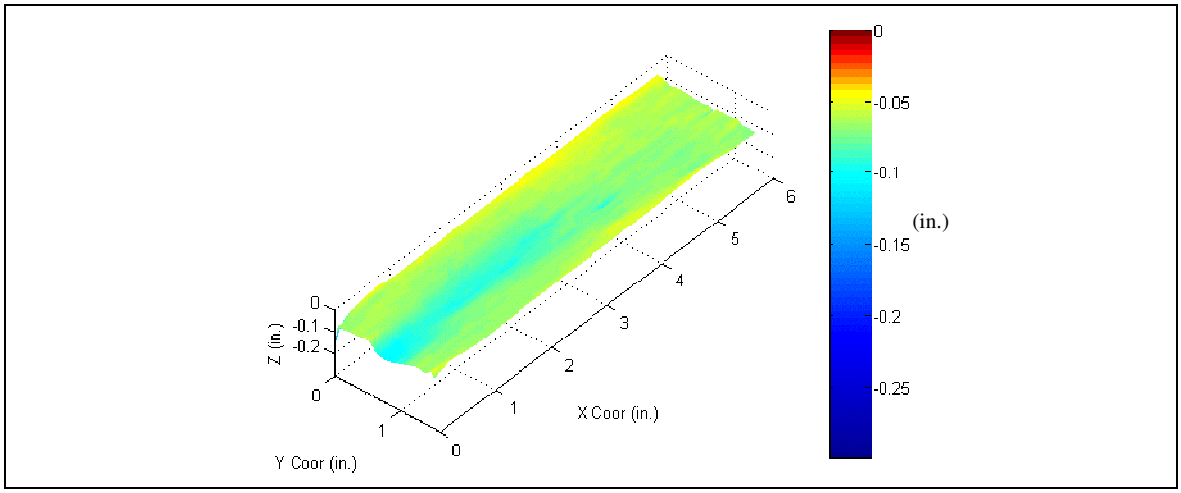

Fig. 5.44—Exp. 4—Waviness 3D surface view for 30-min. rock.

5.2.5. Experiment 5: Viscoelastic Surfactant Acid and Limestone, 200°F, 0.003 ft/min.

Figs. 5.45, 5.46 and 5.47 present the results for Exp. 5. The 3D view unfiltered on all three plots shows that the acid dissolves a big amount of rock progressively (see how the 60-min. surface is blue reflecting the deep surface values). The 3D view valleys plot shows that the amount and size of the wormholes that appear at 30 minutes is almost the same at the 60-min. although the acid continues dissolving the surface.

The increase in the amount of rock dissolved can be seen in Fig. 5.48, where the slope of the curve increases after 30 minutes. The profiles in Fig. 5.49 show how the wormholes that develop at 30 minutes do not become significantly larger when the acidizing time is doubled to 60 minutes; this can be observed in Fig. 5.50, which shows that the hydrodynamic effect present at 30 minutes is eliminated in the 60 minutes profile.

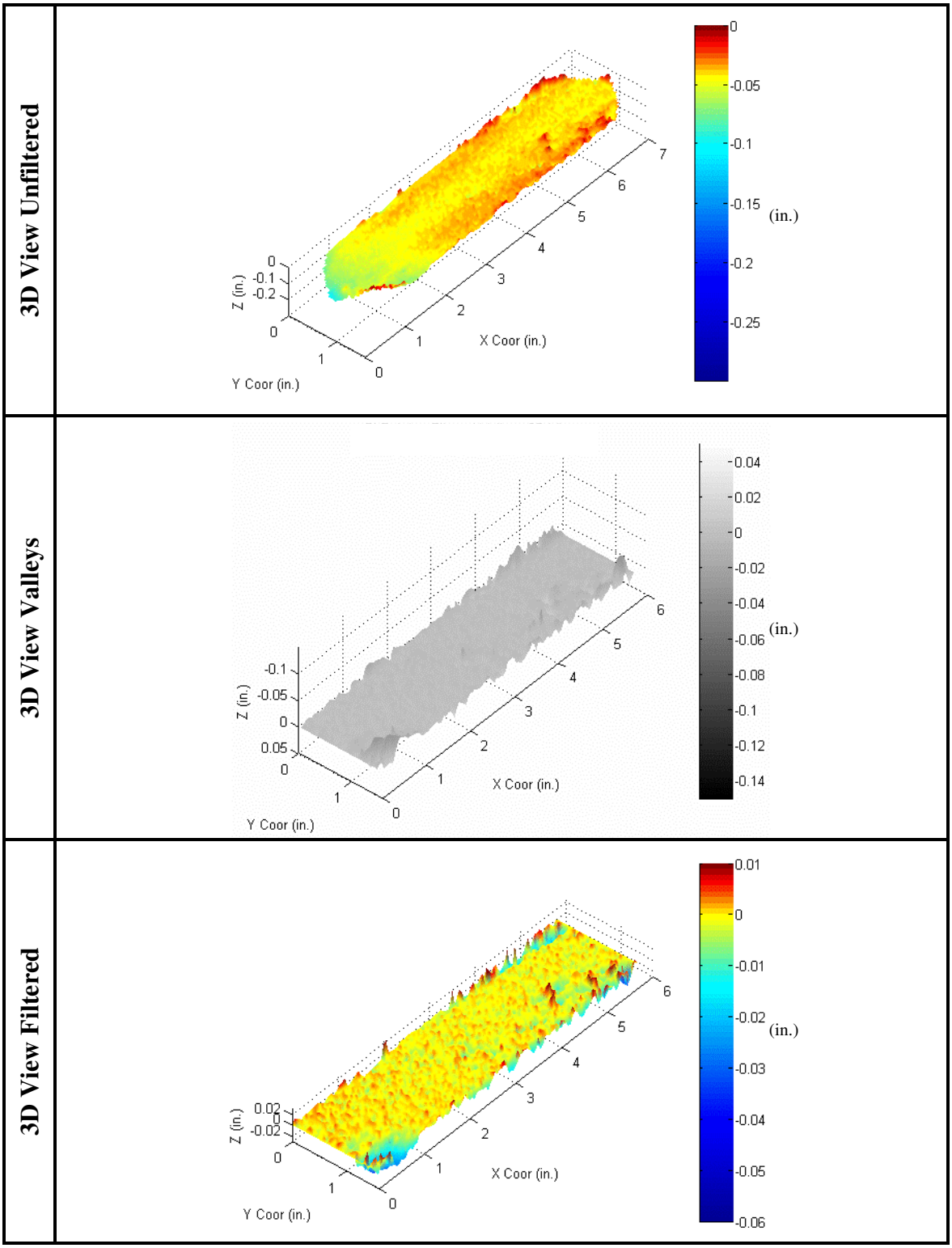

Fig. 5.45—Exp. 5: Visualization 3D surfaces of viscoelastic surfactant acid and limestone—200 °F, 0.003 ft/min., 15 min.

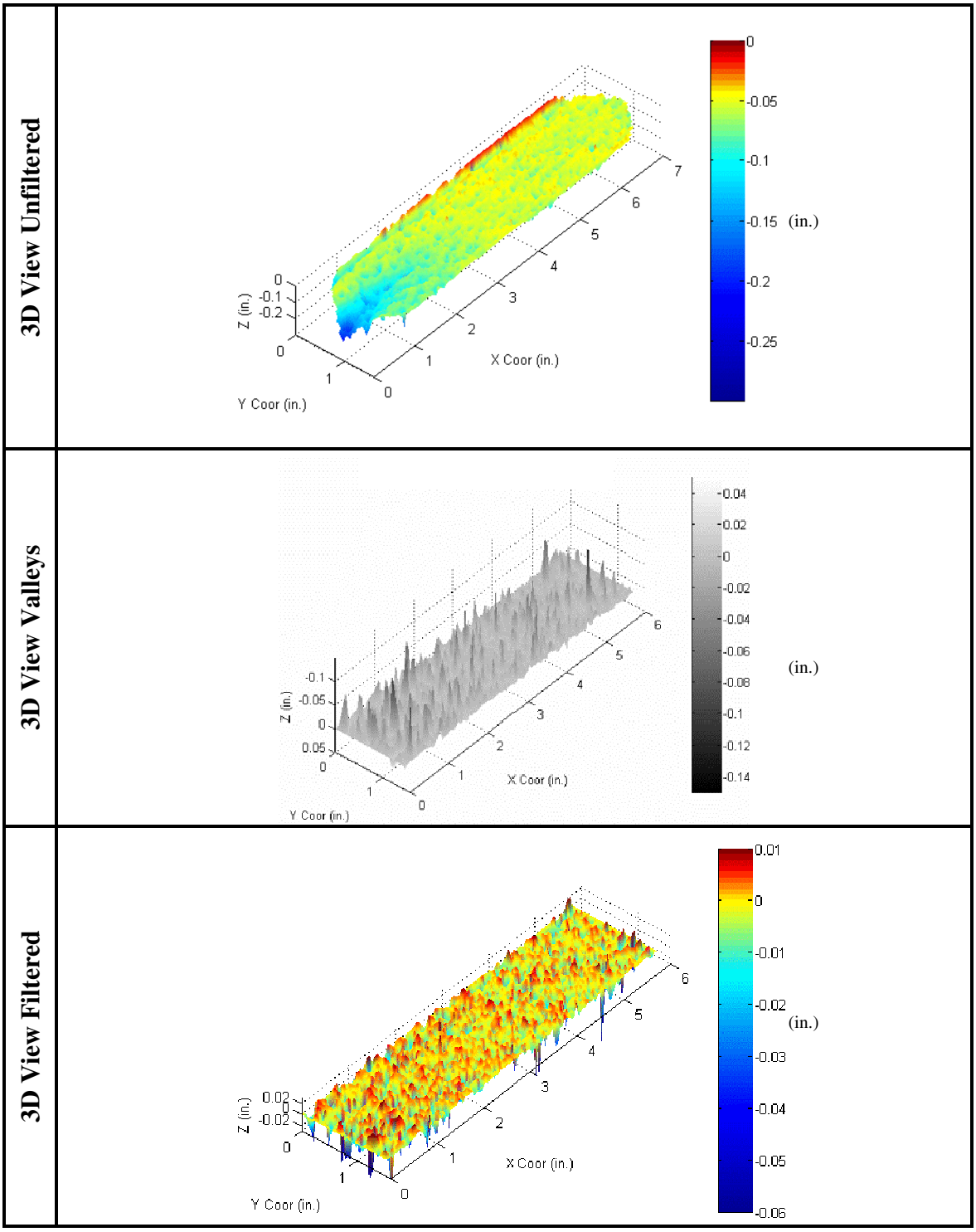

Fig. 5.46—Exp. 5: Visualization 3D surfaces of viscoelastic surfactant acid and limestone—200 °F, 0.003 ft/min., 30 min.

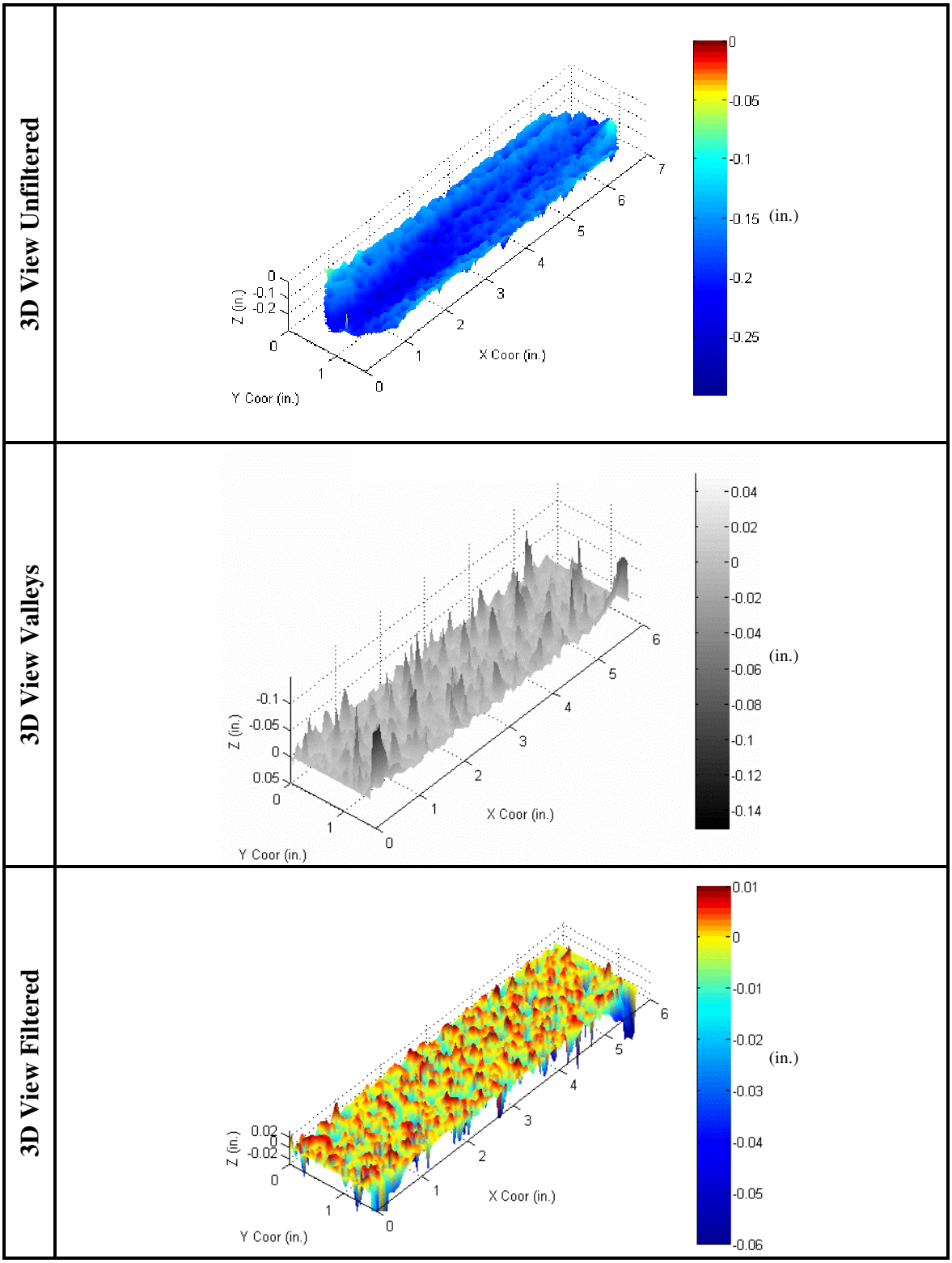

Fig. 5.47—Exp. 5: Visualization 3D surfaces of viscoelastic surfactant acid and limestone—200 °F, 0.003 ft/min., 60 min.

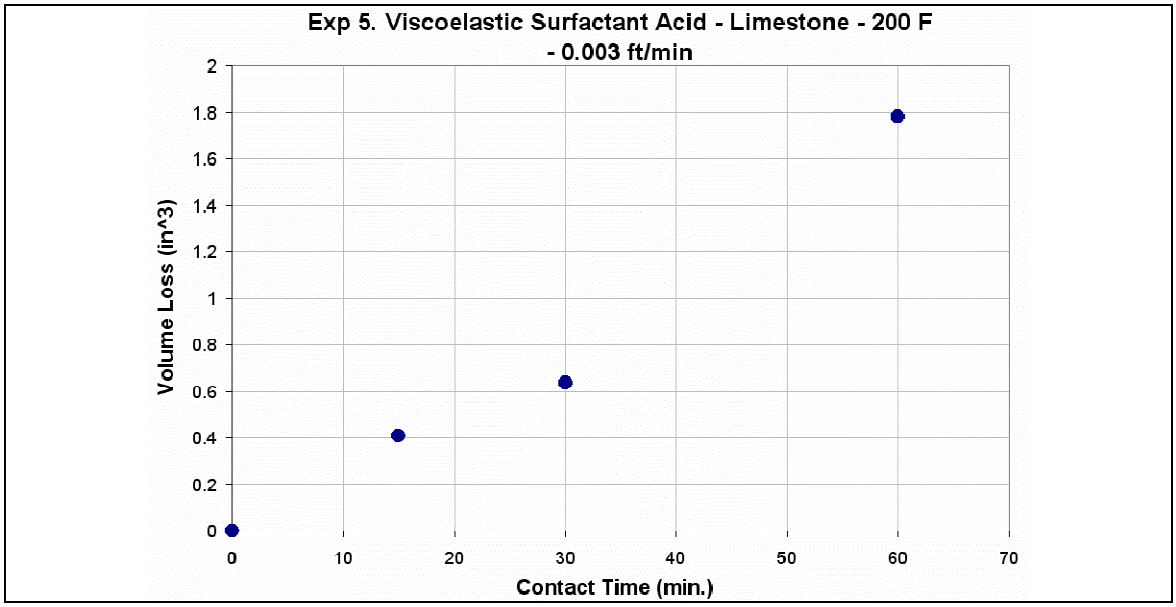

5.48—Exp. 5—Volume of rock dissolved on rock surface.

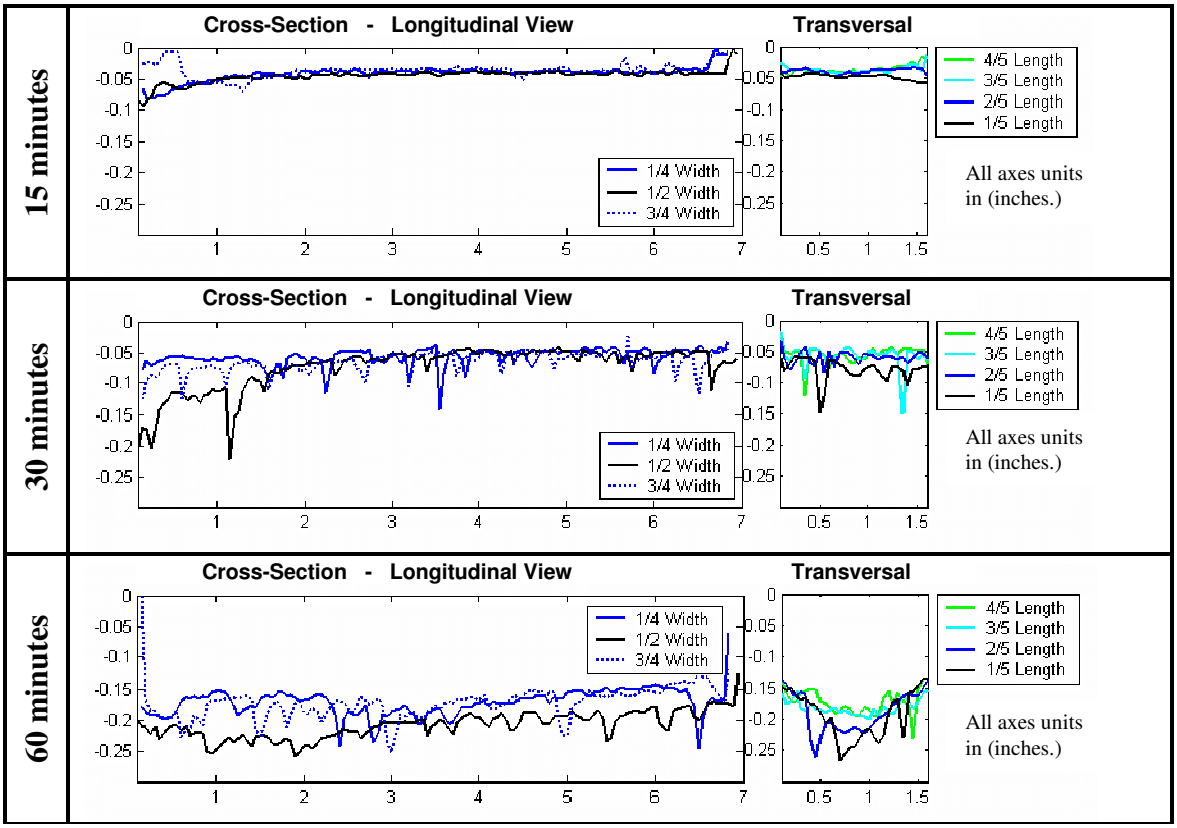

Fig. 5.49—Exp. 5—Longitudinal and transversal cross-section profiles.

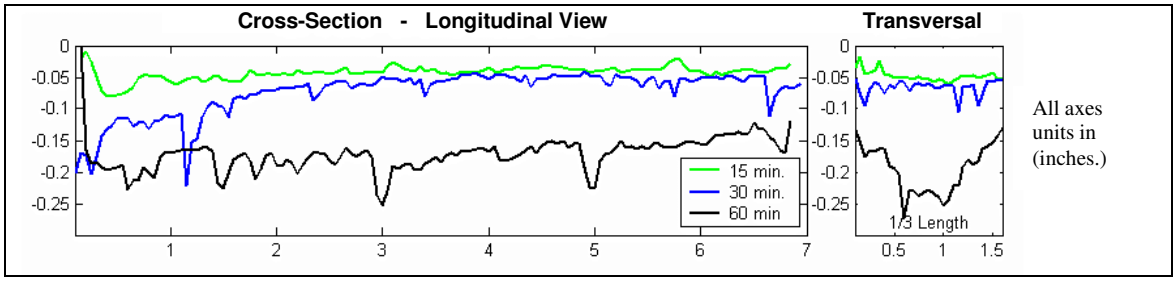

Fig. 5.50—Exp. 5—Comparative cross-section profile.

The roughness in Fig. 5.51 shows that the roughness at 30-min. is close to that at 60-min. This can be confirmed by the roughness parameters in Fig. 5.52, which shows that some of 30-min and 60-min. roughness parameters are close, but far from the 15-min. values.

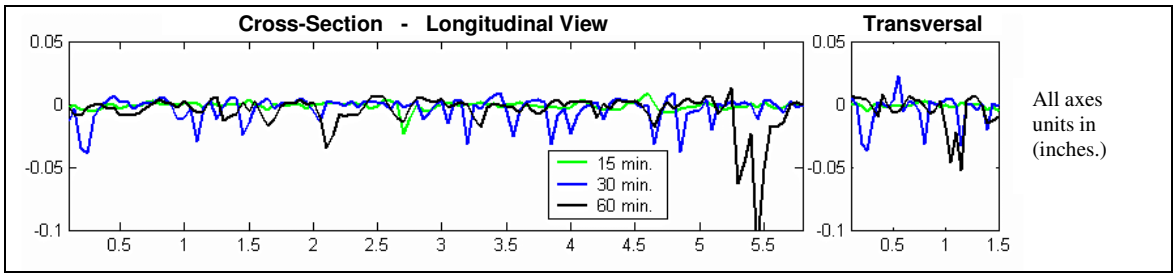

Fig. 5.51—Exp. 5—Comparative roughness cross-section profile.

Notice that the S_a, S_q, S_z and S_c parameters increase with contact time, but S_{Dq} and S_{dr} have a decrease from 30 minutes to 60 minutes. The raw meaning of this is that the surface area starts decreasing, and that the wormholes are not growing at the same rate that the surface is being dissolved. This process can be observed in Fig. 5.53 where the original data MRC plot of the 30 and 60 minutes curves overlap.

The conductivity measurements (Fig. 5.54) show that the 30-min. rock sustained the conductivity better than the other two rocks. That could be attributed to the large

channel created in this experiment. In contrast, the 60-min. rock conductivity falls along the same slope as the 15-min. contact time, even though it has more roughness.

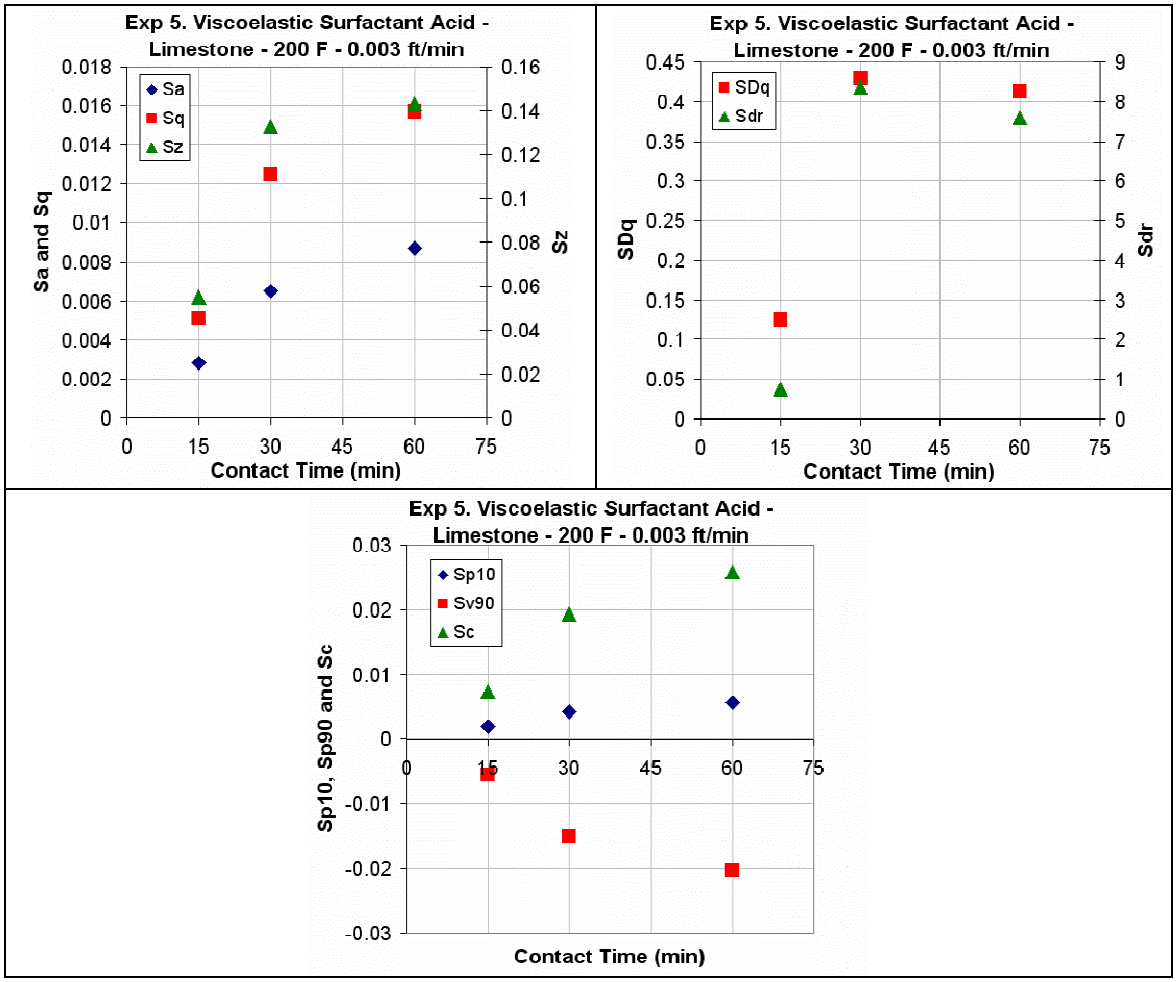

Fig. 5.52—Exp. 5—Roughness parameters.

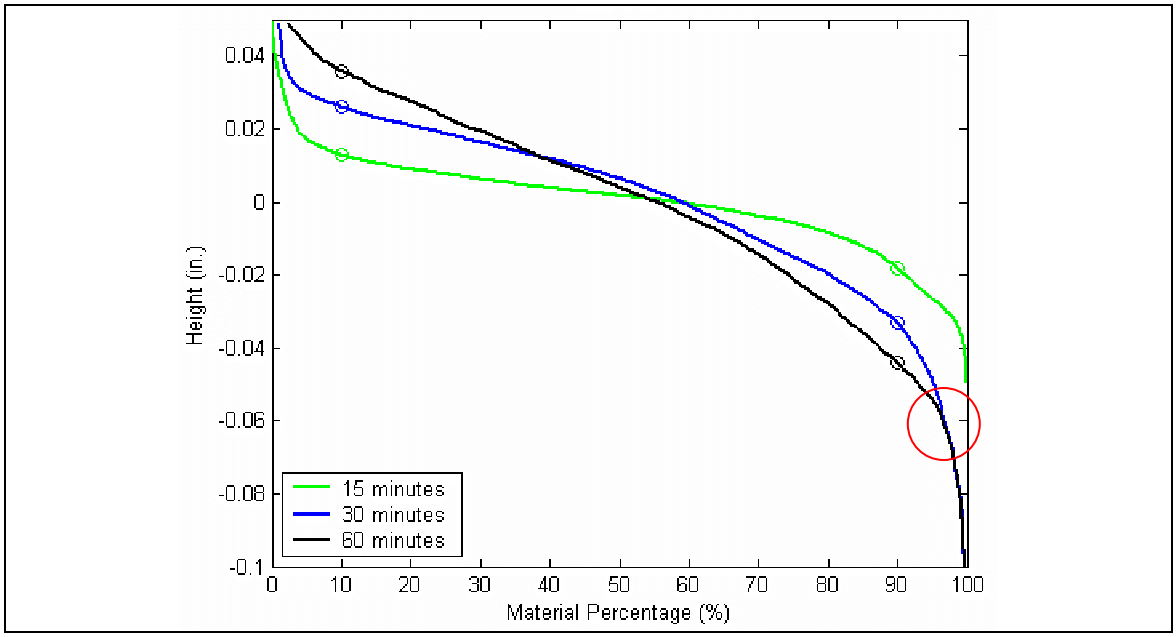

Fig. 5.53—Exp. 5—Original data material ratio curves.

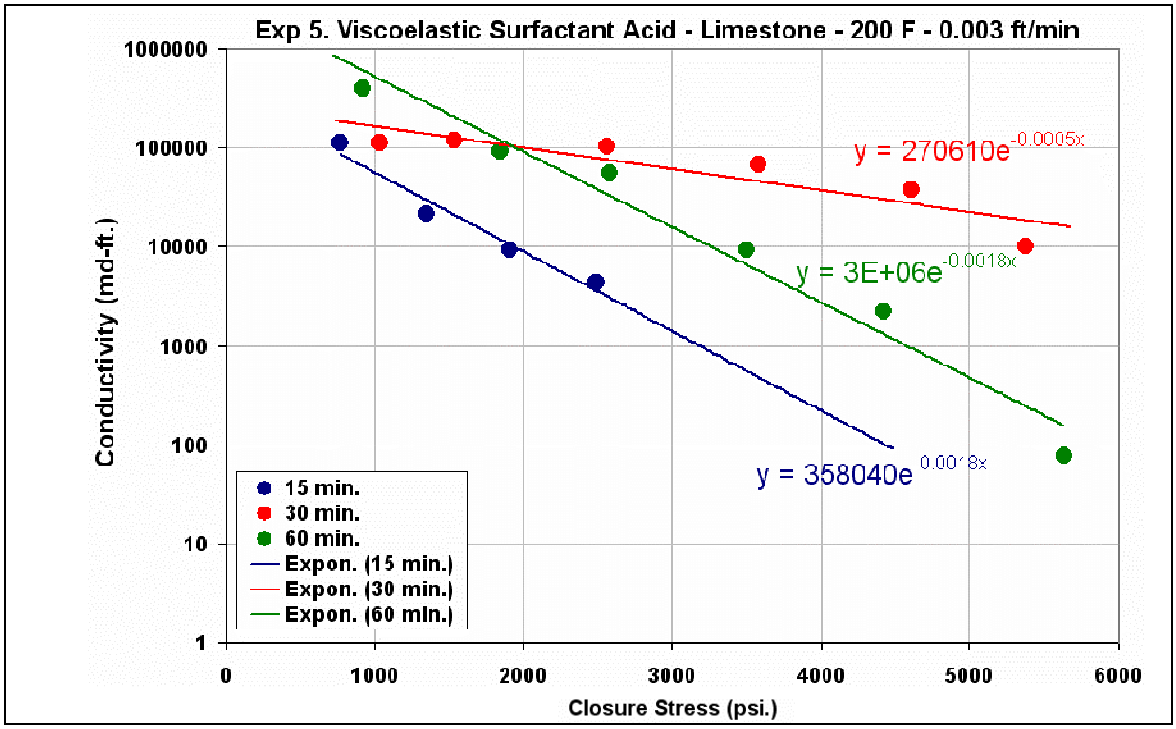

Fig. 5.54—Exp. 5—Conductivity measurements.

5.2.6. Experiment 6: Viscoelastic Surfactant Acid and Dolomite, 200°F, 0.005 ft/min.

The samples in Exp. 6 were treated with viscoelastic surfactant acid. Figs. 5.55, 5.56 and 5.57 show that dolomite has a different dissolution texture; as can be seen on the 3D valley figures, the wormhole density is higher. These wormholes are not as deep as those created in limestone. Unfortunately, the 30-min. rock had different nature than the other two pairs, that fact was apparent before the treatment was performed. Therefore, heterogeneities can be seen in the blue transversal strips on the filtered 3D view on Fig. 5.57. This fact also causes the 30-min. results not to represent the contact time sequence, but again it is clear that the acid system does not allow the wormholes to grow up after a certain point.

Fig. 5.58 shows that the 30-min. experiment has less volume dissolved at the surface than the 20-min. one. The dissolution pattern (Fig. 5.59) occurs along the entire surface and no channel or hydrodynamic effect is visible. Again, the 30-min. rock exhibits fewer wormholes and less dissolution than the 20-min. rock.

Fig. 5.60 compares the roughness profiles. The roughness increases somewhat between 10 an 20 minutes, but the 30-min. roughness is less than 20-min. Fig. 5.61 shows the roughness parameters. Here again, all the parameters show that the 30-min. rock roughness is less than expected.

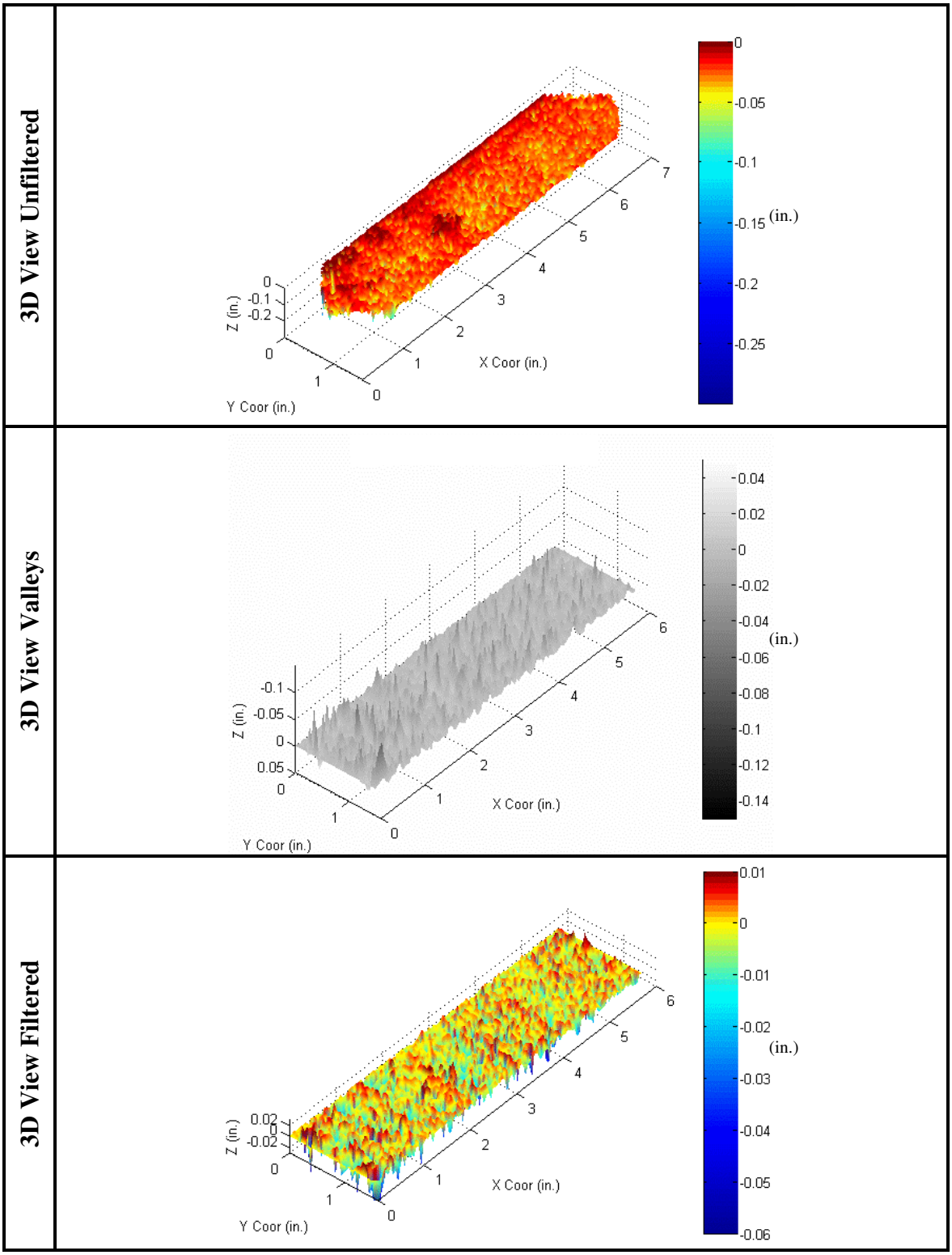

Fig. 5.55—Exp. 6: Visualization 3D surfaces of viscoelastic surfactant acid and dolomite—200 °F, 0.005 ft/min., 10 min.

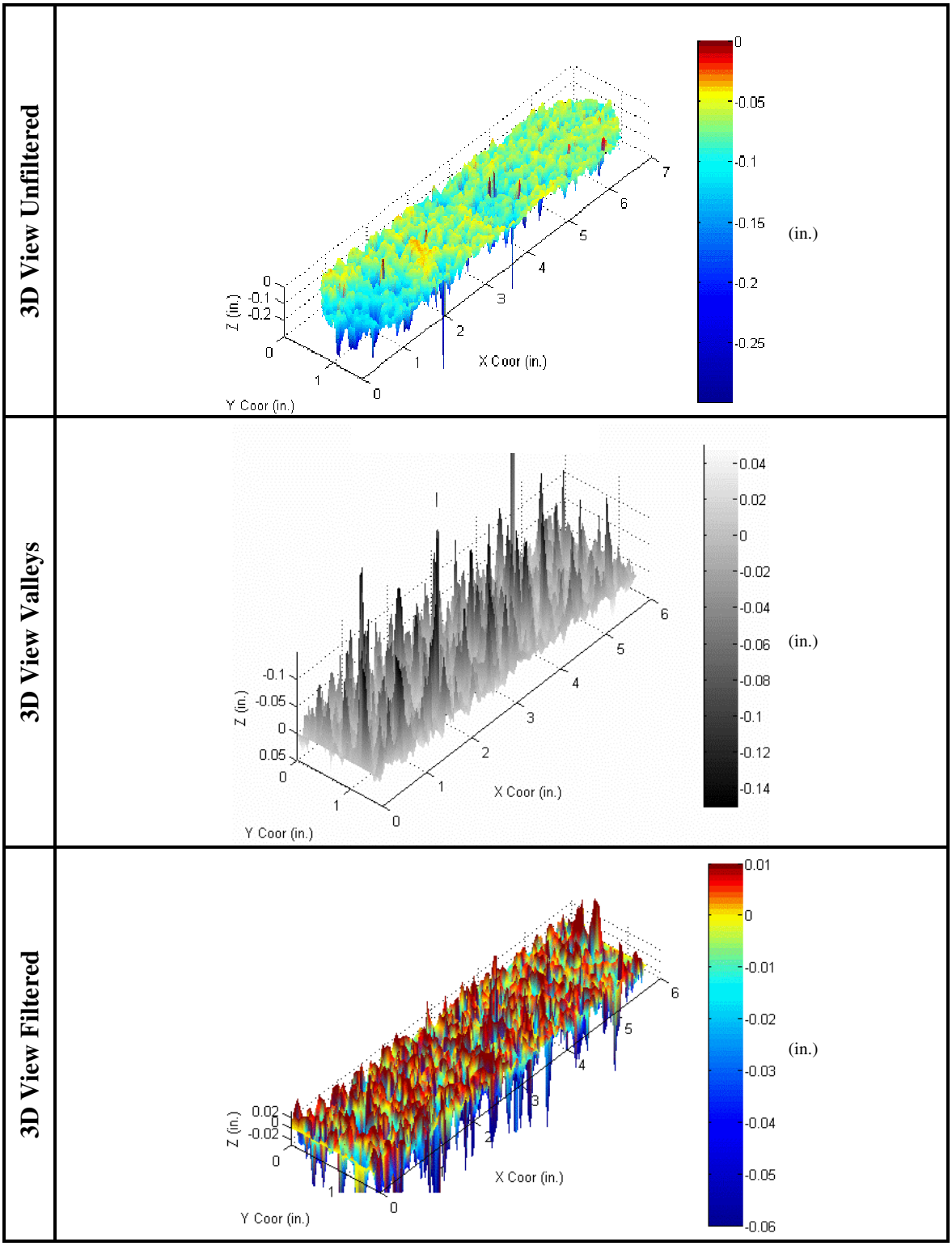

Fig. 5.56—Exp. 6: Visualization 3D surfaces of viscoelastic surfactant acid and dolomite—200 °F, 0.005 ft/min., 20-min.

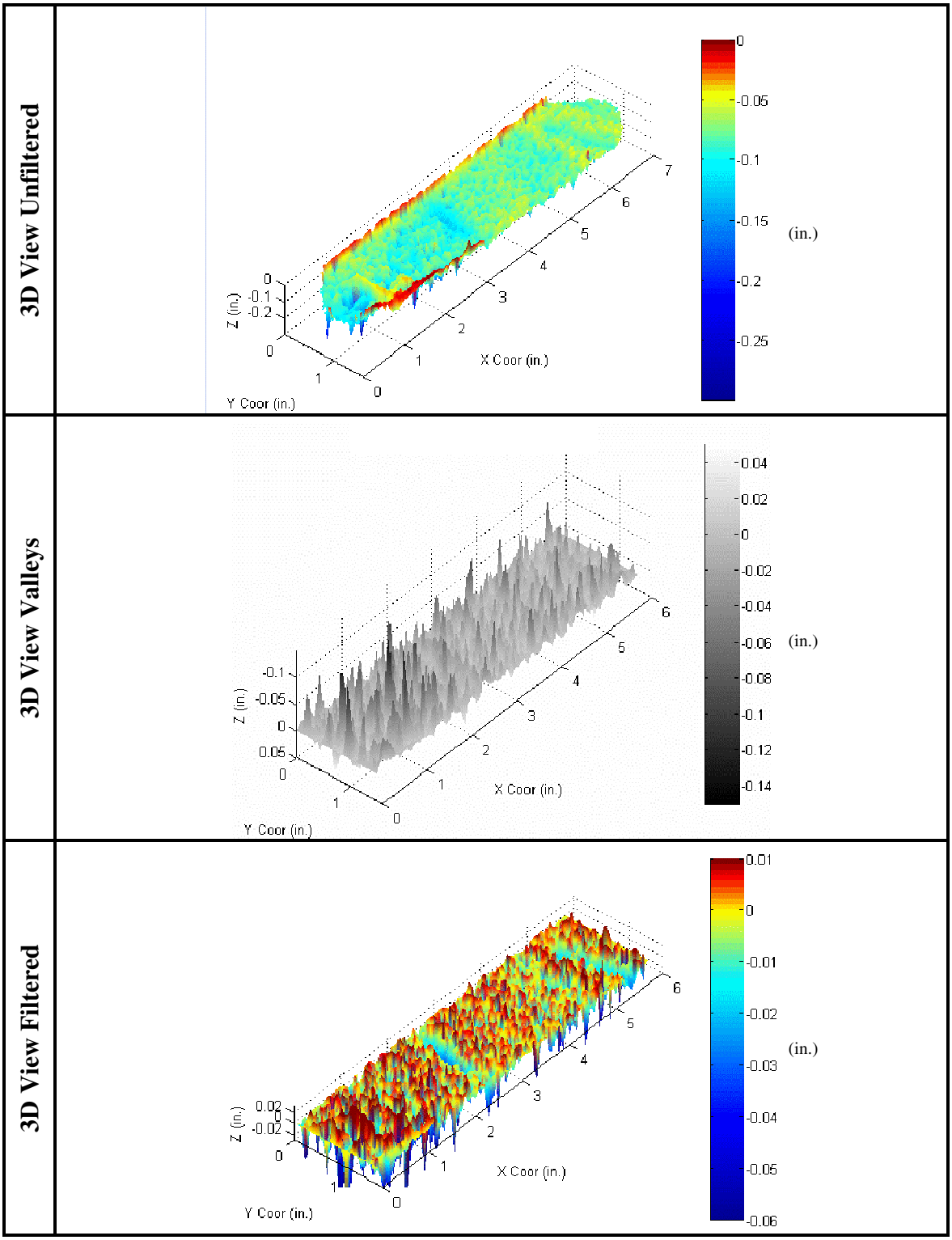

Fig. 5.57—Exp. 6: Visualization 3D surfaces of viscoelastic surfactant acid and dolomite—200 °F, 0.005 ft/min., 30 min.

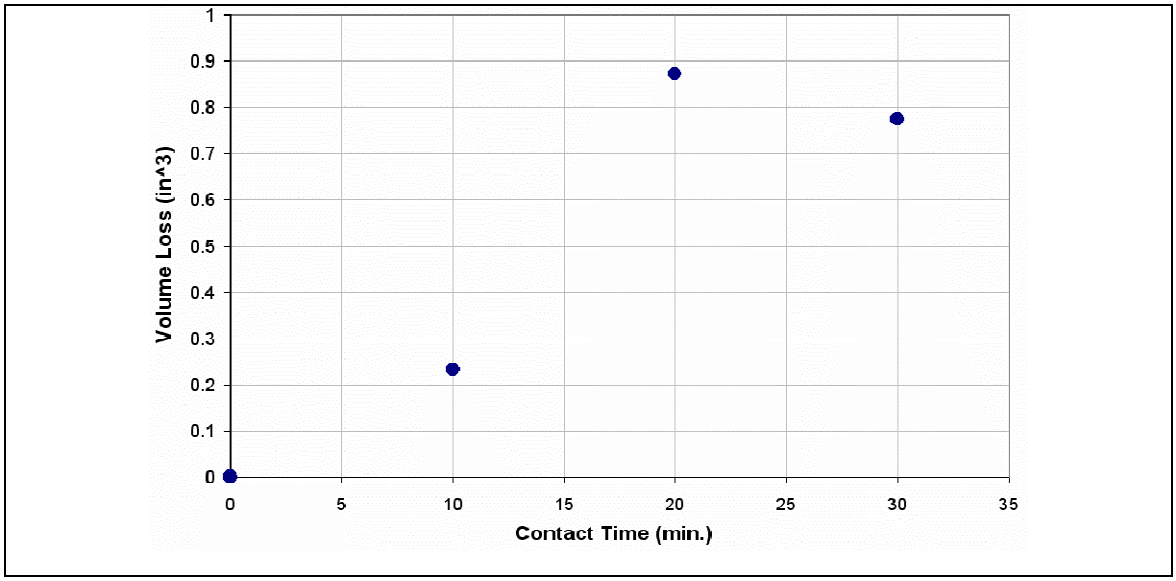

Fig. 5.58—Exp. 6–Volume of rock dissolved on rock surface.

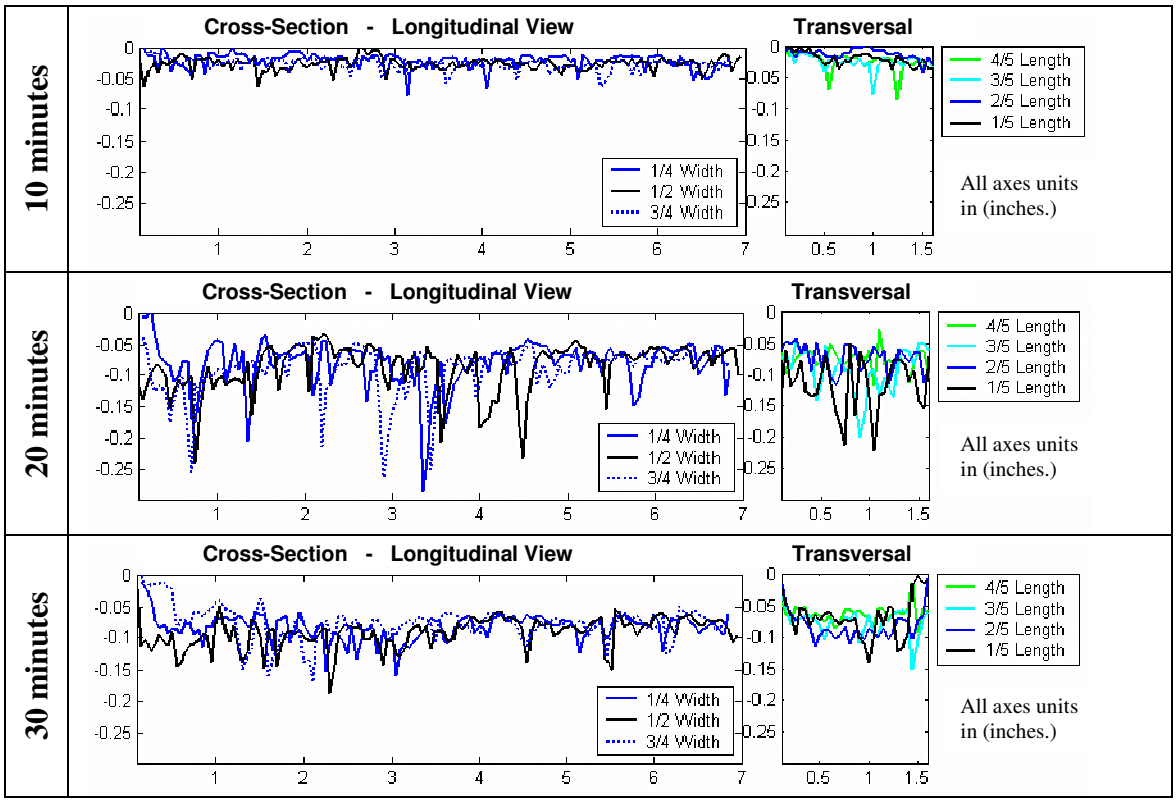

Fig. 5.59—Exp. 6—Longitudinal and transversal cross-section profiles.

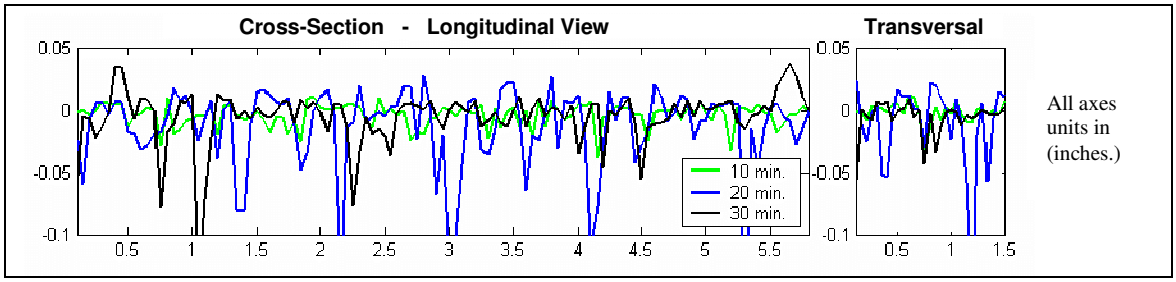

Fig. 5.60—Exp. 6—Comparative roughness cross-section profile.

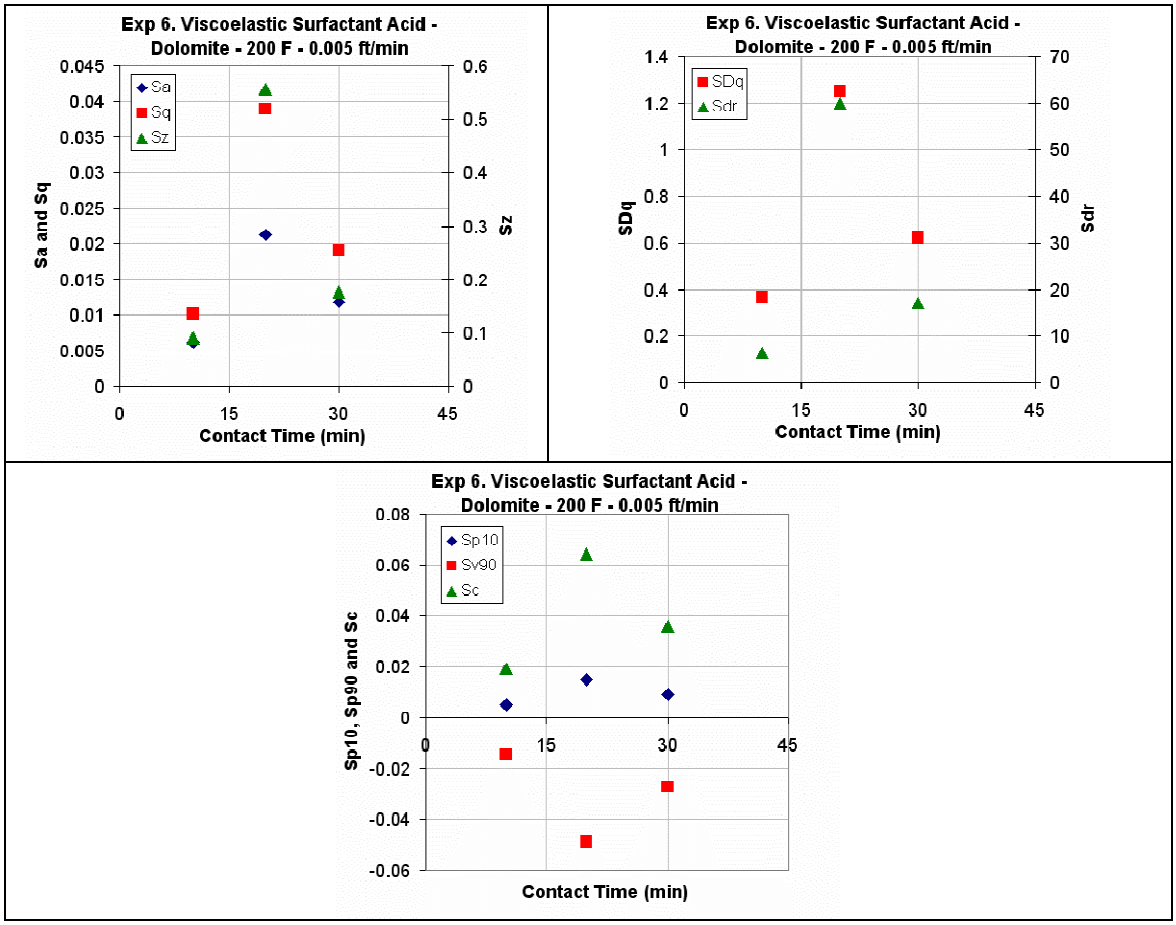

Fig. 5.61—Exp. 6—Roughness parameters.

Fig. 5.62 shows that the 30-min. rock MRC is between the 10- and 20-min. curves. Additionally, Fig. 6.63 shows that the higher slope of the 20-min. sample causes higher

values of the core depth parameter S_c than that observed in the limestone experiments. This is caused by the high-density wormholes that characterize the dolomite dissolution.

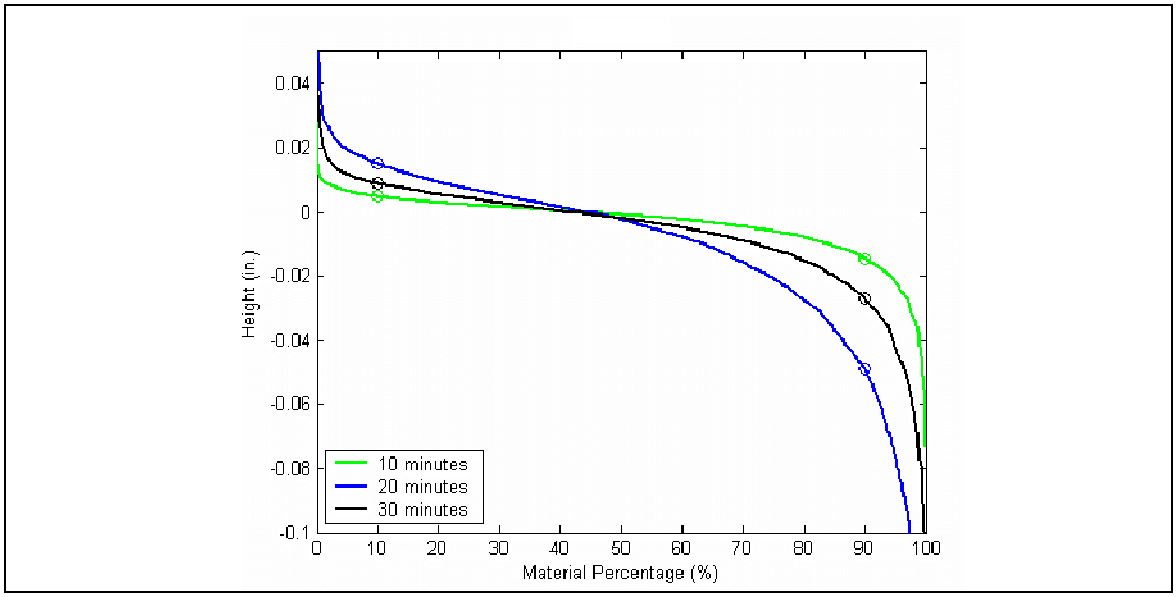

Fig. 5.62—Exp. 6—Roughness comparative of material ratio curves.

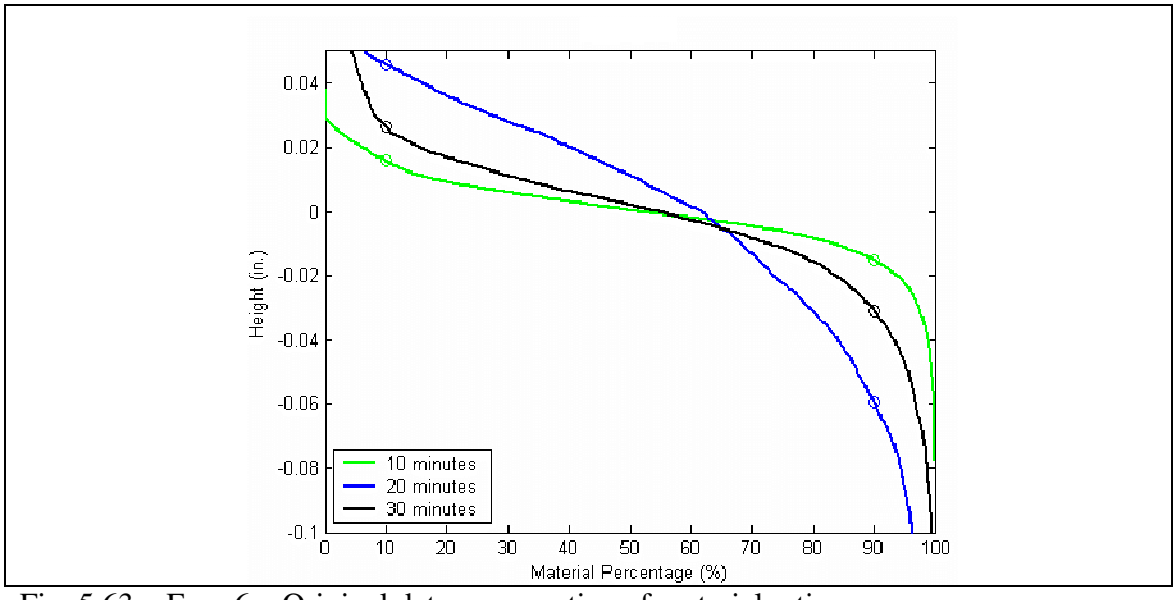

Fig. 5.63—Exp. 6—Original data comparative of material ratio curves.

The conductivity measurement on this set of rocks is shown in Fig. 5.64. The 10-min. contact time sample starts with low conductivity and continues without a considerable decrease. On the other hand, the 20-min. rock has high conductivity at low closure stress, but declines more rapidly than the 10-min. rock at high closure stresses. The 30-min. rock exhibits a behavior close to the 10-min. rock but with slightly higher conductivity decay.

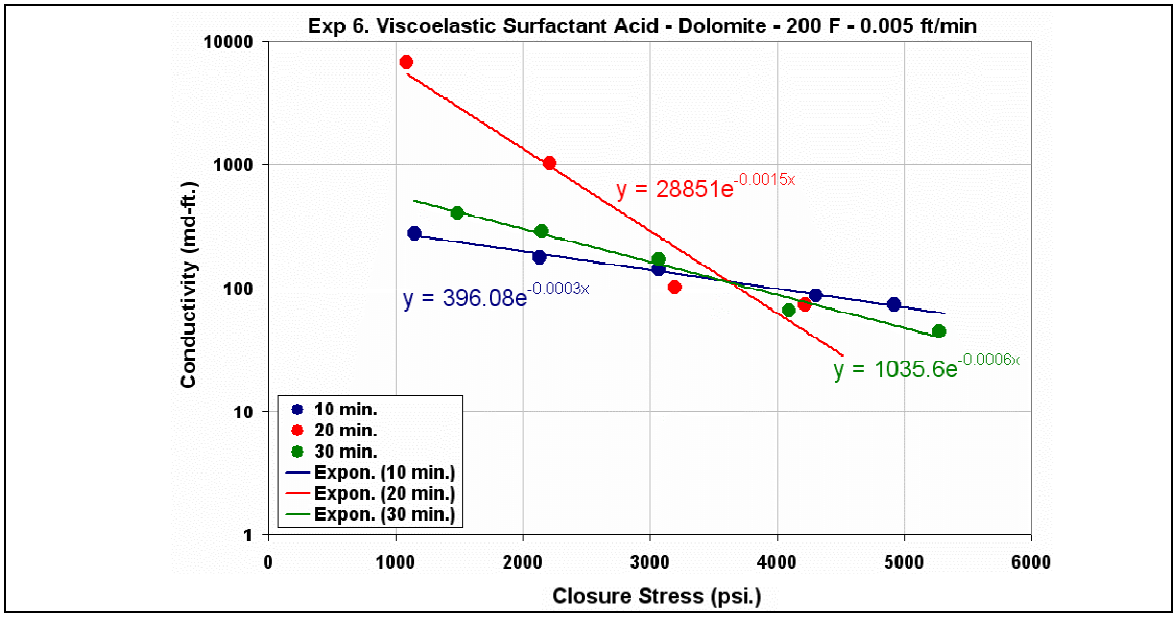

Fig. 5.64—Exp. 6—Conductivity measurements.

5.2.7. Experiment 7 and 8: Straight Acid and Chalk, 100°F, 0.005 ft/min.

Some of the rocks in Exp. 7 were inadvertently protected from the acid by a rock/clay component; therefore only 3- and 5-min. experiments are valid. The experiments were run at 100°F with 0.005 ft/min leakoff rate. The main characteristics of this rock are the big channel features, no roughness, and no large wormholes. The surfaces are presented on Fig. 5.65 and 5.66; notice that the roughness plot has been changed for a mean-line leveled plot. The amount of rock dissolved increases with contact time, as can be observed in Fig. 5.67.

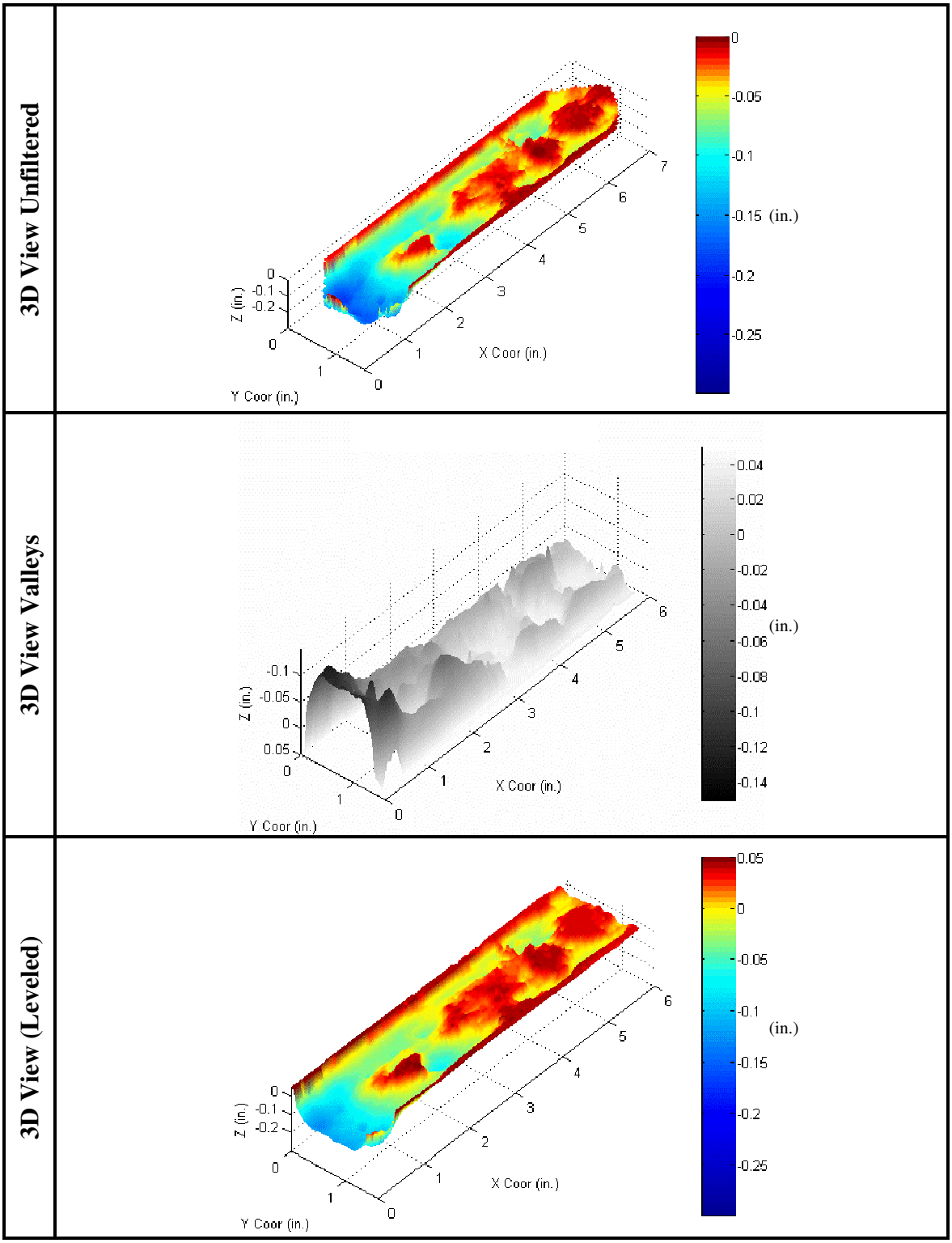

Fig. 5.65—Exp. 7—Visualization 3D surfaces of straight acid and chalk I—100°F, 0.005 ft/min., 3 min.

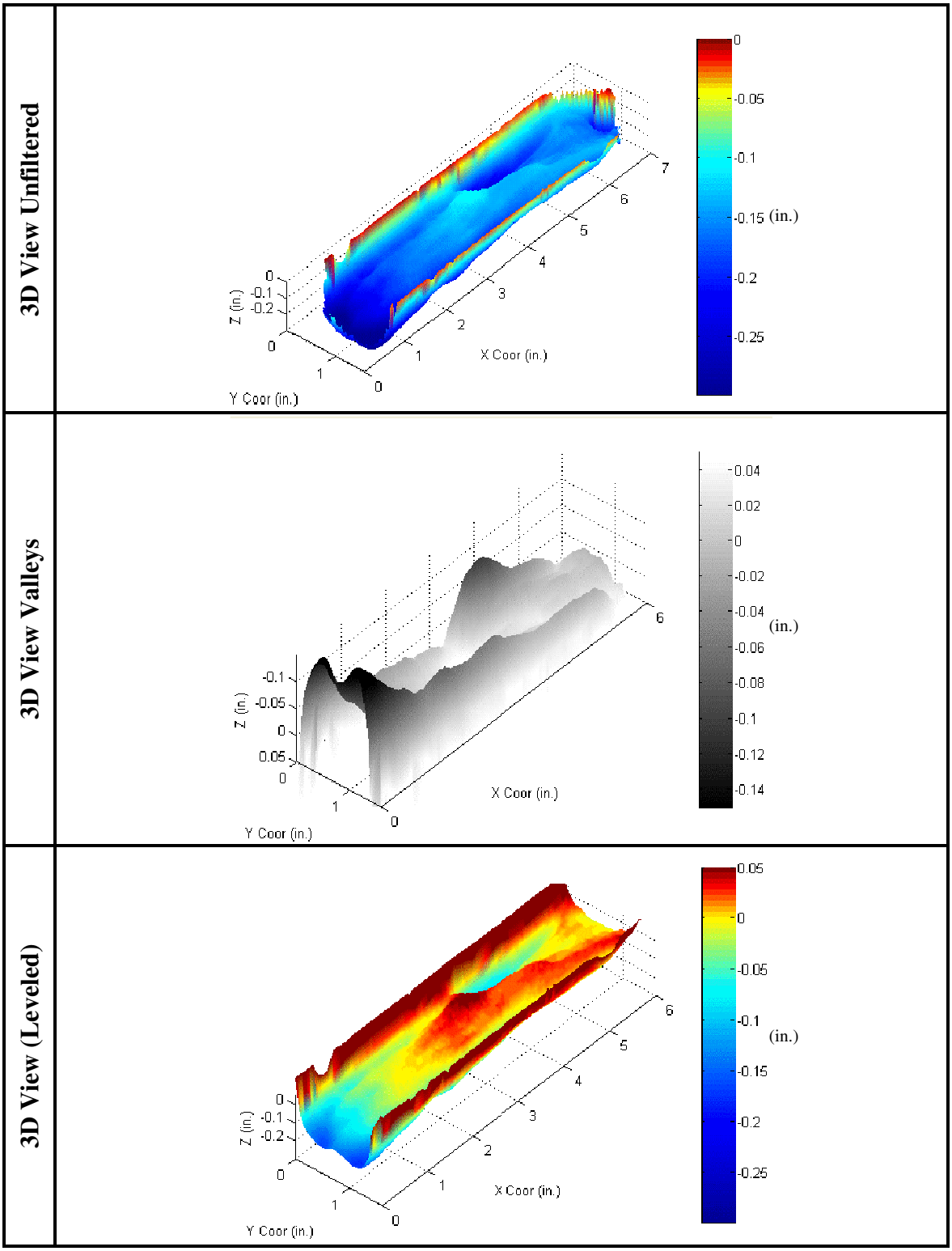

Fig. 5.66—Exp. 7: Visualization 3D surfaces of straight acid and chalk I—100°F, 0.005 ft/min., 5 min.

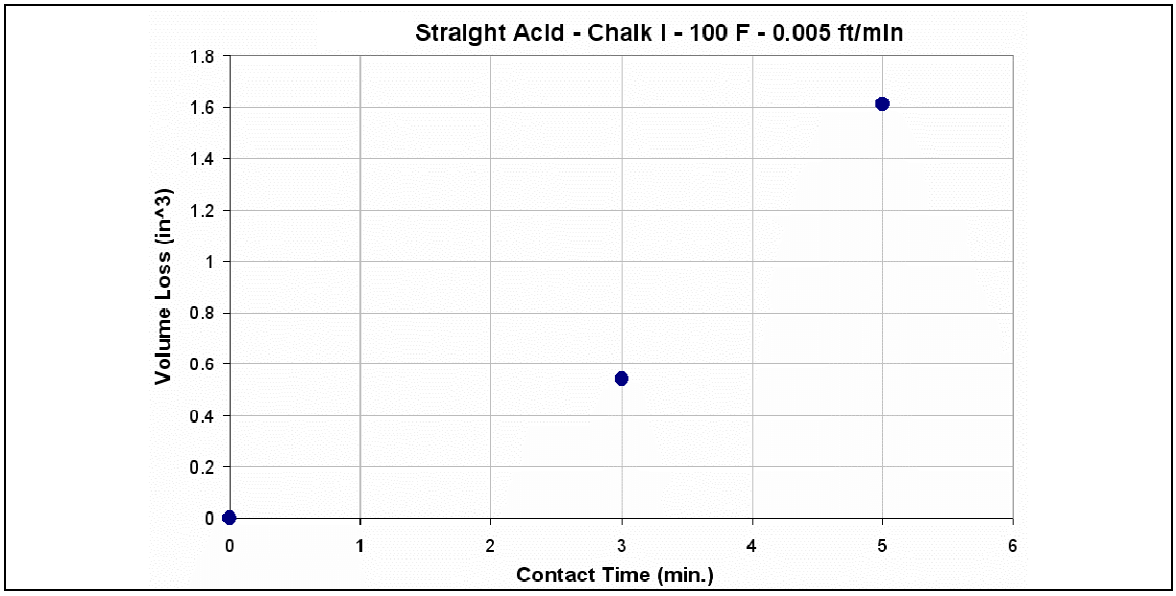

Fig. 5.67—Exp. 7—Volume of rock dissolved on rock surface.

Fig. 5.68 shows the profiles of both tests. The hydrodynamic effect is easily recognizable on the left side of the profile at both contact times.

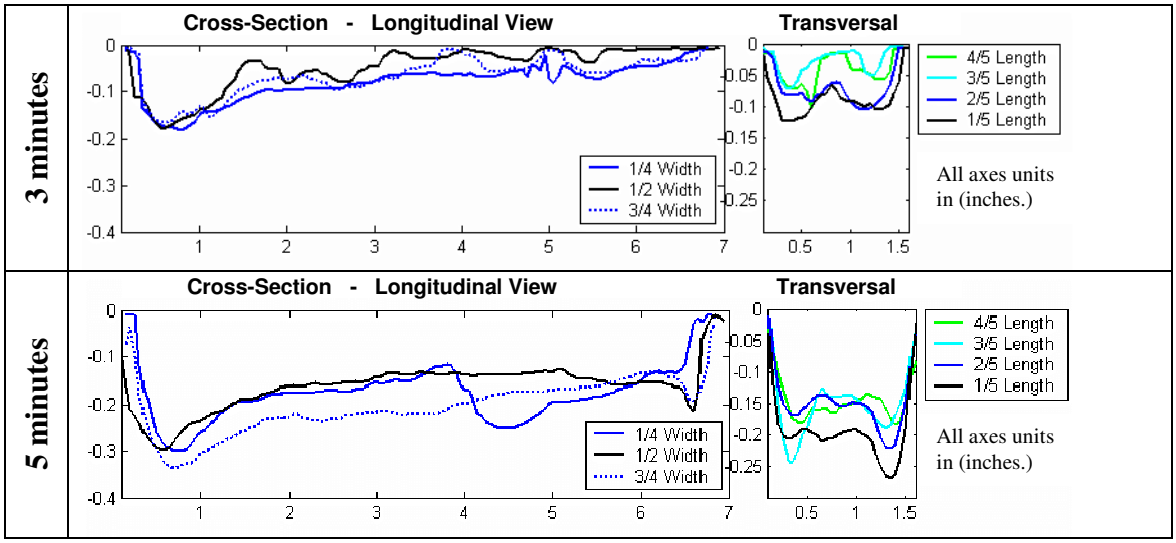

Fig. 5.68—Exp. 7—Longitudinal and transversal cross-section profiles.

Exp. 8 was performed at only one acidizing time, 7.5 minutes. The temperature was 100°F and the leakoff was 0.005 ft/min. Although these rocks differed from the chalk I rock, especially with respect to the strength, similar channel features occur on the sample (Fig. 5.69). No conductivity measurements were conducted.

The profile of Exp. 8 can be seen in Fig. 5.70. The plot shows that the hydrodynamic effect has affected the rock at the inlet.

Since the main features of both experiment channels are on the waviness scale, there is no sense in filtrating them for roughness. Therefore, characterization parameters in Fig. 5.71 have been calculated using the original data set. Those plots combine Exp. 7 and 8; although they are not filtered, all of them increase with the contact time.

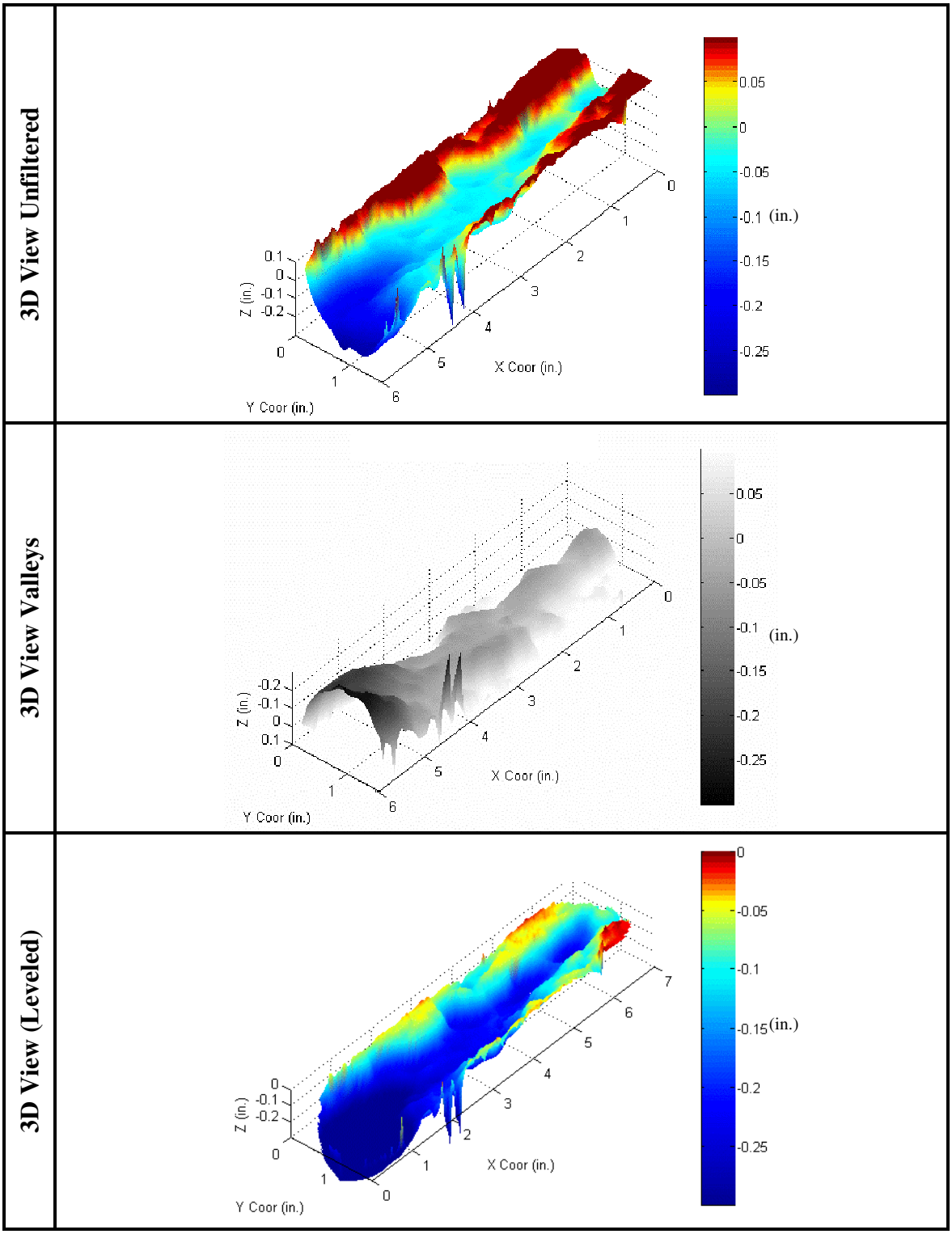

Fig. 5.69—Exp. 8: Visualization 3D surfaces of straight acid and chalk II—100°F, 0.005 ft/min, 7.5 min.

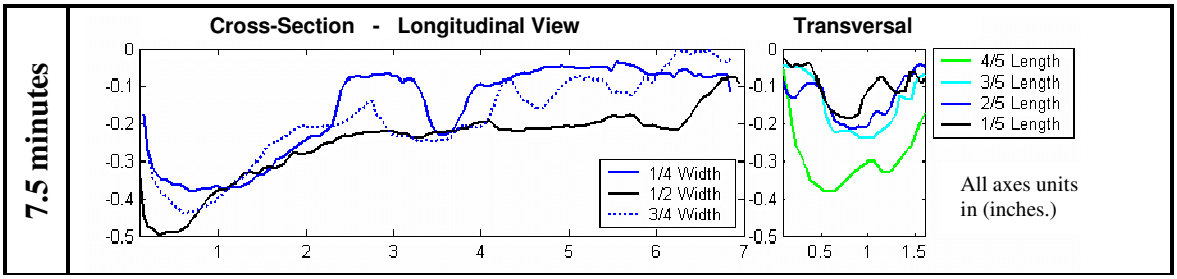

Fig. 5.70—Exp. 8—Longitudinal and transversal cross-section profiles.

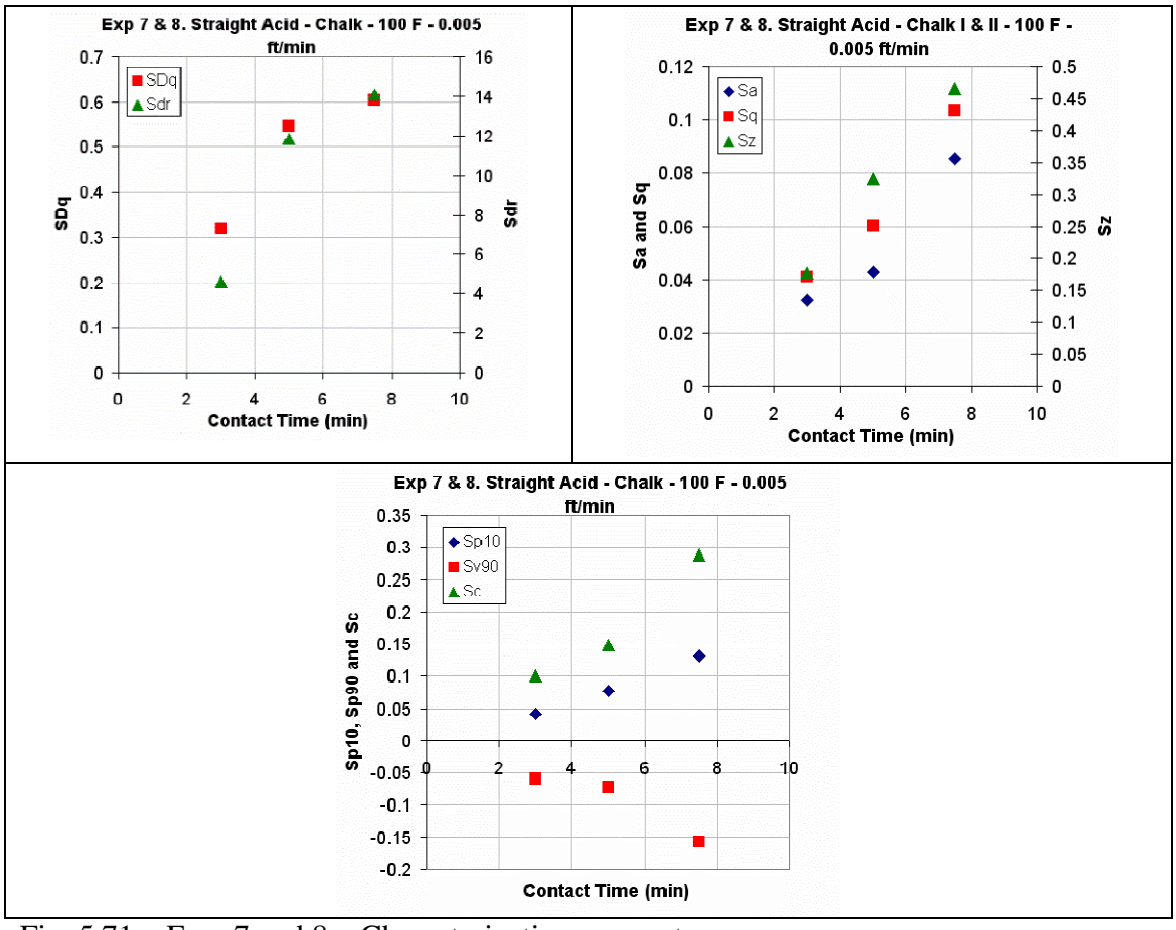

Fig. 5.71—Exp. 7 and 8—Characterization parameters.

6. CONCLUSIONS AND RECOMMENDATIONS

This study showed that the profilometer can represent textural effects of rock dissolution, and models function predictably. However, comprehensive understanding of the effect will require further analysis and testing.

6.1. Characterization Technique

Visualization: The visualization plots were useful in identifying the texture of the acidized surfaces, especially those related with visualizing the hydrodynamic channels and chalk rock that could not be perceived by the naked eye. The Z inverted gray 3D surface was useful to recognize the occurrence and magnitude of the wormholes; the filtered color 3D surface plot revealed rock heterogeneities and the pure action of the dissolution process without the hydrodynamic effect. The longitudinal and transversal plots were more useful to identify uneven dissolution from one experiment to another. The 2D profile plots are helpful to identify dissolution progress and channel patterns.

Statistical Amplitude: Although S_a (mean), S_q (standard deviation) and S_z (ten point height) all responded the same to the degree of roughness, S_q is logically the most reliable of all three. S_a may be skewed by the normalization process that subtracts the value of valleys before the mean is calculated, which might result in higher than accurate values, S_z may also overestimate if the laser beam reflects on anomalous bright spot on the sample. Sq is unaffected by either of these irregularities, so its results are likely more consistent. Using all three would be redundant.

Neither S_{sk} (skewness) nor S_{ku} (kurtosis) was included in the characterization because the S_z they may be highly affected by data set outliers. Both S_{sk} and S_{ku} can lead to misinterpretations when they are not strictly applied to Gaussian distributions.

Hybrid: The hybrid parameters S_{dr} and S_{Dq} represented the relationship between the viscoelastic properties of the surfactant fluid and the growth of wormholes, S_{dr} is the more reliable parameter because it represents percentage of increase at surface area; using both would be redundant.

Functional: The core roughness depth S_c represents both the increasing roughness and the unfiltered material ratio curve, which describes the empty space left by the dissolution. The volume of rock dissolved is useful to understand the degree of dissolution and to verify the validity of the data when longer contact times did not mean big increases on roughness.

6.2. Profilometer

The profilometer hardware and software has been setup, tested, and validated as a useful measurement tool to measure the acidized surface topography, and programs have been developed to perform data preprocessing and visualization and to analyze surface characteristics.

The software calculates the amount of rock dissolves during the test by subtracting the data before and after acidizing. Those values are useful to verify the validity of the experiment, and they can be used as input for future correlation and dissolution modeling.

The technique presented on this work used a filter to separate the two components of the surface data, the roughness and the waviness. The roughness represents the effect of the constant dissolution of the acid along the rock surface, and it is adequate to describe the surface characteristics. The waviness represents the surface features related to localized

dissolution, like the hydrodynamic effect at the inlet of the cell or the less dissolved areas that appear when the rock has geological heterogeneities.

6.3. Experimental Results

Conclusions about treatment conditions and conductivity are premature because of the diverse change of variables for the entire sets of experiments. As shown by Section 5, the texture of the surface responds very differently depending on the type of rock treated and the fluid system used.

The Change on Fluid Type: The fluid system not only creates different degrees of topography but it also can stop the increase in roughness as seen in Exp. 5. This different type of behavior illustrates that any modeling effort must be independent for each type of fluid.

The Change on Rock Type: When Dolomite is treated with viscoelastic acid; it presents more roughness than the limestone. The dolomite lost its volume faster than the limestone, and that it gains empty space much faster, too.

Change on Leak off Rate: Higher leakoff increases the roughness and the amount of rock dissolved of the surface when gel acid is pumped.

The Change on Temperature: The experiment of high temperature resulted in much higher roughness. Additionally, the proportion of the dissolution is very high.

Conductivity: Since different fluids cause different etching patterns and different degrees of dissolution, it is not surprising that they may also create different degrees of

rock weakening. Therefore, the weakening effect may hide the topography interaction in a way prohibits definite conclusions regarding the conductivity response.

When rocks with hydrodynamic effects are put together in the load frame, the channel will not close since its borders will prop it open even at higher loads. That leads to measurement problems: First, the surfaces do not interact along the entire length of the sample, and second, the flow through the channel will overcome the flow through the pressed surfaces. Therefore, the conductivity measurements for most cases can not be related to the roughness parameter S_q since the roughness features are not the ones that direct the flow.

6.4. Recommendations About Conductivity

We recommend the following procedures to improve our understanding of the relationship between conductivity and rock strength.

1. Take rock strength loss into consideration as one of the most important parameters to determine the conductivity response. Measure the rock strength before and after dissolution and add that information to future data sets. Watch for correlation between roughness and rock weakening.

2. Measure the rock compressive strength of pure, nonacidized fractured rock to create a basic understanding of the conductivity closure-stress phenomenon. This knowledge will serve as a basis for the understanding of conductivity of acidized rocks.

3. Perform roughness measurements of the rocks after they come out of the conductivity cell. To analyze the change of the curve, compare the material ratio

curve with the original surface. The material ratio curve may be the basis for modeling conductivity.

4. Improve the conductivity measurement, assuring the nitrogen flows through the rock and not around it. Additionally, use water instead of nitrogen to measure the conductivity so the measurements can be performed faster and with minimal calculation errors.

5. Improve the conductivity stack measurements. Starting at zero load, at small pressure increments (e.g. 100 psi.) and continue to come final pressure such as 7,000 psi.

6.5. General Recommendations

We offer the following recommendations for quality management of future results.

1. Avoid using rocks with heterogeneities or different rock qualities during a set of experiments since heterogeneities alter the sequence of results. This includes labeling and placing of the rocks in the cell carefully. Follow the manual instructions about labeling of the rocks to avoid wrong scanning or misalignment.

2. Explore ways to optimize the fast Fourier transformation of the original data to filter special features from the topography.

3. Incorporate the material ratio curve to model the interaction of the acidized surfaces under closure stress. Use accurate profilometer data and the material ratio curve as presented in the ISO Standard[17] as the next research step to understand the process.

4. To analyze the differences between fractured surfaces and cut surfaces, develop a technique to fracture the rock instead of cutting it.

5. Use the original volume or the dissolved value of the rock to verify the Neirode & Kurk correlation behavior and also as a tool for the future correlation.

6. Take microcopy pictures of the pure and acidized rock to observe the effects of acid dissolution on rock weakening.

7. Explore changes in the conductivity cell to avoid hydrodynamic effects at the rock inlet.

8. Perform conductivity measurements on channeled rocks and verify its response on the amplitude and hybrid parameters.

REFERENCES

1. Barron, A.N., Hendrickson, A.R., and Wieland, D.R.: "The Effect of Flow on Acid Reactivity in Carbonate Fracture," *JPT* (April 1962) 409.

2. Broaddus, G.C., Knox J.A., and Frederickson, S.E.:"Dynamic Etching Tests and Their Use in Planning Acid Treatments," paper SPE 2362 presented at the 1968 SPE Oklahoma Regional Meeting, Stillwater, Oklahoma, 25 October.

3. Williams, B.B. and Nierode, D.E.:"Design of Acid Fracturing Treatments," *JPT* (July 1972) 849.

4. Nierode, D.E., and Kurk, K.F.: "An Evaluation of Acid Fluid Loss Additives, Retarded Acids, and Acidized Fracture Conductivity," paper SPE 4549-MS presented at the 1973 SPE Annual Fall Meeting, Las Vegas, Nevada, 30 September-3 October.

5. Beg, M.S., Kunak, A.O., Gong, M., Zhu D., and Hill, A.D.: "A Systematic Experimental Study of Acid Fracture Conductivity," paper SPE 52402 presented at the 1996 SPE International Symposium on Formation Damage Control, Lafayette, Louisiana, 14-15 February.

6. Ruffet, C.S., Féry, J.J., and Onaisi, A.: "Acid-Fracturing Treatment: A Surface-Topography Analysis of Acid-Etched Fractures To Determine Residual Conductivity," paper SPE 38175 presented at the 1997 SPE European Formation Damage Conference, The Hague, 2-3 June.

7. Gong, M., Lacote, S., and Hill, A.D.: "A New Model of Acid Fracture Conductivity Based on Deformation of Surface Asperities," *JPT* (September 1999) 206.

8. Dong, C., Zhu, D., and Hill, A.D.: "Modeling of the Acidizing Process in Naturally Fractured Carbonates," *JPT* (December 2002) 400.

9. *Acuity Laser Measurement Manual* "AccuRange 200tm Laser Displacement Sensor User's Manual," Schmitt Measurement Systems, Inc., Portland, Oregon. (2004).

10. Creasy C.F.M. and Craggs C.: *Applied Surface Modeling*, Ellis Horwood Ltd., Chichester, England (1990) 61-75.

11. Stout, K.J.: *Development of Methods for the Characterization of Roughness in Three Dimensions*, Prenton Press., London (2000).

12. Thomas, T. R.: *Rough Surfaces*, Longman Inc. New York (1982).

13. "Probability Distribution," http://en.wikipedia.org/wiki/Probability_distribution/, 15 September 2006.

14. *ISO 4287, Geometrical Product Specifications (GPS) – Surface Texture: Profile method- Terms, Definitions and Surface Texture Parameters*. Geneva, Switzerland (1997).

15. *ISO 13565-1, Geometrical Product Specifications (GPS) - Surface Texture: Profile Method; Surfaces Having Stratified Functional Properties. Part 1: Filtering and General Measurement Conditions.* Geneva, Switzerland (1998).

16. Lee, Y.-H., Carr, J. R., Barr, D. J., Haas, C. J.: "The Fractal Dimension as a Measure of the Roughness of Rock Discontinuity Profiles," *Int. J. Rock Mech. Min. Sci. & Geomech. Abstr.* (1990) **27**, No. 6, 435.

17. *ISO 13565-2, Geometrical Product Specifications (GPS) - Surface texture: Profile Method; Surfaces Having Stratified Functional Properties. Part 2: Height Characterization Using the Linear Material Ratio Curve.* Geneva, Switzerland (1998).

APPENDIX A

PROFILOMETER MANUAL

Section 3 of this thesis contains a description of the profilometer and its components. This appendix contains a step-by-step procedure to operate the profilometer.

1. Starting the Software and Hardware

First double click on the LabView file (profilometer.vi) and wait until the software console appears. Fig. A-1. Then press the button with the arrow on the upper right corner of the LabView window.

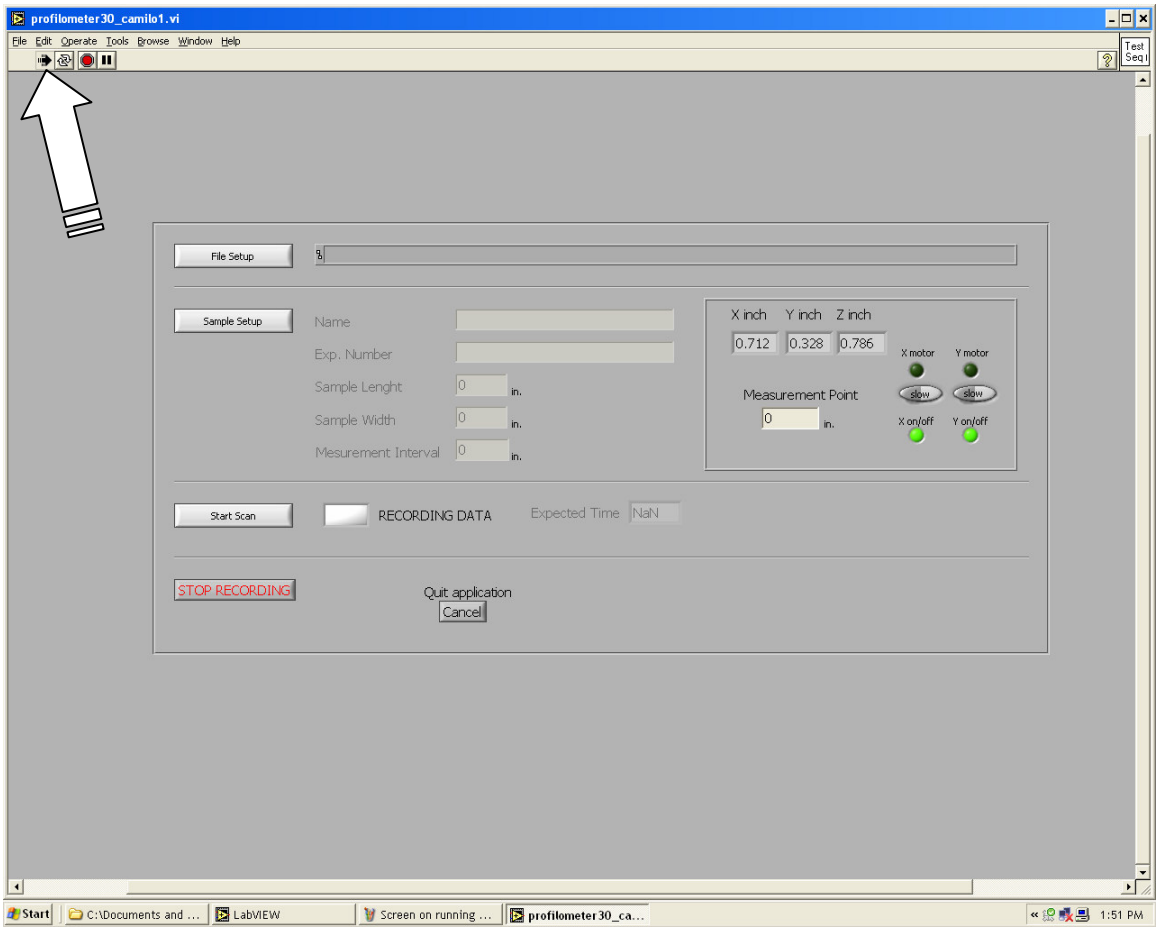

Fig. A-1. LabView profilometer main screen.

Activate the red power source switch on the control box front panel (Fig. A-2). After a few seconds the distance readings start appearing on the software window.

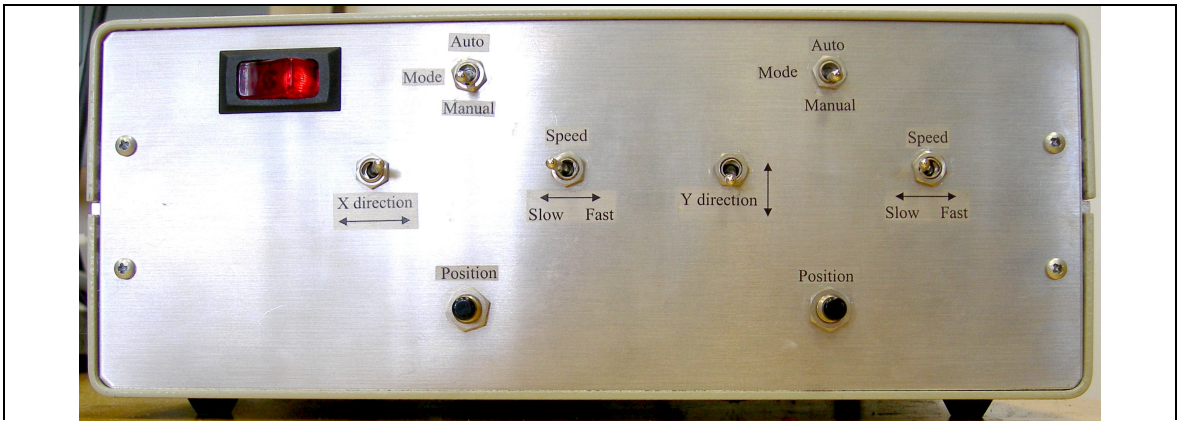

Fig. A-2. Control box front panel.

2. Preparing the rock sample:

Before any other step, make sure of the following:

Use prepared rocks that have rubber compound around then; each rock should have both rock surfaces clear and free of any excess of rubber (Fig. A-3).

Fig. A-3. Cleaning the rock surface.

Verify that the surfaces to be scanned correspond to each other at the time they were cut.

Put both rocks as pictured in Fig. A-4, and label as indicated in Fig. A-5.

The label should have three letters and a one- or two-digit number. The rock on the top is rock "A" and the rock on the bottom is rock "B". The name is written on the center of the rock and repeated on the corner of each sample. The texts are first engraved using a

pin tack and then rewritten using the paint pen. Additionally, the letters “OT” (On Top) are engraved and marked on the side of the sample. Finally, draw two lines to show which ones are the fracture faces.

Fig. A-4. Position of the rocks.

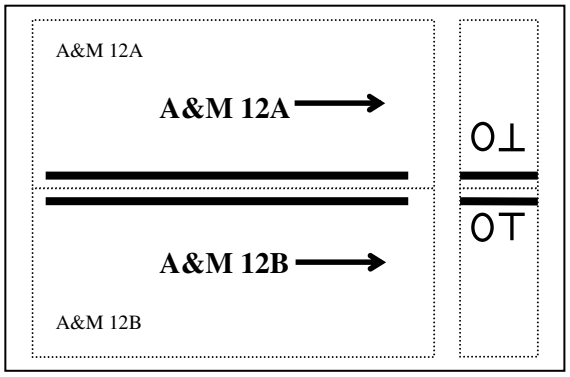

Fig. A-5. Labeling.

3. Placing the Sample.

Clean the aluminum table (Fig. A-6) of any dirt that can alter a stable rock placement.

Place the rock sample on the table and secure it using the table screws. Make sure the sample is secured firmly against the four table rods (Fig. A-7).

Always make sure that the arrow of the flow direction labeled on the sample points left to right on the profilometer. That guarantees that the rock is scanned in the same position before and after the treatment.

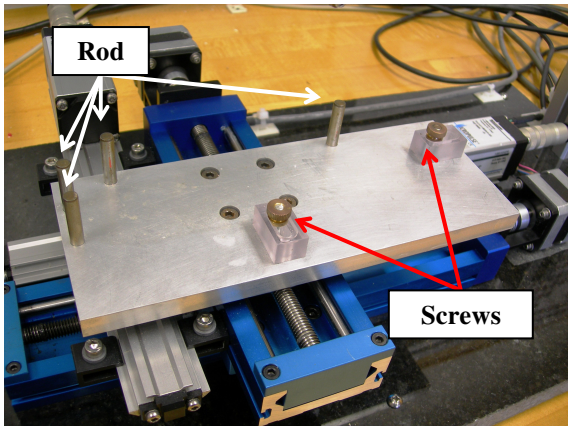

Fig. A-6. Table components.

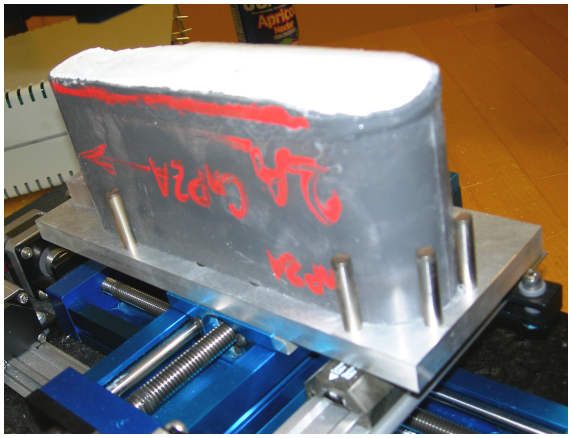
Fig. A-7. Firm rock placement.

4. Adjust the Laser Sensor.

Adjust the laser sensor using the vertical milling table screw to assure full range measurements over the surface topography.

For this propose, put the aluminum ruler on the surface and across the laser beam and verify that you have readings between 0.9 and 0.999 on the Z direction. (Fig A-8)

4. Position Laser at Zero X, Y value.

On the control box front panel, put both switches labeled “Mode” on Manual position. Put the switches “Speed” on Fast and proceed to press the Position button. This causes the motors to move the table.

The controls on the right move the table in the Y direction and the ones on the left in the X direction.

Look at the software window X and Y position indicators, and keep controlling the motor until both are exactly at zero position. When the table position is close to zero, it will be necessary to switch the Speed controls to Slow and press the Position button quickly in order to get the zero value; If you over pass the zero, change the Direction and continue with the positioning.

When finished switch both "Mode" buttons to Auto Position.

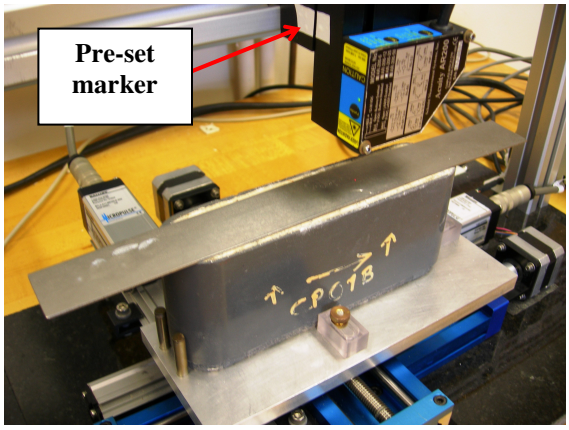

Fig. A-8. Use of ruler to procure full range measurement.

5. Input the file and scan information.

On the software window, first click on the File setup button and select a location to save the data file. Then press the button Sample Setup to open the window shown in Fig. A-9. Start filling the boxes first inputting the name of the experiment or important information that is relevant to the sample; then, input the experiment number as it is labeled on the rock sample. Since all the rocks have the same dimensions, input 7 as the sample length, and 1.7 as the sample width. Finally input as measurement interval 0.05 for a 2 hours scanning, or 0.025 for a 4 hour scanning.

Press OK.

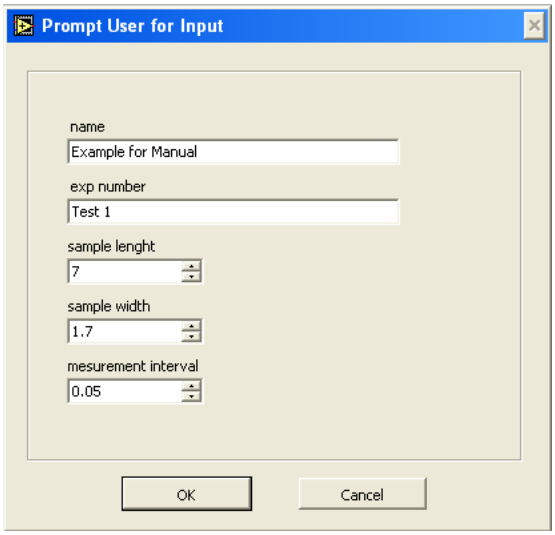

Fig. A-9. Establishing the measurement settings.

6. Start Scanning

Click on the Start Scan button on the software screen. A window will remind you to have the mode switches on Auto mode. Click OK. Immediately the laser will start moving along the sample backward and forward. At the end of the scan, the laser will stay still at the lower right corner of the sample. Turn off the profilometer and then stop the LabView software application.

Safety Measures

Do not leave the equipment working without supervision; some input mistakes or low power surge can make the controls fail and then cause damage to the parts.

If by mistake you need to stop the scanning, first stop the application window by pressing the stop button on the upper menu of the software. Close the software window and then reopen the LabView file and restart the setting process.

Never turn off the profilometer while running the LabView application; that will cause a dangerous abnormal response even if you reset the program. In that case, turn off the profilometer, close the software, and start from the beginning.

Make sure that the measurement interval is a multiple or fraction of 0.05 in. If it is not, it will cause a malfunction that will damage the equipment.

Make sure to keep the same laser sensor height for the before and after measurements; if not, make sure to record the difference in height by measuring it on the marker of the laser screw milling table. Avoid leaving the samples on the table for long periods of

times because although they are clean they still have acid vapors that can cause corrosion of the table. Also, keep the rock from touching the laser sensor since it can scratch the lenses and damage the device. Finally, keep rock particles from falling onto the milling table screws, and lubricate the screws after each 50 scans using only lubricant for plastic nuts (Trigel-300s).

APPENDIX B
MATLAB FUNCTIONS

MatLab was used to process the data obtained from the profilometer. This is done using two programs: Original Data Processor and Final Calculator. The first one is used to convert the vector data from the profilometer in to a 2D height matrix. The second uses different subroutines to perform the filtering, plotting, and parameters calculations. The diagram in Fig. B-1 shows a schematic of the work flow. An explanation of each process follows.

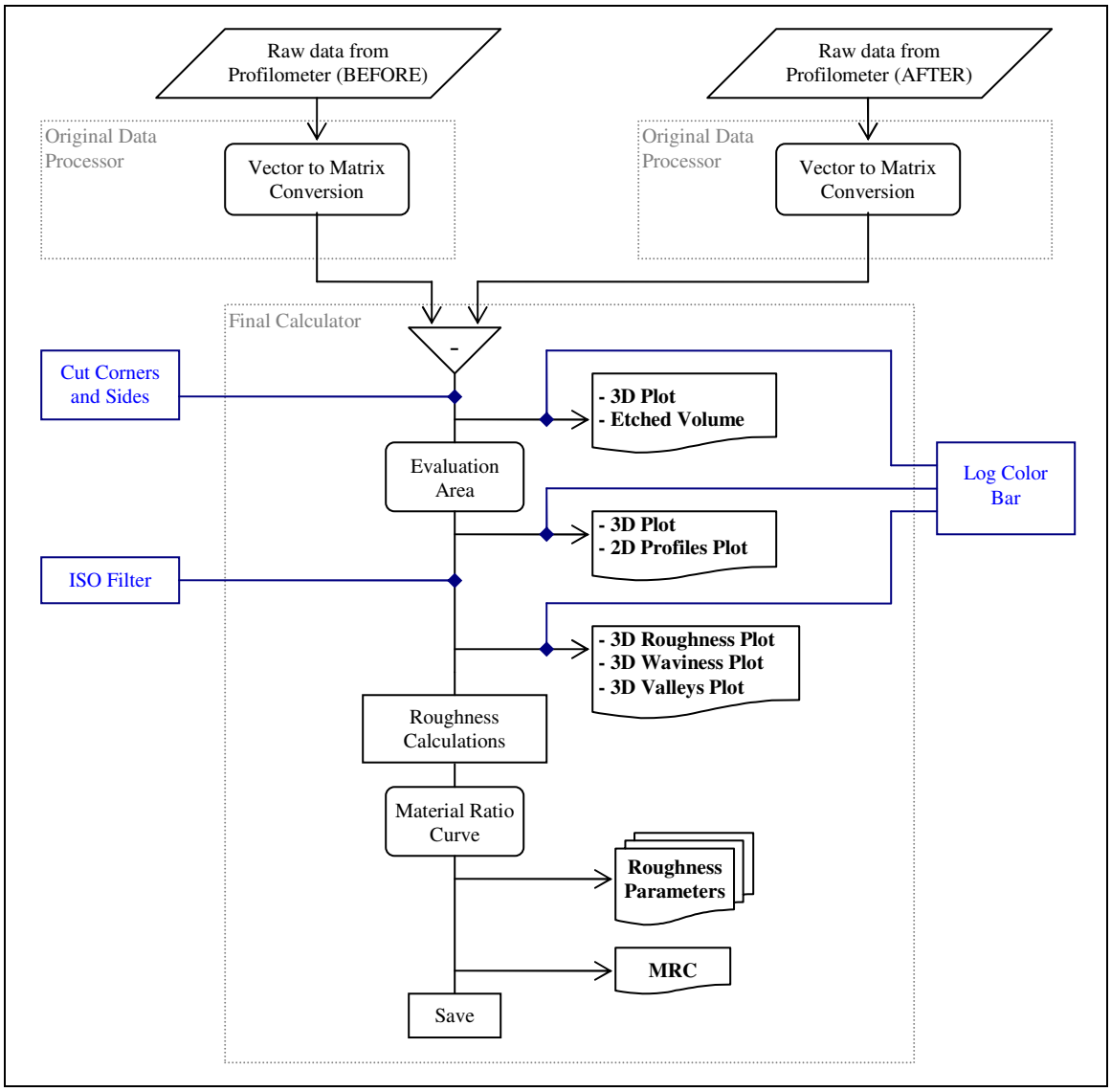

Fig. B-1. Data analysis work flow.

Two sets of data from the profilometer are processed using the Original Data Processor program; it uses a vector-to-matrix algorithm to covert the raw data into a 2D height matrix of data.

The Final Calculator program reads the matrices After and Before, and subtracts them. The new matrix is then processed using a routine to cut the corners and the sides that correspond to the rubber around the sample. After that process the etched volume can be calculated using the eq. 4.10, and a 3D plot of the surface appears on the screeen.

Next, the evaluation area is selected from the surface by cutting the rounded parts of the data. Then a new 3D plot is generated as (see Final Calculator Program on this appendix) as well as the 2D longitudinal and transversal plots. At this point, the ISO Filter algorithm is applied to separate the roughness and the waviness; this allows creating the 3D plots for Roughness, Waviness, and Valleys Views. Some of the plots use a log color bar subroutine that allows the color scale to have more resolution at shallow values.

The data corresponding to the Roughness is then used to calculate the Roughness parameters in eq. 4.1 to 4.9; then the Material Ratio Curve (MRC) is generated and the core depth parameter is calculated. Subsequently, the characterization parameters are presented and the material ratio curve plot is generated.

Finally, all the data is saved for future use i.e for comparative studies. The saved data includes the surface matrix, the MRC data, and all the parameters.

Original Data Processor Program

The original data processor is a data converter program. It is used to convert the file from the profilometer (coordinates data) to a 2D height matrix. First, the program uses the original file location path to open the file, and then it reads and saves the file header,

which includes Experiment Title, Sample Length, Sample Width, and Measurement Interval. Next it reads the three columns of data called X Position, Y Position, and Z Displacement; all the columns are recorded in a data matrix. The size of this matrix is equal to the number of data points recorded.

The dimensions of the 2D matrix are calculated by:

Num. Columns = (Sample Length / Measurement Interval) + 1

Num. Rows = (Sample Width / Measurement Interval) + 1

Then an algorithm takes sections of data from the data matrix at intervals equal to the number of rows and orders them in sequence. As result a 2D matrix is created, its dimensions are the number of columns and the number of rows.

Defining:

data(i,j) = the data matrix

nrows = the number of rows

ncols = the number of columns.

X(i,j), Y(i,j), and Z(i,j) = New 2D matrixes

The algorithm is.

```
for i=1:2:nrows                    % this reads the data points where the laser moves left to right
   k=(i-1)*ncols;
   for j=1:ncols
      k=k+1;
      X(i,j)=data(1,k);
      Y(i,j)=data(2,k);
      Z(i,j)=data(3,k);
   end
end

for i=2:2:nrows                    % this reads the data points where the laser moves right to left
   k=i*ncols;
   for j=1:ncols
      X(i,j)=data(1,k);
      Y(i,j)=data(2,k);
      Z(i,j)=data(3,k);
      k=k-1;
   end
end
```

The program also asks the user if the surface values should be inverted on Y direction; this is necessary when the rock has been placed on the profilometer in the wrong direction. Defining *Z(i,j)* as the 2D surface matrix, the inversion is done by the next algorithm.

```
A=Z;                                % Duplicate the matrix
[ncols,nrows]=size (A);             % Get matrix dimensions
for j=1:ncols
    for i=1:nrows
       Backward=nrows+1-i;          % backwards position counter
       ANew(j,i)=A(j,Backward);     % new matrix with Y values inverted
    end
end
Z=ANew;        % reassigning the inverted matrix to the Z matrix.
end
```

Final Calculator Program

This program is a filtering and visualization program. It starts reading the data from two processed files, the After and the Before; then simply subtracts of the correspondent element of both matrixes to obtain a unique surface matrix.

Then, the data points of the surface that correspond to the rubber are converted to not-a-value (NaN). This is done using a template in a subroutine called "CutCornersSides.m"; this routine contains the positions of the points that need to be converted to NaN. After this, the surface obtained corresponds exactly to the shape of the rock sample. Then the etched volume calculation is performed using the eq. B-1, where *Z'* is the matrix after the corners are cut. This matrix is presented in a 3D color plot, and the etched volume is reported.

$$V_R = \sum_{j=1}^{N-1} \sum_{i=1}^{M-1} Z'_{(x_i, y_j)} \Delta x \Delta y \,. \quad \text{..... B-1.}$$

Next, the matrix is cut again to the evaluation area matrix; this is done by deleting the data from first four rows, the last five rows, and the first and last 12 columns. With this new evaluation area matrix, a new 3D plot is presented as well as the 2D longitudinal

and transversal plot. The longitudinal plot draws Rows 7, 14, and 21; the transversal plot draws the Columns 23, 46, 69, and 92.

The evaluation area is then processed using a subroutine called "ISOFilter.m". This program calculates an approximation to the least mean square line (LMSL) for each longitudinal profile. By definition, the LMSL is the line parallel to the geometrical profile such that the sum of the squares of the deviations of the effective profile from it is a minimum. The program first calculates an approximated mean line by calculating a three-points average for each data point. This process is repeated 100 times until an optimum mean line is obtained. Then the data points that fall below that mean line are subtracted from the profile and a second mean line is calculated over the remaining data by the same process, repeated only 10 times. This last mean line is then subtracted from the original profile data. Subsequently, the resultant matrix corresponds to the roughness and the second mean line corresponds to the waviness. The three most challenging cases of surfaces with big holes and valleys were tested to find that 100 calculations of the first mean line and 10 calculation of the second mean are necessary to achieve an adequate filtering.

If the original matrix is:
Zinput(i,j)= evaluation matrix
The algorithm computes as follows.

```
for f=1:Nrows
   ZL=Zinput(f,:);                  % captures the row of data or profile to be filtrated.
   [nrows,ncols]=size(ZL);
   ZLOriginal=ZL;                   % New matrix to save the original profile for future subtraction.

% THIS "cycle for" is for the FIRST MEAN Calculation.
   for h=1:100                      % 100 has been found to be the optimum for the roughest surfaces
      for i=2:ncols-1
         j=i-1;
         k=i+1;
         ZLlsml(1,1)=ZL(1,1);                          % first data point.
         ZLlsml(1,i)=(ZL(1,j)+ZL(1,i)+ZL(1,k))/3;      % three points average
         ZLlsml(1,ncols)=ZL(1,ncols);                  % last data point.
      end
      ZL=ZLlsml;                              % reassigning the variable for the next h
   end
```

```
% THIS "cycle for" is to subtract the data below the mean line
   for i=1:nrows
      for j=1:ncols
         if ZLOriginal(i,j)>ZL(i,j)              % compares the original to the high wave filtered
            ZLHighWave(i,j)=ZLOriginal(i,j); % If is bigger then keeps the original
         else
            ZLHighWave(i,j)=ZL(i,j);            % if is smaller change to the filtered value
         end
      end
   end

   ZL=ZLHighWave;                  % reassigning to calculate the second mean line

% THIS "cycle for" is for the SECOND MEAN Calculation.
   for h=1:10    %  10 Has been found to be the optimum for the 100 on the FIRST CYCLE
      for i=2:ncols-1
         j=i-1;
         k=i+1;
         ZLlsml(1,1)=ZL(1,1);
         ZLlsml(1,i)=(ZL(1,j)+ZL(1,i)+ZL(1,k))/3;      % three points average
         ZLlsml(1,ncols)=ZL(1,ncols);
      end
      ZL=ZLlsml;
   end

   ZLfinal=ZLOriginal-ZL;          % the final profile is calculated
   Zwaviness(f,:)=ZL;              % Zwavines is the Waviness matrix
   ZFiltered(f,:)=ZLfinal;         % ZFiltered is the Roughness matrix
end
```

After these calculations, the plots of roughness, waviness, and 3D valleys are presented; subsequently, the roughness parameters S_a, S_q, S_z, S_{sk}, S_{ku}, S_{Dq}, and S_{dr} are calculated using the data from the roughness matrix obtained. This is done using Eqs. 4.1 to 4.9 in Section 4.

For the calculation of the parameter S_c (core depth) the MRC is calculated by means of the linearization of the roughness matrix and its ordering by height. Then the values of 90% and 10% are calculated using an interpolation point technique. The linearization is performed by the algorithm.

```
% Linearization = Converting the ZLFinal matrix to a one dimension Matrix ZL.
ZLFinal=ZFinal;                 % this is a new assignation to avoid changing the original ZFinal matrix
[nrows,ncols]=size(ZLFinal);
ZLineal=[];                     % Initializing ZLineal matrix variable.
for i=1:nrows
  for j=1:ncols
    ZLineal=[ZLineal, ZLFinal(i,j)];          % adds each row after row to create a vector variable.
```

```
  end
end

% Creating the MRC
Zsort=sort(ZLineal);                    % Ordering MRC
ZMRC=InvertVectorOrder(Zsort);          % Order for plot by height

[value1,MRCsize]=size(ZLineal);         % size for Xaxis
Xmrc=[0:1:MRCsize-1];                   % creation of X axis matrix
Xmrc=100*Xmrc/MRCsize;                  % X matrix on percentage
Sp10=interp1(Xmrc,ZMRC,10);             % Interpolating for 10%
Sv90=interp1(Xmrc,ZMRC,90);             % Interpolating for 90%
Sc=Sp10-Sv90;                           % calculation of the Sc parameter value
```

The last figures displayed by the program are the MRC plot as well as a histogram of the data. Finally the all the roughness parameters are printed in the MatLab screen and the variables are saved on a MatLab data file that contains the following variables:

ExpTitle = Experiment title
SampleLength = Sample length
SampleWidth = Sample Width
MeasurementInterval = Measurement interval
PhaseApplied = Datum correction applied to the after rock.
X2= X matrix of the coordinates positions of on the X direction.
Y2 = Y matrix of the position coordinates in the Y direction
ZFinal = Height matrix of the Roughness.
Xmrc = X values of the MRC
ZMRC = Matrix of the Material Ratio Curve
Sa, Sq ,Sz, Ssk, Sku, SDq, Sdr,Sp10, Sv90 = Roughness parameters.

APPENDIX C

SAMPLE PICTURES

15 minutes	**N/A**
30 minutes	
60 minutes	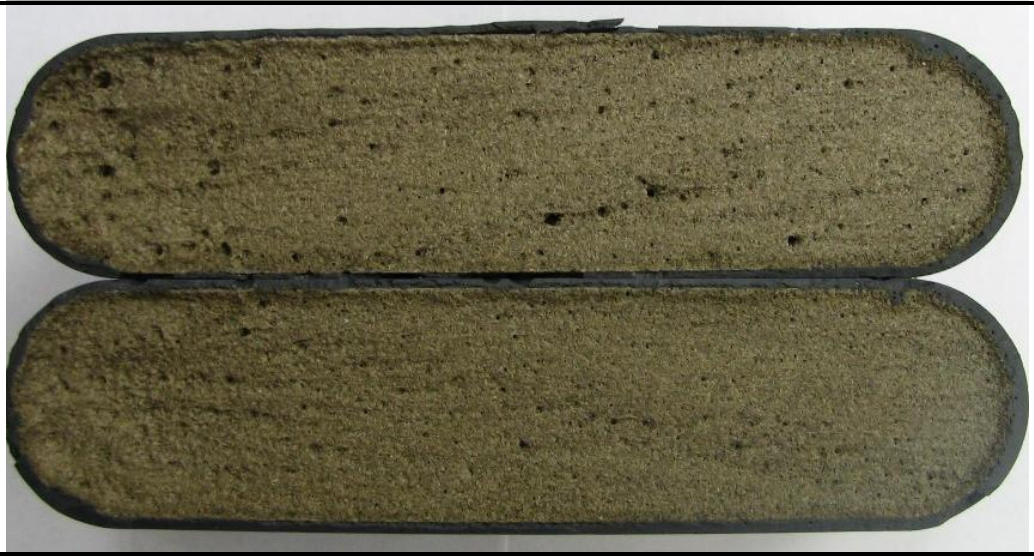

Fig. C-1—Exp. 1: Emulsified acid and limestone, 200 °F, 0.005 ft/min.

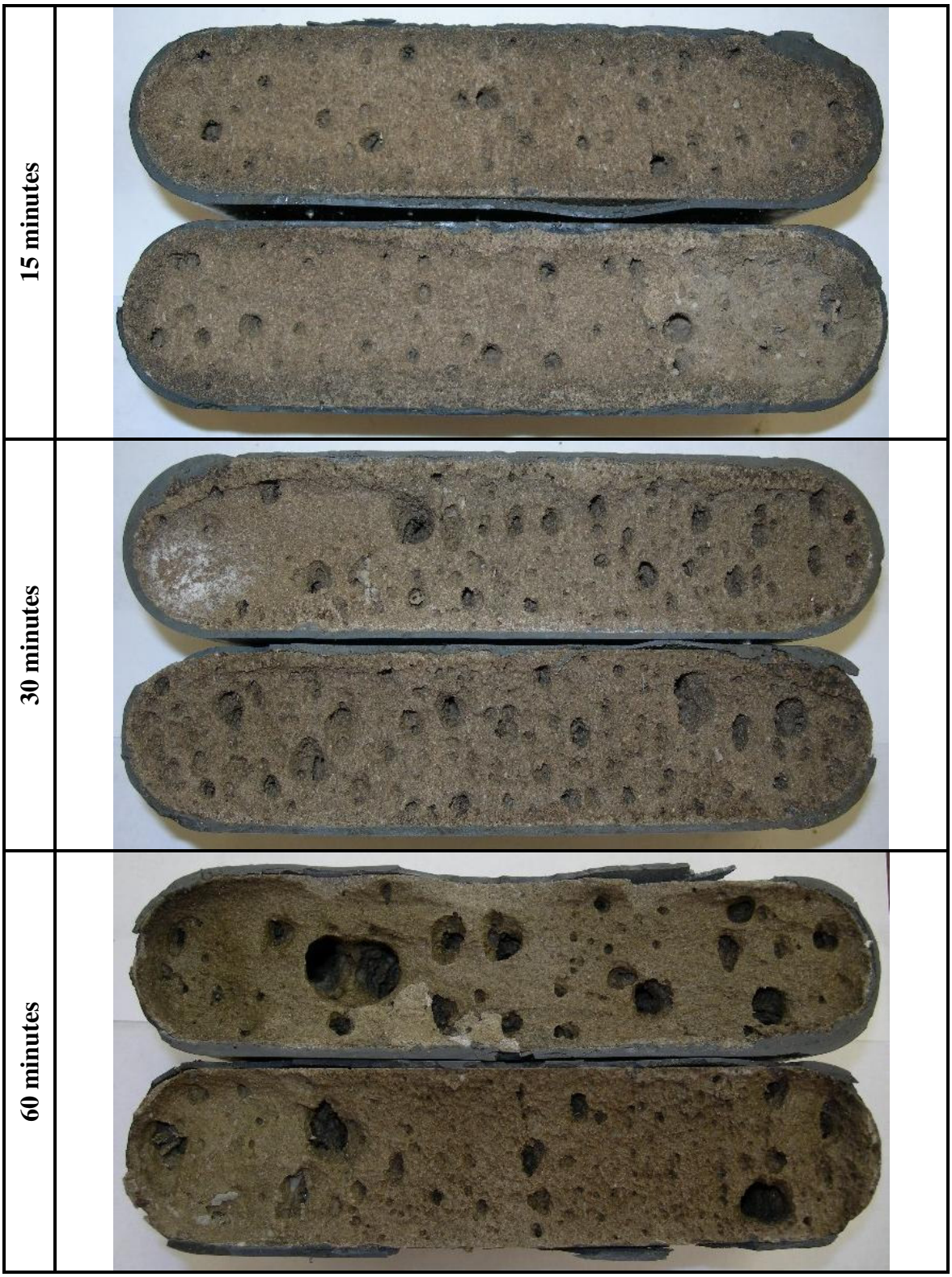

Fig. C-2—Exp 2: Emulsified acid and limestone, 275 °F, 0.005 ft/min.

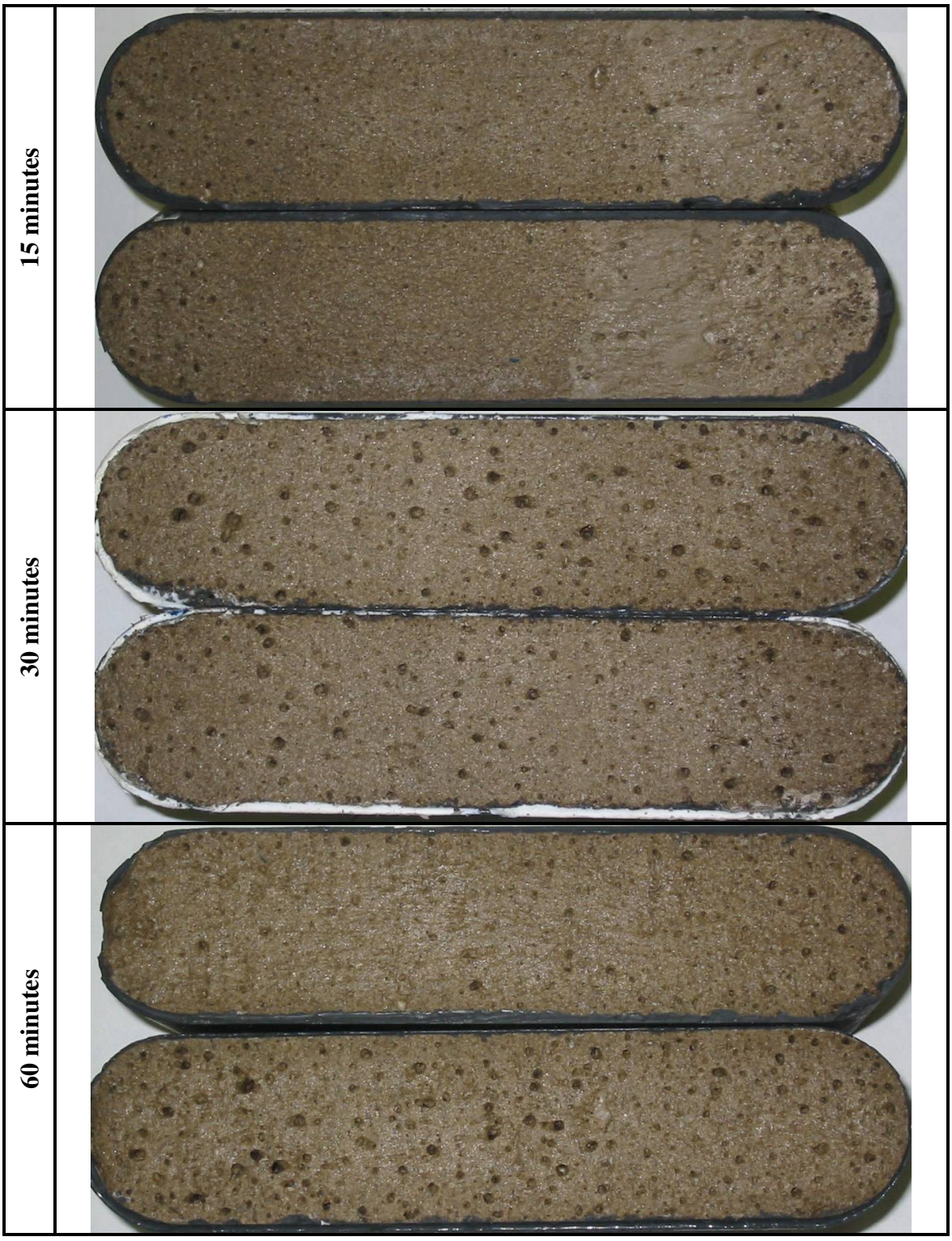

Fig. C-3—Exp. 3: Gelled acid and limestone, 200 °F, 0.005 ft/min.

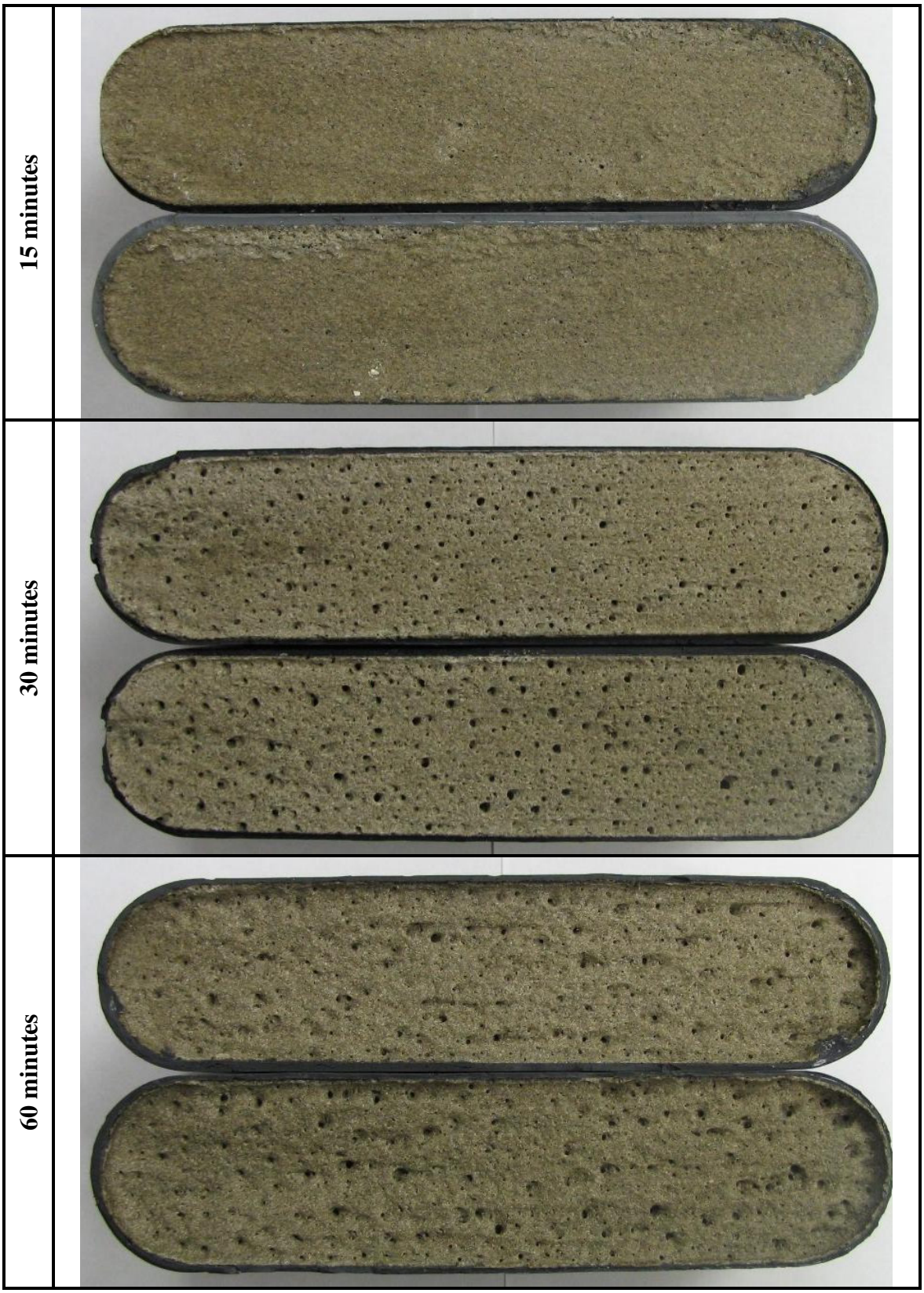

Fig. C-4—Exp. 5: Viscoelastic surfactant acid and limestone, 200 °F, 0.003 ft/min.

Fig. C-5—Exp. 6: Viscoelastic surfactant acid and dolomite, 200 °F, 0.005 ft/min.

Fig. C-6—Exp. 7: Straight acid and chalk I, 100 °F, 0.005 ft/min.

Fig. C-7—Exp. 8: Straight acid and chalk II, 100 °F, 0.005 ft/min.

VITA

CONTACT INFORMATION

Camilo Malagón Nieto
Carrera 58 D # 128B-01 Int. 2-302
Bogotá, Colombia S.A.
(571) 2268879
camilomalagon@hotmail.com

EDUCATION

M.S. Petroleum Engineering. 2007
Texas A&M University, College Station, Texas, USA.
GPR: 3.6

B.S. Petroleum Engineering. 2001
Universidad de America, Bogotá, Colombia.
GPR: 4.0/5.0

RESEARCH

3D Surface Characterization of Acidized Surfaces.
Paper SPE 102167 and SPE 106272.
Advisor Dr. Dan Hill, Texas A&M University.

EXPERIENCE

SCHLUMBERGER (DCS). Part-time Job
College Station, Texas. Feb 2005 – Aug 2005.

OCCIDENTAL INC. Research Internship
Bogotá, Colombia. Mar 2001 – Oct 2001.

ECOPETROL. Internship
Bogotá, Colombia. Oct 1999 – Oct 2000.

OTHER STUDIES

Business Management Certificate for Engineering Students
Mays Business School at Texas A&M. Aug 2006.

HONORS AND LEADERSHIP ACTIVITIES

Meritorious Thesis. Universidad de América. Dec 2001.
Meritorious Student. Second Best GPA. Promotion 2001.
SPE Student Chapter. President. October 1999 - Jan 2001.
Active member of SPE and AAPG.

SKILLS

Computers. MatLab, WellView, CMG, DIMS, AUTOGRAPH, Microsoft Word, Excel, PowerPoint and Access.
Languages. Spanish-mother tongue. English-TOEFL CBT 250.